This is to certify that the
dissertation entitled

EXPLORING MOLECULAR MECHANISMS OF HUMAN GENETIC DISEASES – TWO EXAMPLES: AUTOSOMAL DOMINANT HEARING LOSS (DFNA20/26) AND AUTOSOMAL RECESSIVE LYSOSOMAL STORAGE DISEASE, BETA-MANNOSIDOSIS

presented by

Mei Zhu

has been accepted towards fulfillment
of the requirements for the

Ph.D. degree in Cell and Molecular Biology

Karen Friderici
Major Professor's Signature

12-11-07
Date

MSU is an affirmative-action, equal-opportunity employer

EXPLORING MOLECULAR MECHANISMS OF HUMAN GENETIC DISEASES –TWO EXAMPLES: AUTOSOMAL DOMINANT HEARING LOSS (DFNA20/26) AND AUTOSOMAL RECESSIVE LYSOSOMAL STORAGE DISEASE, BETA-MANNOSIDOSIS

By

Mei Zhu

A DISSERTATION

Submitted to
Michigan State University
In partial fulfillment of the requirements
for the degree of

DOCTOR OF PHILOSOPHY

Cell and Molecular Biology

2007

ABSTRACT

EXPLORING MOLECULAR MECHANISMS OF HUMAN GENETIC DISEASES – TWO EXAMPLES: AUTOSOMAL DOMINANT HEARING LOSS (DFNA20/26) AND AUTOSOMAL RECESSIVE LYSOSOMAL STORAGE DISEASE, BETA-MANNOSIDOSIS

By

Mei Zhu

Two different types of autosomal inherited genetic diseases, namely, a dominant hearing loss (DFNA20/26) and a recessive lysosomal storage disease, β-mannosidosis, have been studied for molecular disease mechanisms. Hearing loss is the most common sensorineural disorder in humans. The disease-causing gene of DFNA20/26 has been identified to be cytoplasmic γ-actin, a highly conserved, ubiquitously expressed, abundant protein in eukaryotic cells. This study was designed to examine the effect of six DFNA20/26 mutations on actin function and elucidate the molecular basis of disease development. In contrast, β-mannosidosis is a rare metabolic disease, which is caused by the deficiency of enzyme activity of β-mannosidase, a ubiquitously expressed house-keeping protein. So far, only a dozen or so human cases have been reported and most of the mutations have been identified. To better understand the molecular pathology of this disease, a β-mannosidase null mouse model was generated and presented in this dissertation.

Six point mutations in γ-actin were identified to be responsible for progressive sensorineural hearing loss in six different families. Here, I tested the

hypothesis that the protein folding pathway and/or its stability play an important role in the development of hearing loss, using a combination of an *in vitro* expression system and a cell culture system. Surprisingly, the only abnormal observation is an altered CAP binding. All six mutants folded properly, copolymerized with wild-type actins and bound to tested actin-binding proteins (thymosin β4, profilin I, DNase I and vitamin D-binding protein) in *in vitro* assays. N-terminally Myc-tagged actin mutants were stable and incorporated into normal actin structure when expressed in COS-7 cells. Since CAP is a key player in the organization and remodeling of cellular actin networks, the altered CAP binding might be directly involved in the development of hearing loss.

A β-mannosidase knockout mouse model was generated by standard homologous recombination. Homozygous mutant mice have undetectable β-mannosidase activity. General appearance and growth of the knockout mice are similar to the wild-type littermates. No dysmorphology or overt neurological problems were observed. The mutant animals have consistent cytoplasmic vacuolation in the central nervous system and minimal vacuolation in most visceral organs. Thin-layer chromatography demonstrated an accumulation of disaccharide in epididymis and brain. This mouse model resembles human β-mannosidosis in many respects and provides a useful tool for studying the phenotypic variation in different species and will facilitate the study of potential therapies for lysosomal storage diseases.

This dissertation is dedicated to my extended family:

my faithful husband: Hongwei, my two lovely daughters: Anqi and Annie,
my respected parents-in-law: Shuzhen Wei and Deshun Gao,
and my parents: Yulan Chen and Xiucheng Zhu

For their unconditional Love and Support

ACKNOWLEDGMENTS

First of all, I would like to thank my mentor, Dr. Karen H. Friderici for her great guidance, absolute support and strong encouragement through the completion of my dissertation research. Her love and caring for all people, her hard working in science, and her own special way of motivating and encouraging people around her have made her a role model for me over the past ten years. She always told me using her own experiences that life is a learning experience when I had concerns. For that, I am very grateful. I appreciate that she gave me a lot of freedom to pursue new scientific ideas and guided me when I needed it. I feel extremely fortunate to have Karen as my very first and only mentor since my scientific career started in the US ten years ago, and from now on.

I thank my committee members: Dr. Jerry B. Dodgson, Dr. John C. Fyfe, Dr. Richard C. Schwartz, and Dr. Susan E. Conrad for their encouragement, support, and input through my dissertation research. A special thanks to Dr. Fyfe, who has also served as my M.S. degree's committee years ago, for his continuing support and help, and for being a good model of a biologist. I am also very thankful for the help and support provided by Dr. Conrad and the CMB admission committee.

I owe great thanks to my lab members: Meghan Drummond, Soumya Korrapati, Kathy Jernigan, Ellen Wilch, Donna Housley, and Tychele Turner for their friendship and support. Their existence, love, and wisdom have made the lab full of fun and happiness through the years. I appreciate that they are always

there whenever I need them. I thank Meghan, Soumya and Ellen for their comments on this dissertation. A special thanks to Meghan for her great help on many computer-related problems.

Finally, I would like to give my special thanks to my fabulous family. I thank my husband, Hongwei, for his love, belief in me, and encouragement toward completing my degree. My two lovely daughters, Anqi and Annie, have been the strength for me to continue this work. I am thankful for the love and support provided by my respected parents and parents-in-law. I would like especially to thank my mother-in-law who has always been there helping me through the toughest part of my life and career thus far. She took care of my older daughter when I pursued my M.S. degree eight years ago, and has been helping to take care of my younger daughter during my Ph. D.. For that, I am very grateful.

TABLE OF CONTENTS

LIST OF TABLES

CHAPTER 2

LIST OF FIGURES

CHAPTER 1

CHAPTER 2

CHAPTER 3

LIST OF ABBREVIATIONS

ABP	Actin-binding protein
ADF	Actin depolymerizing factor
ADP-actin	Adenosine diphosphate-actin
ATP-actin	Adenosine 5′-triphosphate-actin
Arp2/3 complex	Actin-related proteins 2 and 3
BSA	Bovine serum albumin
CAP	Cyclase-associated protein
CBB	Coomassie brilliant blue
CCT	Chaperonin containing TCP-1
CDC20	Cell division cycle 20 homolog
CHX	Cycloheximide
DAPI	4′,6-Diamidino-2-phenylindole
DNA	Deoxyribonucleic acid
DNase I	Deoxyribonuclease I
EDTA	Ethylenediaminetetraacetic acid
EGFP	Enhanced green fluorescence protein
ES cells	Embryonic stem cells
F-actin	Filamentous actin
G-actin	Globular actin
GimC	Genes involved in microtubule biogenesis complex
HRP	Horseradish Peroxidase

neo	Neomycin
NIH	National Institutes of Health
PBS	Phosphate buffer solution
PCR	Polymerase chain reaction
PFA	Paraformaldehyde
PFD	Prefoldin
pH	potential of hydrogen
PQC	Protein quality control
psi	Pounds per square inch
PVDF	Polyvinylidene difluoride
RNA	Ribonucleic acid
RT-PCR	Reverse transcription polymerase chain reaction
SCAD	Short chain acyl-CoA dehydrogenase
SDS-PAGE	Sodium dodecyl sulfate polyacrylamide gel electrophoresis
TCP-1	T-complex protein 1
3′ UTR	Three prime untranslated region
VDBP	Vitamin D-binding protein

INTRODUCTION

The major focus of my graduate studies has been to explore the molecular pathogenesis mechanisms of human genetic diseases. I have been primarily studying two distinct types of human genetic diseases, namely an autosomal dominant progressive sensorineural hearing loss (DFNA20/26) and an autosomal recessive lysosomal storage disease, β-mannosidosis (MIM no. 248510). The major project that I am currently working on and will be presenting for my defense is to investigate the molecular mechanism of dominant hearing loss. Recently, we and others identified six missense mutations in highly conserved cytoplasmic γ-actin that caused autosomal dominant hearing loss (1-3). These mutations were identified from six different unrelated families. The six amino acids substitutions are not clustered, but are distributed across three of the four subdomains of native γ-actin. γ-Actin is ubiquitously expressed and plays an important role in many cellular activities. Surprisingly, progressive sensorineural hearing loss is the only symptom observed from all six families. To investigate the molecular mechanism of hearing loss caused by these mutations, I examined the effect of these mutations on actin folding, binding ability to actin monomer binding proteins, copolymerization ability, and stability of the protein and transcripts using an *in vitro* cell free expression system and cell culture. In chapter 1, I provide a brief introduction to actin biology, including actin molecular properties, actin-binding proteins, actin mutations and related diseases, and hearing loss. Finally I introduce diseases of protein folding and misfolding and discuss current understanding of the actin folding process. In chapter 2, I

describe in detail different experiments conducted to examine the actin functionalities that are more likely to be affected by the mutations. In chapter 3, I describe the generation and characterization of a mouse model of β-mannosidosis.

β-Mannosidosis is a rare lysosomal storage disease that is caused by a deficiency of β-mannosidase activity. It was first identified in Nubian goats (4) and subsequently in humans and cows (5, 6). The two ruminant models demonstrate severe disease phenotypes and usually die in the neonatal period. In contrast, human cases display a milder and heterogeneous clinical expression. To investigate the phenotypic differences between human and ruminant β-mannosidosis, and to develop potential therapeutic strategies we created a mouse model of β-mannosidosis. This study has been published in *Human Molecular Genetics*, vol.15, No. 3, 493-500 (7). I was responsible for this study and have been working on and following the mouse colony since I initiated this project. As a graduate student, I cloned and sequenced the cDNA of the mouse β-mannosidase gene, screened the mouse genomic library, designed and constructed the targeting vector and set up all robotic screening strategies for screening ES clones, and litter mates and functional tests (including the β-mannosidase activity assay and protein assay). I also carried out the remainder of the breeding and characterization of the β-mannosidase null mice during my employment as a research technician. Currently, I am still maintaining the knockout mice for further characterization and future studies.

REFERENCES

1. Zhu, M., T. Yang, S. Wei, A. T. DeWan, R. J. Morell, J. L. Elfenbein, R. A. Fisher, S. M. Leal, R. J. Smith, and K. H. Friderici. 2003. Mutations in the gamma-actin gene (ACTG1) are associated with dominant progressive deafness (DFNA20/26). *Am J Hum Genet* 73:1082-1091.

2. van Wijk, E., E. Krieger, M. H. Kemperman, E. M. De Leenheer, P. L. Huygen, C. W. Cremers, F. P. Cremers, and H. Kremer. 2003. A mutation in the gamma actin 1 (ACTG1) gene causes autosomal dominant hearing loss (DFNA20/26). *J Med Genet* 40:879-884.

3. Rendtorff, N. D., M. Zhu, T. Fagerheim, T. L. Antal, M. Jones, T. M. Teslovich, E. M. Gillanders, M. Barmada, E. Teig, J. M. Trent, K. H. Friderici, D. A. Stephan, and L. Tranebjaerg. 2006. A novel missense mutation in ACTG1 causes dominant deafness in a Norwegian DFNA20/26 family, but ACTG1 mutations are not frequent among families with hereditary hearing impairment. *Eur J Hum Genet* 14:1097-1105.

4. Jones, M. Z., and G. Dawson. 1981. Caprine beta-mannosidosis. Inherited deficiency of beta-D-mannosidase. *J Biol Chem* 256:5185-5188.

5. Cooper, A., C. E. Hatton, M. Thornley, and I. B. Sardharwalla. 1990. Alpha- and beta-mannosidoses. *J Inherit Metab Dis* 13:538-548.

6. Abbitt, B., M. Z. Jones, T. R. Kasari, R. W. Storts, J. W. Templeton, P. S. Holland, and P. E. Castenson. 1991. Beta-mannosidosis in twelve Salers calves. *J Am Vet Med Assoc* 198:109-113.

7. Zhu, M., K. L. Lovell, J. S. Patterson, T. L. Saunders, E. D. Hughes, and K. H. Friderici. 2006. Beta-mannosidosis mice: a model for the human lysosomal storage disease. *Hum Mol Genet* 15:493-500.

CHAPTER 1

LITERATURE REVIEW

INTRODUCTION

Molecular properties of actin

Actin is the most abundant and conserved protein in eukaryotic cells. It is a 42 kDa globular protein (G-actin), which can polymerize into filaments (F-actin) under physiological salt concentrations both *in vivo* and *in vitro*. The filaments are further organized into higher-order structures such as networks or bundles to perform various cellular functions including muscle contraction, cell motility, cell division, endocytosis, vesicle and organelle movement, and maintenance of cell shape and cell integrity. F-actin has been regarded as the only functional form of actin in cells, but recent emerging evidence has suggested that G-actin may play a role in the nucleus; both G- and F-actin have been implicated in many nuclear functions, such as transcription, mRNA processing, chromatin remodeling and nuclear matrix association (2).

Actin filaments are polarized, characterized by a fast-growing (plus or barbed) end and a slow-growing (minus or pointed) end. The addition of ATP-actin monomers to the barbed end is accompanied by dissociation of ADP-actin monomers from the pointed end, a process known as treadmilling. The driving force behind the treadmilling is the hydrolysis of ATP by actin and a number of other factors including a large number of actin-binding proteins (ABPs). Hydrolysis of ATP occurs after the actin monomer is incorporated into the filament while the inorganic phosphate (Pi) remains trapped in the nucleotide site for several minutes before being released (3). Therefore, the actin filament has

three distinct regions: an ATP-bound region near the fast growing barbed end, an intermediate ADP-P_i region where the P_i is retained, and an ADP-bound region at the slow-growing pointed end of the filament. The different nucleotide states of the filament have slightly different conformations (4), which is also reinforced by the fact that certain ABPs preferentially interact with one or more of these states of filament. For example, the Arp-2/3 complex, mediating filament branching at the leading edge of the cell, binds 25-fold better to ATP filaments than to ADP filaments; and cofilin/ADF has been shown to bind 10- to 50-fold better to ADP-actin than to ATP-actin (reviewed in (3)). This nucleotide effect on actin structure is also true for G-actin and it is supported by many lines of evidence including the preferential binding of ABPs to different nucleotide states of G-actin (which will be disscussed in the section on ABPs), the observations from spectroscopic and electron microscopic studies (5), and atomic structures of G-actin with ATP or ADP (5-7).

To date, more than 40 crystal and cocrystal structures of actin have been solved (3). The overall structures of actin in complexed (with an ABP) or uncomplexed states (monomeric actin) with either ATP or ADP are very similar though not identical. The actin molecule consists of a small domain (subdomains 1 and 2) and a large domain (subdomains 3 and 4) with a cleft containing one molecule of ATP and a single cation (Ca^{2+} or Mg^{2+}) (Figure 1-1). Both the amino- and carboxy-termini of actin reside in subdomain 1 of the small domain, which consists of residues 1-144 and 338-375. The large domain is made up of residues 145-337. Subdomains 1 and 3 constitute the barbed end of globular

Figure 1-1: The three-dimensional structure of actin. Actin consists of a small and a large domain with one molecule of ATP (wire diagram) and one metal atom (sphere) residing in the cleft between the two domains. The small domain contains subdomain 1 (residues 1-32, 70-144, and 338-375) and subdomain 2 (residues 33-69); the large domain contains subdomain 3 (residues 145-180 and 270-337) and subdomain 4 (residues 181-269). The numbers indicate residues at either end of α-helices (cylinders) or β-sheet (arrows) (adapted from Hennessey et al., Biochem. J. 1993, 282, 657-671).

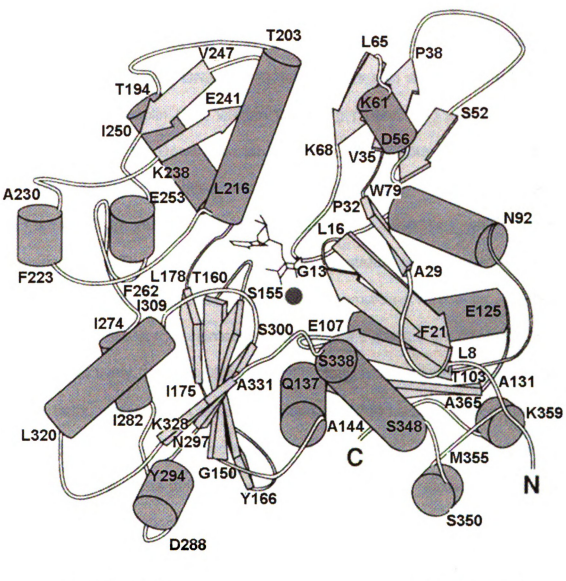
Subdomain 4
Subdomain 2
T203
V247
T194
E241
I250
K238
A230
E253
L216
F223
L178
T160
F262
I309
S155
I274
S300
E107
I175
A331
Q137
I282
K328
N297
L320
Y294
G150
Y166
D288
L65
P38
K61
S52
D56
K68
V35
W79
P32
N92
L16
G13
A29
E125
F21
L8
S338
T103
A131
A365
K359
A144
S348
C
M355
N
S350
Subdomain 3
Subdomain 1

actin, which is located at the barbed end of the filament during polymerization (8).

Due to the inherent strong tendency to polymerize, the atomic structure of actin had to be determined from a complex with an actin-binding protein that keeps actin in a monomeric state. The first crystal structure of ATP-G-actin was solved in a complex with DNase I (9), later it was also determined with other ABPs, including gelsolin (10), vitamin D-binding protein (11) and profilin (12). Recently, however, the Dominguez lab (5, 7) was able to obtain crystal structures of uncomplexed actin in both ADP and ATP states using covalent modification with tetramethylrhodamine-5-maleimide (TMR) to Cys374, which blocks polymerization. The uncomplexed ADP-actin structure has revealed some differences compared to those structures of uncomplexed ATP-actin and those complexed with ABPs: the orientation of subdomains 2 and 4 are rotated by ~10° and 5°, respectively, and the DNase I-binding loop within subdomain 2 is folded as an α helix, whereas it is either disordered or folded as a β turn in previous complexed structures and uncomplexed ATP-actin (5, 7). In addition, in comparing the dynamics of G-actin in ATP, ADP-P_i and ADP states via molecular dynamics (MD) simulations, Zheng et al. (3) have observed that the DNase I loop is an α helix in the ADP state but forms an unstructured coil domain in the ADP-P_i and ATP states. In summary, hydrolysis of ATP changes the conformations of both G- and F-actin, and these conformations control or regulate interaction of actin with itself and with other proteins, which play a key role in the rapid turnover dynamics of actin *in vivo*.

Actin-binding proteins

The structure and dynamics of actin filaments are essential for various cellular functions and are tightly regulated *in vivo* by the hydrolysis of ATP by actin as well as interactions with a substantial number of proteins collectively called actin-binding proteins (ABPs) (13). These include proteins that sever or cap actin filaments (gelsolin), nucleate polymerization (the Arp2/3 complex, formins), affect the depolymerization of filaments (ADF/cofilin), or associate with monomeric actin to sequestrate and regulate its availability for polymerization (profilin and thymosin β4) (14). To date, more than 160 ABPs have been identified (15). Here, I only focus on a few monomeric actin-binding proteins that are essential for maintaining and regulating G-actin for rapid actin filament turnover. These proteins (thymosin 4, profilin, DNase I, vitamin D-binding protein, cyclase-associated protein, and cofilin) are widely distributed and very important factors for maintaining the G-actin pool and regulating the dynamics of actin in cells. In addition, most of them have been well studied both *in vivo* and *in vitro*.

Thymosin β4 (Tβ4) is a highly conserved, 43-amino acid acidic polypeptide (pI 5.1) with a molecular weight of 4.964 kDa (16). It was isolated originally from a thymic extract (17) but is now known to be present in other tissues and circulating cells, but not in red blood cells (18). It forms a 1:1 complex with monomeric actin and is the principal *in vivo* regulator of unpolymerized actin. Tβ4 is essential for maintaining the cytoplasmic pool of actin monomers required for

rapid filament formation. It has a 50-fold higher affinity for MgATP-actin (K_d ~ 0.5-2 uM) than for MgADP-actin (19). Acting alone, Tβ4 inhibits polymerization and the exchange of the actin-bound nucleotide. This contrasts with the action of profilin which facilitates the nucleotide exchange of ADP for ATP and promotes actin filament formation. Tβ4 has multiple biological functions in addition to actin binding and sequestration. It was identified as an angiogenic factor involved in endothelial cell migration, angiogenesis and wound healing (16). NMR studies show that Tβ4 is mostly unstructured in aqueous solution (20) and folds upon binding to G-actin (21). The exact Tβ4 binding sites on G-actin are unknown. There is a general agreement that subdomains 1 and 3 of actin form part of the interface, and the C-terminal region of Tβ4 binds directly to the DNase I-binding loop in subdomain 2 of actin (22) (Figure 1-2A).

Profilin is a low molecular weight protein (12-19 kDa) and is among the most highly expressed (20-100 μM) of cytoplasmic proteins (15, 23). It was isolated initially from calf thymus, but it was later found in all other cells and species investigated to date, including yeast, flies and plants (23). In mice and humans, three profilin isoforms have been identified. Profilin I is expressed in nearly all cell types, whereas profilin II is expressed exclusively in the nervous system (23). Human profilin I and profilin II were shown to have similar biochemical properties and their atomic structures are almost superimposable (24). The biochemical properties and expression pattern of the newly identified profilin III have not been determined (23). Profilin was among the first actin-binding proteins to be

Figure 1-2: The ribbon structure models of actin and actin-binding proteins. Actin is indicated by four subdomains in all structure complexes illustrated in this figure. (**A**) The modeled complex of actin and thymosin β4. No crystal structure is avilable for this complex. Based on the cross-linking analysis, it is suggested that the N-terminal region of thymosin β4 interacts with subdomains 1 and 3 of the actin while the C-terminal region of thymosin β4 binds directly to the DNase I-binding loop in subdomain 2 of the actin. (**B**) The crystal structure of profilin and actin. Profilin binds subdomains 1 and 3 of the actin monomer. (**C**) The atomic structure of DNase I and actin. DNase I binds primarily to a loop in subdomain 2 of the actin monomer. The complex structures of A-C were reviewed by Dos Remedios et al. Physiol Rev 83: 433-473, 2002. (**D**) The crystal structure of vitamin D-binding protein and actin. VDBP binds to actin subdomains 1 and 3 with an unusually large actin-binding interface. This structure was adapted from Head et al. Biochemistry, 41 (29), 9015-9021, 2002.

A. Actin and thymosin β4

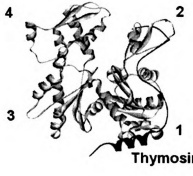

B. Actin and profilin

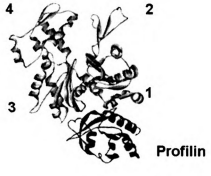

C. Actin and DNase I

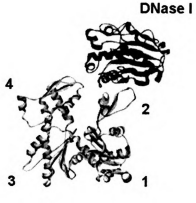

D. Actin and VDBP

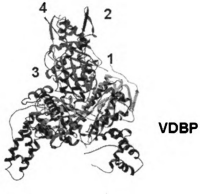

characterized and has several cellular functions. Profilin has a higher affinity for ATP-G-actin (K_d = 0.1 μM) than for ADP-G-actin (K_d = 0.5 μM) (25). It is best known for its ability to promote the exchange of nucleotide in actin monomers released from filaments; it accelerates the ADP-ATP exchange on G-actin by 1000 fold (23). Profilin enhances filament turnover in the presence of cofilin, which depolymerizes actin filaments at the opposite end. Profilin also inhibits the hydrolysis of ATP bound to actin, thus maintaining the ATP-bound G-actin pool ready for the growing barbed end of filaments. More recently, Bertling et al. (26) showed in yeast that profilin directly interacts with Srv2 (a yeast homolog of cyclase-associated protein) to recycle newly depolymerized actin monomers from ADF/cofilin for subsequent rounds of polymerization. Profilin has been cocrystallized with actin (27) and the atomic structure of the complex is illustrated in Figure 1-2B. Profilin binds subdomains 1 and 3, and its main crystal contacts with actin are as follows: subdomain 1: 113, 354, 355, 361, 364, 369, 371, 373, 375; subdomain 3: 166, 167, 169, 171-173, 284, 286-288, 290.

DNase I (Deoxyribonuclease I) is an endonuclease that cleaves double-stranded DNA to yield 5′-phosphorylated polynucleotides. It has a molecular mass of 31 kDa and an optimum pH of 7.8. DNase I is secreted by exocrine glands such as the pancreas and the parotid but it has a much wider tissue distribution. It was one of the first nonmuscle actin-binding proteins to be identified (28). DNase I binds very tightly to monomeric actin (1:1 ratio) with K_d ~ 2 nM (29), which makes it a useful tool for affinity purification of actin from cells

and in other studies (30-32). However, there are conflicting reports regarding DNase I binding to filamentous actin (F-actin): DNase I binds F-actin with either equal or drastically different K_d values (0.12$\pm$ 0.09 mM) compared to G-actin (29, 32). Recently, however, by developing a high-throughput DNase I inhibition assay, Morrison et al (33) showed that DNase I binds G-actin and F-actin with similar affinity. The enzymatic activity of DNase I is inhibited by binding of G-actin but remains when bound to the pointed end of F-actin (29, 34). Although the function of DNase I in cytoskeletal dynamics has yet to be elucidated, the tight binding with actin and its wide distribution suggests it has a biological role. The first atomic resolution structure of G-actin was obtained from crystals of DNase I bound to actin (9). DNase I binds primarily to a loop in subdomain 2 at the pointed end of actin (Figure 1-2C).

Vitamin D-binding protein (VDBP), also known as group-specific component or Gc-globulin, is a multifunctional plasma protein with a molecular mass of 51-58 kDa (52 kDa in humans). The major function of VDBP is binding, solubilization, and transport of vitamin D and its metabolites. Other important biological functions of VDBP include actin-scavenging, fatty acid transport, macrophage activation and chemotaxis (35). Interestingly, only a minority of (5% of total) plasma VDBP is occupied by vitamin D, leaving the majority free for scavenging and other functions (36). VDBP acts as an actin-sequestering agent in the extracellular space. VDBP together with gelsolin, the only other plasma protein that binds actin avidly, play a crucial role in the clearance of actin filaments

released by necrotic cell destruction into the circulation, thus protecting against disseminated intravascular coagulation induced by polymerized forms of actin (37). VDBP binds ATP-G-actin with high affinity (K_d = 10 nM) and inhibits filament formation. The crystal structure of actin-VDBP complex was determined at 2.4 Å resolution by Verboven et al. (38). VDBP binds to actin subdomains 1 and 3 with an unusually large actin-binding interface, which far exceeds the binding-interface areas reported for other actin-binding proteins such as profilin, DNase I and gelsolin. The barbed end of G-actin is completely blocked by the binding of VDBP, demonstrating how VDBP effectively interferes with actin-filament formation. A model structure of VDBP and G-actin is shown in Figure 1-2D.

Cyclase-associated protein (CAP) is a highly conserved actin monomer binding protein (50-60 kDa) found in all eukaryotic organisms examined (39). CAP (also called Srv2 in yeast) was first identified in budding yeast as a protein that interacts with adenylyl cyclase and facilitates its activation by RAS (40, 41). A role for CAP in actin dynamics was initially suggested by the observation that overexpression of profilin suppressed the cytoskeletal defects associated with CAP^- cells in yeast (42). The N-terminal region of CAP (Srv2) binds to adenylyl cyclase in yeast, although this binding activity does not appear to be conserved in animals and plants and the function of the N-terminus in higher eukaryotes is unknown. In contrast, the C-terminal half of this protein which binds actin monomers with a 1:1 stoichiometry and regulates actin dynamics is conserved in all Srv2/CAPs tested so far (39, 43). Recently, several studies have

demonstrated that Srv2/CAPs are not simple actin monomer-sequestering proteins, but instead regulate actin dynamics by recycling actin monomers and cofilin/ADF for new rounds of actin filament assembly (44-46). Mattila et al. (47) have shown that yeast CAP binds with strong preference to ADP-actin (K_d 0.02 μM) compared with ATP-actin (K_d 1.9 μM) and competes directly with cofilin for binding ADP-actin. In addition, CAP has been suggested to interact with profilin through the conserved proline-rich motif (Fig. 1-3) to promote exchange of nucleotide (ATP for ADP) on G-actin, followed by release of profilin-bound ATP-G-actin to replenish the actin monomer pool (26, 48). In a recent study in plants, Chaudhry et al. (43) reported that *Arabidopsis* CAP1 can increase the rate of nucleotide exchange (ADP for ATP) on actin. Furthermore, CAP has been proposed to bind ADF/cofilin-G-actin complexes through its N-terminus (44) and interact with F-actin through actin filament binding protein Abp1 (49, 50). The current view of binding motifs in Srv2/CAP is illustrated in Fig. 1-3 (1). The binding sites as indicated from the N-terminus to the C-terminus are adenylyl cyclase, cofilin-G-actin, profilin, actin (?), abp1, and G-actin. Unlike most actin monomer binding proteins, CAP oligomerizes, likely into hexamers (45). Taken together, the macromolecular complex of CAP seems to serve as a multifunctional center where multiple actin-binding proteins interact to recycle actin monomers and cofilin for subsequent filament assembly and disassembly.

Deletion of the Srv2 gene in yeast results in abnormally large cell size, random budding pattern, and defects in actin distribution (42, 51). Consistent with a role in regulating actin dynamics, the loss of CAP results in cytoskeletal

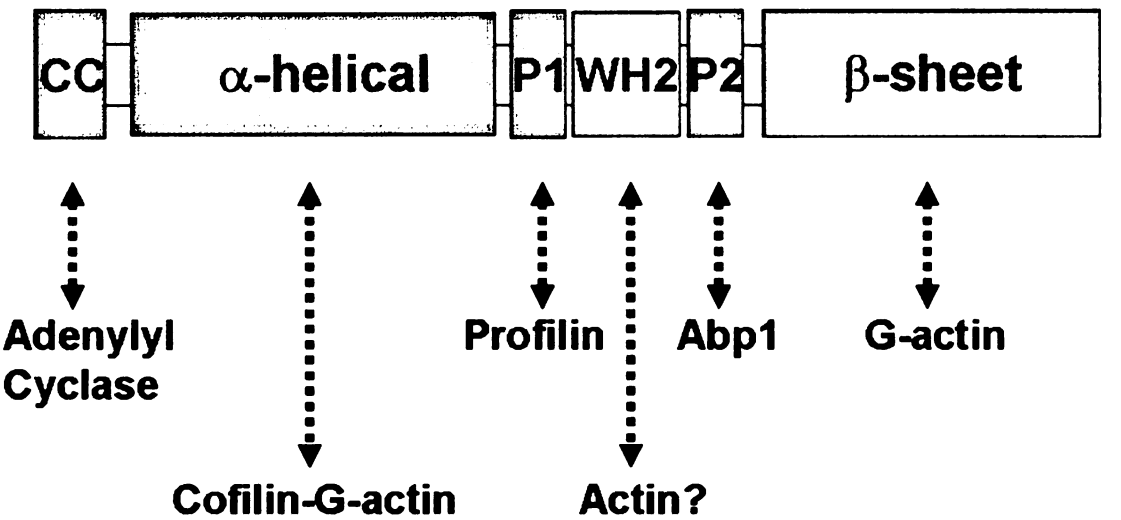

Figure 1-3: The current view of binding motifs on Srv2/CAP. Srv2/CAP is a mutifunctional protein, consisting of multiple binding motifs to interact with proteins. They are arranged in the following order, from its N-terminus to C-terminus: adneylyl cyclase, cofilin-G-actin, profilin, Actin ?, Abp1, and G-actin. These binding motifs were proposed by Dr. Bruce Goode (1)

defects that have been observed in other organisms, including *Dictyostelium discoideum*, *Drosophila*, plants and mammals (46, 52-55). In mammals, there are at least two CAP homologs, CAP1 and CAP2, which are closely related. Both CAP1 and 2 have been reported to bind to G-actin at their C-terminal domains (39). The biological role of CAPs in mammalian cells has not been well studied. Several studies using mice and cell lines have shown that CAP1 is widely expressed in different tissues and localizes to dynamic actin structures (colocalized with cofilin in active sites) , whereas CAP2 is only significantly expressed in limited tissues including brain, heart, skeletal muscle, and skin (46, 56). CAP1 has been demonstrated to promote assembly of the actin cytoskeleton by recycling cofilin and G-actin (44, 46, 57). Observations from an alanine mutagenesis scan of actin (58) and the crystal structure of actin binding domain of CAP (59) suggeste that CAP likely binds in the subdomain 1-3 cleft of the actin monomer.

Cofilin and actin depolymerizing factor (ADF) are two members of a family of small (15-20 kDa) actin-binding proteins that disassemble actin filaments. Multiple isoforms exist in this family. All eukaryotic cells have at least one member of this family. Although cofilin and ADF are commonly regarded synonymous to each other (cofilin/ADF), they are different and are coded by two different genes (15). In mammals, only one isoform of ADF is known, whereas there are two known isoforms for cofilin: cofilin 1 and 2. Cofilin 1 is expressed in most tissues and cofilin 2 is primarily expressed in muscle cells, while ADF is

limited to epithelial cells and endothelial cells (60). Cofilin/ADF (hereafter called cofilin) binds to both G-actin and F-actin in a 1:1 molar ratio with high affinity (K_d < 1 μM), and the binding is pH dependent; in general, cofilins tend to bind to F-actin around pH 6.5 and to G-actin around pH 8.0 (61). Cofilin causes depolymerization at the pointed (minus) end of filaments, thereby preventing their reassembly. In addition, cofilin can also sever actin filaments and thus generate more barbed (positive) ends on filament fragments. Cofilin binds to ADP-actin with about two orders of magnitude greater affinity than to ATP-actin or ADP-P_i-actin for both the G- and F-actin. Cofilin is regulated by phosphorylation (Ser3), pH and phosphatidylinositol 4,5-bisphosphate (PIP2) (15). It also appears to be regulated by CAP. Moriyama et al. (44) demonstrated that CAP could stimulate the release of cofilin from the cofilin-G-actin heterodimer. No atomic structure has been reported for any vertebrate cofilin. Structure homologies between cofilin, gelsolin and profilin suggest they might bind to the same region of G-actin at subdomains 1 and 3.

Actin isoforms

According to the differences in mobility in isoelectric focusing, actins have been classified as α-, β-, and γ-isotypes in order of increasing basicity. In mammals, there are six isoforms consisting of four muscle actins (skeletal α-actin, vascular α-actin, cardiac α-actin, enteric γ-actin) and two non-muscle actins (cytoplasmic β-actin and γ-actin). Although the six isoforms are coded by separate genes residing on different chromosomes, the primary sequence of the

six isoforms is very similar. The non-muscle actins differ from the muscle actins at 25 of 375 amino acid residues that make up their primary structure. Cytoplasmic β- and γ-actin are strikingly similar, differing by only four amino acids at the N-terminus. Besides sharing very high homology, each of the six actins is also completely conserved across vertebrate species ranging from birds to humans. Actin isoforms cannot substitute for each other *in vivo* and are functionally specialized for the tissue in which they predominate (62). Very little is known at the molecular level about the functional differences between actin isoforms. So far, the only breakthrough finding on discrimination between β- and γ-actins is the posttranslational arginylation of β-actin at its N-terminus (63), which prevents actin filaments from clustering. Arginylated β-actin forms single F-actin filaments, whereas non-arginylated γ-actin forms dense parallel bundles of filaments (64), which could be the molecular basis of spatial differences observed in these two cytoplasmic actins: β-actin is concentrated near the leading edge of a moving cell whereas γ-actin is distributed throughout the central region of the cell. Currently, it is still not clear if actin isoforms copolymerize *in vivo* and whether such filaments have different function. Moreover, little is known about whether certain ABPs prefer to bind to particular isoforms, especially in the case of the two cytoplasmic actins, β- and γ-actin. Several studies have shown that β-actin preferentially interacts with the plasmin-fimbrin family (65, 66) and with ezrin (67-69), while only one study reported a possible preferential binding of γ-actin to annexin V (70).

Actin and Disease

Because actin is remarkably conserved and is essential for many cell activities and viability, it is thought that most actin mutations likely have been eliminated rather than tolerated in nature. Therefore, it is unexpected to see many disease-causing mutations in actin. However, more than one hundred mutations in the α-skeletal muscle actin gene (*ACTA1*) have been reported to be associated with different types of congenital myopathies (71) and nine mutations in α-cardiac muscle actin (*ACTC*) causing hypertrophic and dilated cardiomyopathy have also been reported (72). The majority of muscle actin mutations are *de novo* missense mutations with three instances of stop codon mutations (73) and four cases of single base pair deletion (74, 75). In addition, there are ten cases with recessive inheritance that are either compound heterozygotes for two missense mutations or homozygotes of null mutations. A few dominant traits were also found (74, 75). The myopathies caused by *ACTA1* mutations are very heterogeneous, ranging from complete lack of spontaneous movement at birth requiring immediate mechanical ventilation, to mild and even adult-onset symptoms. To date, there have been rare reports of non-muscle actin mutations associated with disease. Two missense mutations in β-actin (*ACTB*) have been reported: one mutation was found in a single patient with recurrent infection (76), and the other was identified in monozygotic twins with developmental malformations and deafness (77). Recently, our lab along with others identified six missense mutations in γ-actin that cause nonsyndromic, autosomal dominant, sensorineural hearing loss (78-80).

Hearing loss

Hearing loss is the most common disabling sensory defect in humans. Approximately one in 1,000 individuals is affected by severe or profound deafness at birth or during early childhood, and the prevalence of hearing loss increases dramatically with age. Sensorineural hearing loss, which results from defects in inner ear or auditory nerve function, is the most prevalent form of hearing impairment. It can be caused by noise- or drug-induced damage, aging, viral infections, and genetic factors (which account for at least 60% of congenital hearing loss). Genetic deafness is divided into syndromic forms (in which hearing loss is associated with other anomalies) and non-syndromic forms. The syndromic forms of deafness account for 30% of deafness with genetic etiology (81) and several hundred syndromes which include hearing loss have been described (82). According to the Hereditary Hearing Loss Homepage (Van Camp G, Smith RJH. http://dnalab-www.uia.ac.be/dnalab/hhh), more than 100 loci have been mapped for non-syndromic deafness, and about 45 genes have been identified to date. Many of these genes are involved in maintaining and regulating the structural integrity and proper function of the hair cells within the cochlea of the inner ear. Hair cells are mechanosensors of the inner ear and are responsible for transduction of mechanical stimuli (sound waves) into electrical signals, which is a crucial event in the normal hearing process. Some of the deafness genes related to hair cell function include proteins interacting with actins, such as whirlin, harmonin, espin, cadherin, myosin VIIa, myosin XV, myosin VI (reviewed in (81)), and γ-actin (78-80).

γ-Actin and Mutations

γ-Actin is one of the two actin isoforms that are ubiquitously expressed in non-muscle cells. It is the predominant form of actin in intestinal epithelial cells (83) and in auditory hair cells (65), while in most other cells β-actin and γ-actin coexist at a constant ratio of approximately 2:1 (62). In chicken hair cells, β-actin is restricted primarily to the stereocilia whereas γ-actin is found throughout the hair cells. The actin cytoskeleton is essential for maintaining the specific structure and proper function of hair cells. It is well accepted that γ-actin is distributed throughout the central region of the cell and is likely involved with the stable parts of the cytoskeleton. In addition, γ-actin is also known to be the exclusive isoform expressed at very low levels in skeletal muscle costameres (84), the cytoskeletal networks that couple peripheral myofibrils to the sarcolemma. Several lines of evidences have suggested that γ-actin plays an important and unique role in maintaining skeletal muscle function. It may participate in sarcomere assembly (85). Recently, Hanft and colleagues have demonstrated that γ-actin contributes to a compensatory remodeling response in several animal models, including dystrophin-deficient mice and dogs (86, 87), in which γ-actin expression were all dramatically increased. In addition, skeletal muscle-specific γ-actin knockout mice were also generated, and they exhibited muscle weakness accompanied by a progressive pattern of muscle fiber necrosis and regeneration (88), implying a potent role of γ-actin in muscle.

γ-Actin mutations. Recently, we and others discovered six point mutations in γ-actin causing dominant hearing loss (78-80). These mutations are T89I, K118M,

P264L, T278I, P332A, and V370A. Five of the six are located in subdomains 1 and 3, with P264L located in subdomain 4, as shown in Fig. 1-4B. All mutations result in substitution of highly conserved amino acids. What is unexpected is that these mutations cause only hearing loss, and that the pattern of progressive hearing loss is very similar among the six different families, differing only in the age of onset and rate of progression. These findings imply that γ-actin may play a very specific role in the ear. One hypothesis is that these mutations may interfere with actin-related ear-specific functions; for instance, the mutations may diminish the ability of γ-actin to interact with other proteins in the ear. On the other hand, these amino acids that are mutated are across the coding region of the γ-actin gene (Fig. 1-4A) and are predicted to be involved in different functions, such as filament formation (T278I, P264L), myosin interaction (P332A T89I, K118M), and bundling or gelation protein interaction (T89I, K118M, V370A). This implies that the mutations may not directly disrupt specific γ-actin function, but may result in a common defect, such as decreased stability of the mutated proteins.

γ-Actin mutations in yeast. In collaboration with Peter Rubenstein (University of Iowa) I engineered all six mutations separately into the single yeast actin gene to investigate the effects of these mutations on actin function (89). All six yeast mutants are viable but four mutants (K118M, T278I, P332A, V370A) exhibited significant growth deficiencies in complete medium and an inability to grow on glycerol as the sole carbon source, implying a mitochondrial defect. These four mutants also exhibited abnormal mitochondrial morphology. Five of the six

Figure 1-4: Location of *ACTG1* mutations in the actin structure. (**A**) The six mutations in the genomic structure of γ-actin. The human γ-actin gene consists six exons, including a small 5′ UTR, 5 coding exons and a relatively long 3′ UTR, which are indicated by filled blocks. The six mutations are scattered across the coding region (larger filled blocks) from exon 3 to exon 6. (**B**) The six mutations in the three-dimensional structure of actin (PDB accession number 1ATN). The six missense mutations identified are located in three of the four subdomains of actin: T89I, K118M, and V370A in subdomain 1, P264L in subdomain 4, and T278I and P332A in subdomain 3. Mutations P264L and P332A are near the ATP binding site while the remaining four mutations are located near the barbed end of the actin monomer.

A


T89I
K118M
P264L
T278I
P332A
V370A
5′
3′

B

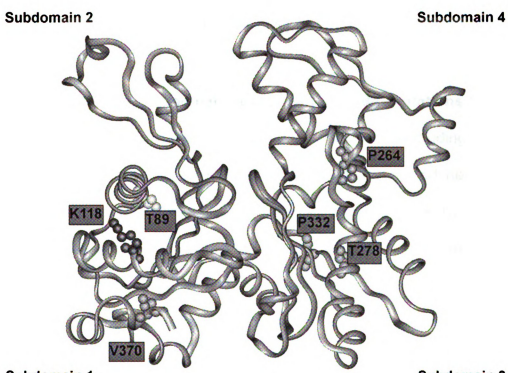
Subdomain 2
Subdomain 4
P264
K118
T89
P332
T278
V370
Subdomain 1
Subdomain 3

mutants (all except T89I) displayed strain-specific vacuole morphological abnormalities. Two mutant actins (P264L and P332A) showed decreased thermal stabilities (decreased melting temperature of 6 and 5°C respectively) and increased nucleotide exchange rates (5 and 3.5 times faster respectively). The T89I mutation showed a retarded rate of nucleotide exchange, although the K118M and T278I mutants behaved virtually identifical to wild-type actin. All mutants exhibited abnormal actin cytoskeletons (fragmentation) and all mutant actins polymerized into filaments. Only V370A actin polymerized faster than wild-type actin. These results suggest that the deafness caused by these mutations may be due to an altered ability of actin filaments to be properly regulated by ABPs rather than an inability to polymerize.

Current understanding of molecular mechanism of actin mutations. Actin mutations have also been described in other organisms, including yeast (*Saccharomyces cerevisiae*), fruitfly (*Drosophila melanogaster*), and nematode (*Caenorhabditis elegans*), and mutations have been studied either by *in vitro* transcription translation systems or *in vivo* (reviewed in (90)). A common feature of actin mutants in these organisms is 'antimorphism' or 'dominant negative complementation'. The mutant actin monomers interfere or 'poison' the assembly of wild-type monomers into F-actin. This notion was further supported by the observations from *ACTA1* mutations. The majority of *ACTA1* mutations are *de novo* missense mutations resulting in severe clinical presentations. In addition, three stop codon mutations (TAG > TAT (Tyr), TAG > CAG (Glu), and

TAG > TGG (Trp)), all introducing 47 additional amino acids, also caused severe nemaline myopathy in patients who carry one copy of these mutations (73). Moreover, ten nemaline myopathy patients who carry either compound heterozygous missense and/or deletion mutations (Glu259Val/Leu94Pro and trunc188/Glu259Val, respectively) or homozygous null mutations (p.Arg41X, p.Tyr364fsX1, and p.Asp181fsX10, respectively) have severe myopathy phenotypes whereas all their parents, who carry one copy of these mutations (all resulting in non-functional protein), are unaffected (74, 75). All these suggested that haploinsufficiency is not the case for *ACTA1* and dominant-negative effect (for the majority of *ACTA1* myopathies) or loss of function (for the only 10 cases of recessive *ACTA1* myopathies) is likely the cause of disease. Recent *in vitro* studies of muscle actin variants (skeletal and cardiac actins) have shown that myopathy mutations cause a range of molecular defects in the protein folding pathway. Some variant monomers can incorporate into F-actin in both *in vitro* assays and in cultured cells (91, 92). All these studies led me to test the hypothesis that the protein folding pathway of γ-actin is affected due to these mutations, ultimately causing hearing loss.

Diseases of protein folding and misfolding

A central process in biology is the conversion of genetic information into functional proteins. In this process ribosomes play an essential role as they translate the mRNA into polypeptides; then, newly translated polypeptides must go through a folding process to attain their functional structure. *In vitro* studies

have shown that the amino acid sequence of a polypeptide contains all the necessary information for determining the three-dimensional structure of a given protein (93). However, many proteins in living cells cannot reach this final state themselves and their folding requires the help of a large family of proteins called chaperones (94). Chaperones are a class of proteins whose function is to assist the correct folding of other proteins. There are two general families of chaperones: molecular chaperones, which bind and stabilize unfolded or partially folded proteins thereby preventing these proteins from being degraded, and chaperonins, which directly facilitate protein folding. Amino acid changes caused by genetic mutation as well as cellular events such as chemical or temperature stress can result in protein misfolding. The proteosome together with the chaperones constitute the cellular protein quality control (PQC) system to determine the fate of variant proteins (95-97). The fate of misfolded proteins depends on the nature of the protein, the activity of the PQC system, the cell type and environmental conditions. Protein misfolding may lead to disease through loss-of-function, resulting from the rapid degradation of misfolded proteins; a dominant negative effect, where misfolded proteins interfere with the activity of normal proteins, or gain-of-function, due to toxicity or other novel function of the accumulated misfolded proteins. Some disease conditions can also be caused by a combination of both loss- and gain-of-function (98). However, despite the diversity of pathogenic mechanism these diseases are often collectively called protein misfolding diseases or conformational diseases (98, 99).

For missense mutations, the pathogenic nature of the mutation is not directly evident. In many studies, missense mutations have been shown to impair the propensity of the affected polypeptide to fold into its functional conformation or to decrease the stability of the functional conformation. In human genetic diseases, missense variation accounts for approximately half of all the known gene lesions (100). Due to the lack of knowledge about the folding pathway of most of the known proteins, we do not know how many of these missense variants have folding defects. Fortunately, the folding pathway of actin is well known and it has been used to study the functionality of many actin variants (91, 92, 101).

Actin folding pathway

Actin folding is a complex process and is assisted by at least two cytosolic chaperones: chaperone prefoldin (PFD, also termed GimC, (102)) and chaperonin CCT (chaperonin containing TCP-1, also termed c-cpn or Tric; (103, 104)). Both PFD and CCT are found in archaeabacteria and eukaryotic organisms. Eukaryotic PFD is a heterohexameric protein (~90 kD) composed of six different subunits, whereas its archaeal counterpart contains only two different proteins (two α and four β subunits). The crystal structure of eukaryotic PFD has not been solved; the crystal structure of the archeal PFD resembles a jellyfish, with six α-helical coiled-coil tentacles emanating from a β-barrel body. The tips of the tentacles were proposed to interact with target proteins (105). CCT is a hetero-oligomeric complex (~800 kD) consisting of two back-to-back rings of eight different subunits each (106). Each subunit consists of three

domains: the apical domain, which is responsible for target protein (substrate) interaction, the equatorial domain with the nucleotide binding site, and the intermediate domain, that transfers nucleotide-dependent conformational changes in the equatorial domain to the substrate-binding apical domain (107). Both biochemical and genetic studies have shown that CCT is required for the biogenesis of the major cytoskeletal proteins actin and tubulin (104, 108, 109). There is also evidence that CCT participates in the folding of other proteins including actin-related proteins (ARPs), cofilin/ADF, the heavy meromyosin subunit (HMM), cyclin E, histone deacetylases, CDC20, and proteins with WD40 motifs (110, 111). During actin synthesis, PFD cotranslationally binds and stabilizes the incompletely folded nascent polypeptide. Once synthesis is complete, the actin-PFD complex is thought to form a transient ternary complex with CCT and the non-native actin (partially folded) is transferred to this chaperonin (112). CCT assists in the folding of actin in an ATP-dependent manner and releases it as a fully folded monomer. However, actin binding and release by PFD is ATP-independent. Little is known about how these chaperones recognize the non-native forms of target proteins and the exact folding mechanism of CCT is not yet well understood. Several studies using mutagenesis and peptide array screens have provided evidence that PFD and CCT interact with target proteins through discrete binding determinants, and a multi-step binding transition-release model for CCT-mediated actin folding has been proposed by Neirynck et al. (113). Actin regions at residues 60-79, 170-183, and 194-199 are found to be important for PFD binding. The binding

determinants for CCT are situated at actin residues 30-34, 135-139,170-174, 240-254, 265-274 and 340-349. However, these findings have not been studied *in vivo*. Some interesting findings from the *in vitro* experiments are that the majority of mutants lacking binding determinants for CCT recognition show only delayed CCT release. Actin mutants that are CCT-arrested demonstrate that some regions neighboring the recognition sites are involved in modulating the correct folding or release of actin from CCT.

As described above, at least two actin-containing complexes are formed during the actin folding process. A number of studies have shown that these actin-associated species can be visualized by autoradiography when actin is synthesized *in vitro* as radioactively labeled protein and analyzed by native gel electrophoresis. In the presence of ATP, three labeled species are evident: a fast-migrating band corresponding to released native actin, a slow-migrating band corresponding to actin-CCT complex (~ 800 kD), and an intermediate band corresponding to actin-PFD complex (~150 kD) (112, 114). This method has been widely used for studying the folding pathway of actin variants and forms the basis for my studies.

REFERENCES

1. Goode, B. L. 2006. Srv2/cyclase-associated protein (CAP): a multi-functional recycling center for actin monomers and cofilin. In "*Actin monomer binding proteins*," Editor: P. Lappalainen. *Landes Bioscience*, pp. 45-52.

2. Chen, M., and X. Shen. 2007. Nuclear actin and actin-related proteins in chromatin dynamics. *Curr Opin Cell Biol* 19:326-330.

3. Zheng, X., K. Diraviyam, and D. Sept. 2007. Nucleotide effects on the structure and dynamics of actin. *Biophys J* 93:1277-1283.

4. Belmont, L. D., A. Orlova, D. G. Drubin, and E. H. Egelman. 1999. A change in actin conformation associated with filament instability after Pi release. *Proc Natl Acad Sci U S A* 96:29-34.

5. Graceffa, P., and R. Dominguez. 2003. Crystal structure of monomeric actin in the ATP state. Structural basis of nucleotide-dependent actin dynamics. *J Biol Chem* 278:34172-34180.

6. Rould, M. A., Q. Wan, P. B. Joel, S. Lowey, and K. M. Trybus. 2006. Crystal structures of expressed non-polymerizable monomeric actin in the ADP and ATP states. *J Biol Chem* 281:31909-31919.

7. Otterbein, L. R., P. Graceffa, and R. Dominguez. 2001. The crystal structure of uncomplexed actin in the ADP state. *Science* 293:708-711.

8. Holmes, K. C., D. Popp, W. Gebhard, and W. Kabsch. 1990. Atomic model of the actin filament. *Nature* 347:44-49.

9. Kabsch, W., H. G. Mannherz, D. Suck, E. F. Pai, and K. C. Holmes. 1990. Atomic structure of the actin:DNase I complex. *Nature* 347:37-44.

10. McLaughlin, P. J., J. T. Gooch, H. G. Mannherz, and A. G. Weeds. 1993. Structure of gelsolin segment 1-actin complex and the mechanism of filament severing. *Nature* 364:685-692.

11. Otterbein, L. R., C. Cosio, P. Graceffa, and R. Dominguez. 2002. Crystal structures of the vitamin D-binding protein and its complex with actin: structural basis of the actin-scavenger system. *Proc Natl Acad Sci U S A* 99:8003-8008.

12. Schutt, C. E., J. C. Myslik, M. D. Rozycki, N. C. Goonesekere, and U. Lindberg. 1993. The structure of crystalline profilin-beta-actin. *Nature* 365:810-816.

13. Pollard, T. D., and G. G. Borisy. 2003. Cellular motility driven by assembly and disassembly of actin filaments. *Cell* 112:453-465.

14. Disanza, A., A. Steffen, M. Hertzog, E. Frittoli, K. Rottner, and G. Scita. 2005. Actin polymerization machinery: the finish line of signaling networks, the starting point of cellular movement. *Cell Mol Life Sci* 62:955-970.

15. dos Remedios, C. G., D. Chhabra, M. Kekic, I. V. Dedova, M. Tsubakihara, D. A. Berry, and N. J. Nosworthy. 2003. Actin binding proteins: regulation of cytoskeletal microfilaments. *Physiol Rev* 83:433-473.

16. Goldstein, A. L., E. Hannappel, and H. K. Kleinman. 2005. Thymosin beta4: actin-sequestering protein moonlights to repair injured tissues. *Trends Mol Med* 11:421-429.

17. Low, T. L., S. K. Hu, and A. L. Goldstein. 1981. Complete amino acid sequence of bovine thymosin beta 4: a thymic hormone that induces terminal deoxynucleotidyl transferase activity in thymocyte populations. *Proc Natl Acad Sci U S A* 78:1162-1166.

18. Huff, T., C. S. Muller, A. M. Otto, R. Netzker, and E. Hannappel. 2001. beta-Thymosins, small acidic peptides with multiple functions. *Int J Biochem Cell Biol* 33:205-220.

19. Carlier, M. F., C. Jean, K. J. Rieger, M. Lenfant, and D. Pantaloni. 1993. Modulation of the interaction between G-actin and thymosin beta 4 by the ATP/ADP ratio: possible implication in the regulation of actin dynamics. *Proc Natl Acad Sci U S A* 90:5034-5038.

20. Zarbock, J., H. Oschkinat, E. Hannappel, H. Kalbacher, W. Voelter, and T. A. Holak. 1990. Solution conformation of thymosin beta 4: a nuclear magnetic resonance and simulated annealing study. *Biochemistry* 29:7814-7821.

21. Domanski, M., M. Hertzog, J. Coutant, I. Gutsche-Perelroizen, F. Bontems, M. F. Carlier, E. Guittet, and C. van Heijenoort. 2004. Coupling of folding and binding of thymosin beta4 upon interaction with monomeric actin monitored by nuclear magnetic resonance. *J Biol Chem* 279:23637-23645.

22. Dedova, I. V., O. P. Nikolaeva, D. Safer, E. M. De La Cruz, and C. G. dos Remedios. 2006. Thymosin beta4 induces a conformational change in actin monomers. *Biophys J* 90:985-992.

23. Witke, W. 2004. The role of profilin complexes in cell motility and other cellular processes. *Trends Cell Biol* 14:461-469.

24. Nodelman, I. M., G. D. Bowman, U. Lindberg, and C. E. Schutt. 1999. X-ray structure determination of human profilin II: A comparative structural analysis of human profilins. *J Mol Biol* 294:1271-1285.

25. Paavilainen, V. O., E. Bertling, S. Falck, and P. Lappalainen. 2004. Regulation of cytoskeletal dynamics by actin-monomer-binding proteins. *Trends Cell Biol* 14:386-394.

26. Bertling, E., O. Quintero-Monzon, P. K. Mattila, B. L. Goode, and P. Lappalainen. 2007. Mechanism and biological role of profilin-Srv2/CAP interaction. *J Cell Sci* 120:1225-1234.

27. Chik, J. K., U. Lindberg, and C. E. Schutt. 1996. The structure of an open state of beta-actin at 2.65 A resolution. *J Mol Biol* 263:607-623.

28. Lazarides, E., and U. Lindberg. 1974. Actin is the naturally occurring inhibitor of deoxyribonuclease I. *Proc Natl Acad Sci U S A* 71:4742-4746.

29. Mannherz, H. G., R. S. Goody, M. Konrad, and E. Nowak. 1980. The interaction of bovine pancreatic deoxyribonuclease I and skeletal muscle actin. *Eur J Biochem* 104:367-379.

30. Cook, R. K., W. T. Blake, and P. A. Rubenstein. 1992. Removal of the amino-terminal acidic residues of yeast actin. Studies in vitro and in vivo. *J Biol Chem* 267:9430-9436.

31. Schuler, H., U. Lindberg, C. E. Schutt, and R. Karlsson. 2000. Thermal unfolding of G-actin monitored with the DNase I-inhibition assay stabilities of actin isoforms. *Eur J Biochem* 267:476-486.

32. Thulasiraman, V., R. G. Ferreyra, and J. Frydman. 2000. Monitoring actin folding. Purification protocols for labeled proteins and binding to DNase I-sepharose beads. *Methods Mol Biol* 140:161-167.

33. Morrison, S. S., and J. F. Dawson. 2007. A high-throughput assay shows that DNase-I binds actin monomers and polymers with similar affinity. *Anal Biochem* 364:159-164.

34. Pinder, J. C., and W. B. Gratzer. 1982. Investigation of the actin-deoxyribonuclease I interaction using a pyrene-conjugated actin derivative. *Biochemistry* 21:4886-4890.

35. Speeckaert, M., G. Huang, J. R. Delanghe, and Y. E. Taes. 2006. Biological and clinical aspects of the vitamin D binding protein (Gc-globulin) and its polymorphism. *Clin Chim Acta* 372:33-42.

36. White, P., and N. Cooke. 2000. The multifunctional properties and characteristics of vitamin D-binding protein. *Trends Endocrinol Metab* 11:320-327.

37. Lee, W. M., and R. M. Galbraith. 1992. The extracellular actin-scavenger system and actin toxicity. *N Engl J Med* 326:1335-1341.

38. Verboven, C., I. Bogaerts, E. Waelkens, A. Rabijns, H. Van Baelen, R. Bouillon, and C. De Ranter. 2003. Actin-DBP: the perfect structural fit? *Acta Crystallogr D Biol Crystallogr* 59:263-273.

39. Hubberstey, A. V., and E. P. Mottillo. 2002. Cyclase-associated proteins: CAPacity for linking signal transduction and actin polymerization. *FASEB J* 16:487-499.

40. Fedor-Chaiken, M., R. J. Deschenes, and J. R. Broach. 1990. SRV2, a gene required for RAS activation of adenylate cyclase in yeast. *Cell* 61:329-340.

41. Field, J., A. Vojtek, R. Ballester, G. Bolger, J. Colicelli, K. Ferguson, J. Gerst, T. Kataoka, T. Michaeli, S. Powers, and et al. 1990. Cloning and characterization of CAP, the S. cerevisiae gene encoding the 70 kd adenylyl cyclase-associated protein. *Cell* 61:319-327.

42. Vojtek, A., B. Haarer, J. Field, J. Gerst, T. D. Pollard, S. Brown, and M. Wigler. 1991. Evidence for a functional link between profilin and CAP in the yeast S. cerevisiae. *Cell* 66:497-505.

43. Chaudhry, F., C. Guerin, M. von Witsch, L. Blanchoin, and C. J. Staiger. 2007. Identification of Arabidopsis cyclase-associated protein 1 as the first nucleotide exchange factor for plant actin. *Mol Biol Cell* 18:3002-3014.

44. Moriyama, K., and I. Yahara. 2002. Human CAP1 is a key factor in the recycling of cofilin and actin for rapid actin turnover. *J Cell Sci* 115:1591-1601.

45. Balcer, H. I., A. L. Goodman, A. A. Rodal, E. Smith, J. Kugler, J. E. Heuser, and B. L. Goode. 2003. Coordinated regulation of actin filament turnover by a high-molecular-weight Srv2/CAP complex, cofilin, profilin, and Aip1. *Curr Biol* 13:2159-2169.

46. Bertling, E., P. Hotulainen, P. K. Mattila, T. Matilainen, M. Salminen, and P. Lappalainen. 2004. Cyclase-associated protein 1 (CAP1) promotes cofilin-induced actin dynamics in mammalian nonmuscle cells. *Mol Biol Cell* 15:2324-2334.

47. Mattila, P. K., O. Quintero-Monzon, J. Kugler, J. B. Moseley, S. C. Almo, P. Lappalainen, and B. L. Goode. 2004. A high-affinity interaction with ADP-actin monomers underlies the mechanism and in vivo function of Srv2/cyclase-associated protein. *Mol Biol Cell* 15:5158-5171.

48. Drees, B. L., B. Sundin, E. Brazeau, J. P. Caviston, G. C. Chen, W. Guo, K. G. Kozminski, M. W. Lau, J. J. Moskow, A. Tong, L. R. Schenkman, A. McKenzie, 3rd, P. Brennwald, M. Longtine, E. Bi, C. Chan, P. Novick, C. Boone, J. R. Pringle, T. N. Davis, S. Fields, and D. G. Drubin. 2001. A

protein interaction map for cell polarity development. *J Cell Biol* 154:549-571.

49. Freeman, N. L., Z. Chen, J. Horenstein, A. Weber, and J. Field. 1995. An actin monomer binding activity localizes to the carboxyl-terminal half of the Saccharomyces cerevisiae cyclase-associated protein. *J Biol Chem* 270:5680-5685.

50. Lila, T., and D. G. Drubin. 1997. Evidence for physical and functional interactions among two Saccharomyces cerevisiae SH3 domain proteins, an adenylyl cyclase-associated protein and the actin cytoskeleton. *Mol Biol Cell* 8:367-385.

51. Gerst, J. E., K. Ferguson, A. Vojtek, M. Wigler, and J. Field. 1991. CAP is a bifunctional component of the Saccharomyces cerevisiae adenylyl cyclase complex. *Mol Cell Biol* 11:1248-1257.

52. Gottwald, U., R. Brokamp, I. Karakesisoglou, M. Schleicher, and A. A. Noegel. 1996. Identification of a cyclase-associated protein (CAP) homologue in Dictyostelium discoideum and characterization of its interaction with actin. *Mol Biol Cell* 7:261-272.

53. Baum, B., W. Li, and N. Perrimon. 2000. A cyclase-associated protein regulates actin and cell polarity during Drosophila oogenesis and in yeast. *Curr Biol* 10:964-973.

54. Benlali, A., I. Draskovic, D. J. Hazelett, and J. E. Treisman. 2000. act up controls actin polymerization to alter cell shape and restrict Hedgehog signaling in the Drosophila eye disc. *Cell* 101:271-281.

55. Barrero, R. A., M. Umeda, S. Yamamura, and H. Uchimiya. 2002. Arabidopsis CAP regulates the actin cytoskeleton necessary for plant cell elongation and division. *Plant Cell* 14:149-163.

56. Peche, V., S. Shekar, M. Leichter, H. Korte, R. Schroder, M. Schleicher, T. A. Holak, C. S. Clemen, Y. B. Ramanath, G. Pfitzer, I. Karakesisoglou, and A. A. Noegel. 2007. CAP2, cyclase-associated protein 2, is a dual compartment protein. *Cell Mol Life Sci.*

57. Freeman, N. L., and J. Field. 2000. Mammalian homolog of the yeast cyclase associated protein, CAP/Srv2p, regulates actin filament assembly. *Cell Motil Cytoskeleton* 45:106-120.

58. Rommelaere, H., D. Waterschoot, K. Neirynck, J. Vandekerckhove, and C. Ampe. 2003. Structural plasticity of functional actin: pictures of actin binding protein and polymer interfaces. *Structure* 11:1279-1289.

59. Dodatko, T., A. A. Fedorov, M. Grynberg, Y. Patskovsky, D. A. Rozwarski, L. Jaroszewski, E. Aronoff-Spencer, E. Kondraskina, T. Irving, A. Godzik, and S. C. Almo. 2004. Crystal structure of the actin binding domain of the cyclase-associated protein. *Biochemistry* 43:10628-10641.

60. Vartiainen, M. K., T. Mustonen, P. K. Mattila, P. J. Ojala, I. Thesleff, J. Partanen, and P. Lappalainen. 2002. The three mouse actin-depolymerizing factor/cofilins evolved to fulfill cell-type-specific requirements for actin dynamics. *Mol Biol Cell* 13:183-194.

61. Blondin, L., V. Sapountzi, S. K. Maciver, E. Lagarrigue, Y. Benyamin, and C. Roustan. 2002. A structural basis for the pH-dependence of cofilin. F-actin interactions. *Eur J Biochem* 269:4194-4201.

62. Khaitlina, S. Y. 2001. Functional specificity of actin isoforms. *Int Rev Cytol* 202:35-98.

63. Karakozova, M., M. Kozak, C. C. Wong, A. O. Bailey, J. R. Yates, 3rd, A. Mogilner, H. Zebroski, and A. Kashina. 2006. Arginylation of beta-actin regulates actin cytoskeleton and cell motility. *Science* 313:192-196.

64. Bulinski, J. C. 2006. Cell biology. Actin discrimination. *Science* 313:180-181.

65. Hofer, D., W. Ness, and D. Drenckhahn. 1997. Sorting of actin isoforms in chicken auditory hair cells. *J Cell Sci* 110 (Pt 6):765-770.

66. Prassler, J., S. Stocker, G. Marriott, M. Heidecker, J. Kellermann, and G. Gerisch. 1997. Interaction of a Dictyostelium member of the plastin/fimbrin family with actin filaments and actin-myosin complexes. *Mol Biol Cell* 8:83-95.

67. Shuster, C. B., and I. M. Herman. 1995. Indirect association of ezrin with F-actin: isoform specificity and calcium sensitivity. *J Cell Biol* 128:837-848.

68. Yao, X., C. Chaponnier, G. Gabbiani, and J. G. Forte. 1995. Polarized distribution of actin isoforms in gastric parietal cells. *Mol Biol Cell* 6:541-557.

69. Yao, X., L. Cheng, and J. G. Forte. 1996. Biochemical characterization of ezrin-actin interaction. *J Biol Chem* 271:7224-7229.

70. Tzima, E., P. J. Trotter, M. A. Orchard, and J. H. Walker. 2000. Annexin V relocates to the platelet cytoskeleton upon activation and binds to a specific isoform of actin. *Eur J Biochem* 267:4720-4730.

71. Laing, N. G., N. F. Clarke, D. E. Dye, K. Liyanage, K. R. Walker, Y. Kobayashi, S. Shimakawa, T. Hagiwara, R. Ouvrier, J. C. Sparrow, I. Nishino, K. N. North, and I. Nonaka. 2004. Actin mutations are one cause of congenital fibre type disproportion. *Ann Neurol* 56:689-694.

72. Bookwalter, C. S., and K. M. Trybus. 2006. Functional consequences of a mutation in an expressed human alpha-cardiac actin at a site implicated in familial hypertrophic cardiomyopathy. *J Biol Chem* 281:16777-16784.

73. Wallefeld, W., S. Krause, K. J. Nowak, D. Dye, R. Horvath, Z. Molnar, M. Szabo, K. Hashimoto, C. Reina, J. De Carlos, J. Rosell, A. Cabello, C. Navarro, I. Nishino, H. Lochmuller, and N. G. Laing. 2006. Severe nemaline myopathy caused by mutations of the stop codon of the skeletal muscle alpha actin gene (ACTA1). *Neuromuscul Disord* 16:541-547.

74. Agrawal, P. B., C. D. Strickland, C. Midgett, A. Morales, D. E. Newburger, M. A. Poulos, K. K. Tomczak, M. M. Ryan, S. T. Iannaccone, T. O. Crawford, N. G. Laing, and A. H. Beggs. 2004. Heterogeneity of nemaline myopathy cases with skeletal muscle alpha-actin gene mutations. *Ann Neurol* 56:86-96.

75. Nowak, K. J., C. A. Sewry, C. Navarro, W. Squier, C. Reina, J. R. Ricoy, S. S. Jayawant, A. M. Childs, J. A. Dobbie, R. E. Appleton, R. C. Mountford, K. R. Walker, S. Clement, A. Barois, F. Muntoni, N. B. Romero, and N. G. Laing. 2007. Nemaline myopathy caused by absence of alpha-skeletal muscle actin. *Ann Neurol* 61:175-184.

76. Nunoi, H., T. Yamazaki, H. Tsuchiya, S. Kato, H. L. Malech, I. Matsuda, and S. Kanegasaki. 1999. A heterozygous mutation of beta-actin associated with neutrophil dysfunction and recurrent infection. *Proc Natl Acad Sci U S A* 96:8693-8698.

77. Procaccio, V., G. Salazar, S. Ono, M. L. Styers, M. Gearing, A. Davila, R. Jimenez, J. Juncos, C. A. Gutekunst, G. Meroni, B. Fontanella, E. Sontag, J. M. Sontag, V. Faundez, and B. H. Wainer. 2006. A mutation of beta - actin that alters depolymerization dynamics is associated with autosomal dominant developmental malformations, deafness, and dystonia. *Am J Hum Genet* 78:947-960.

78. Zhu, M., T. Yang, S. Wei, A. T. DeWan, R. J. Morell, J. L. Elfenbein, R. A. Fisher, S. M. Leal, R. J. Smith, and K. H. Friderici. 2003. Mutations in the gamma-actin gene (ACTG1) are associated with dominant progressive deafness (DFNA20/26). *Am J Hum Genet* 73:1082-1091.

79. van Wijk, E., E. Krieger, M. H. Kemperman, E. M. De Leenheer, P. L. Huygen, C. W. Cremers, F. P. Cremers, and H. Kremer. 2003. A mutation in the gamma actin 1 (ACTG1) gene causes autosomal dominant hearing loss (DFNA20/26). *J Med Genet* 40:879-884.

80. Rendtorff, N. D., M. Zhu, T. Fagerheim, T. L. Antal, M. Jones, T. M. Teslovich, E. M. Gillanders, M. Barmada, E. Teig, J. M. Trent, K. H. Friderici, D. A. Stephan, and L. Tranebjaerg. 2006. A novel missense mutation in ACTG1 causes dominant deafness in a Norwegian DFNA20/26 family, but ACTG1 mutations are not frequent among families with hereditary hearing impairment. *Eur J Hum Genet* 14:1097-1105.

81. Petit, C., J. Levilliers, and J. P. Hardelin. 2001. Molecular genetics of hearing loss. *Annu Rev Genet* 35:589-646.

82. Nance, W. E. 2003. The genetics of deafness. *Ment Retard Dev Disabil Res Rev* 9:109-119.

83. Vandekerckhove, J., and K. Weber. 1981. Actin typing on total cellular extracts: a highly sensitive protein-chemical procedure able to distinguish different actins. *Eur J Biochem* 113:595-603.

84. Rybakova, I. N., J. R. Patel, and J. M. Ervasti. 2000. The dystrophin complex forms a mechanically strong link between the sarcolemma and costameric actin. *J Cell Biol* 150:1209-1214.

85. Lloyd, C. M., M. Berendse, D. G. Lloyd, G. Schevzov, and M. D. Grounds. 2004. A novel role for non-muscle gamma-actin in skeletal muscle sarcomere assembly. *Exp Cell Res* 297:82-96.

86. Hanft, L. M., I. N. Rybakova, J. R. Patel, J. A. Rafael-Fortney, and J. M. Ervasti. 2006. Cytoplasmic gamma-actin contributes to a compensatory remodeling response in dystrophin-deficient muscle. *Proc Natl Acad Sci U S A* 103:5385-5390.

87. Hanft, L. M., D. J. Bogan, U. Mayer, S. J. Kaufman, J. N. Kornegay, and J. M. Ervasti. 2007. Cytoplasmic gamma-actin expression in diverse animal models of muscular dystrophy. *Neuromuscul Disord* 17:569-574.

88. Sonnemann, K. J., D. P. Fitzsimons, J. R. Patel, Y. Liu, M. F. Schneider, R. L. Moss, and J. M. Ervasti. 2006. Cytoplasmic gamma-actin is not required for skeletal muscle development but its absence leads to a progressive myopathy. *Dev Cell* 11:387-397.

89. Bryan, K. E., K. K. Wen, M. Zhu, N. D. Rendtorff, M. Feldkamp, L. Tranebjaerg, K. H. Friderici, and P. A. Rubenstein. 2006. Effects of human deafness gamma-actin mutations (DFNA20/26) on actin function. *J Biol Chem* 281:20129-20139.

90. Hennessey, E. S., D. R. Drummond, and J. C. Sparrow. 1993. Molecular genetics of actin function. *Biochem J* 291 (Pt 3):657-671.

91. Vang, S., T. J. Corydon, A. D. Borglum, M. D. Scott, J. Frydman, J. Mogensen, N. Gregersen, and P. Bross. 2005. Actin mutations in hypertrophic and dilated cardiomyopathy cause inefficient protein folding and perturbed filament formation. *FEBS J* 272:2037-2049.

92. Costa, C. F., H. Rommelaere, D. Waterschoot, K. K. Sethi, K. J. Nowak, N. G. Laing, C. Ampe, and L. M. Machesky. 2004. Myopathy mutations in alpha-skeletal-muscle actin cause a range of molecular defects. *J Cell Sci* 117:3367-3377.

93. Anfinsen, C. B. 1973. Principles that govern the folding of protein chains. *Science* 181:223-230.

94. Hartl, F. U., and M. Hayer-Hartl. 2002. Molecular chaperones in the cytosol: from nascent chain to folded protein. *Science* 295:1852-1858.

95. Barral, J. M., S. A. Broadley, G. Schaffar, and F. U. Hartl. 2004. Roles of molecular chaperones in protein misfolding diseases. *Semin Cell Dev Biol* 15:17-29.

96. McClellan, A. J., and J. Frydman. 2001. Molecular chaperones and the art of recognizing a lost cause. *Nat Cell Biol* 3:E51-53.

97. Goldberg, A. L. 2003. Protein degradation and protection against misfolded or damaged proteins. *Nature* 426:895-899.

98. Gregersen, N., P. Bross, S. Vang, and J. H. Christensen. 2006. Protein Misfolding and Human Disease. *Annu Rev Genomics Hum Genet.*

99. Stefani, M. 2004. Protein misfolding and aggregation: new examples in medicine and biology of the dark side of the protein world. *Biochim Biophys Acta* 1739:5-25.

100. Stenson, P. D., E. V. Ball, M. Mort, A. D. Phillips, J. A. Shiel, N. S. Thomas, S. Abeysinghe, M. Krawczak, and D. N. Cooper. 2003. Human Gene Mutation Database (HGMD): 2003 update. *Hum Mutat* 21:577-581.

101. Rommelaere, H., D. Waterschoot, K. Neirynck, J. Vandekerckhove, and C. Ampe. 2004. A method for rapidly screening functionality of actin mutants and tagged actins. *Biol Proced Online* 6:235-249.

102. Geissler, S., K. Siegers, and E. Schiebel. 1998. A novel protein complex promoting formation of functional alpha- and gamma-tubulin. *EMBO J* 17:952-966.

103. Frydman, J., E. Nimmesgern, H. Erdjument-Bromage, J. S. Wall, P. Tempst, and F. U. Hartl. 1992. Function in protein folding of TRiC, a cytosolic ring complex containing TCP-1 and structurally related subunits. *EMBO J* 11:4767-4778.

104. Gao, Y., J. O. Thomas, R. L. Chow, G. H. Lee, and N. J. Cowan. 1992. A cytoplasmic chaperonin that catalyzes beta-actin folding. *Cell* 69:1043-1050.

105. Siegert, R., M. R. Leroux, C. Scheufler, F. U. Hartl, and I. Moarefi. 2000. Structure of the molecular chaperone prefoldin: unique interaction of multiple coiled coil tentacles with unfolded proteins. *Cell* 103:621-632.

106. Rommelaere, H., M. Van Troys, Y. Gao, R. Melki, N. J. Cowan, J. Vandekerckhove, and C. Ampe. 1993. Eukaryotic cytosolic chaperonin contains t-complex polypeptide 1 and seven related subunits. *Proc Natl Acad Sci U S A* 90:11975-11979.

107. Villebeck, L., M. Persson, S. L. Luan, P. Hammarstrom, M. Lindgren, and B. H. Jonsson. 2007. Conformational rearrangements of tail-less complex polypeptide 1 (TCP-1) ring complex (TRiC)-bound actin. *Biochemistry* 46:5083-5093.

108. Chen, X., D. S. Sullivan, and T. C. Huffaker. 1994. Two yeast genes with similarity to TCP-1 are required for microtubule and actin function in vivo. *Proc Natl Acad Sci U S A* 91:9111-9115.

109. Vinh, D. B., and D. G. Drubin. 1994. A yeast TCP-1-like protein is required for actin function in vivo. *Proc Natl Acad Sci U S A* 91:9116-9120.

110. Melki, R., I. E. Vainberg, R. L. Chow, and N. J. Cowan. 1993. Chaperonin-mediated folding of vertebrate actin-related protein and gamma-tubulin. *J Cell Biol* 122:1301-1310.

111. Camasses, A., A. Bogdanova, A. Shevchenko, and W. Zachariae. 2003. The CCT chaperonin promotes activation of the anaphase-promoting complex through the generation of functional Cdc20. *Mol Cell* 12:87-100.

112. Vainberg, I. E., S. A. Lewis, H. Rommelaere, C. Ampe, J. Vandekerckhove, H. L. Klein, and N. J. Cowan. 1998. Prefoldin, a chaperone that delivers unfolded proteins to cytosolic chaperonin. *Cell* 93:863-873.

113. Neirynck, K., D. Waterschoot, J. Vandekerckhove, C. Ampe, and H. Rommelaere. 2006. Actin interacts with CCT via discrete binding sites: a

binding transition-release model for CCT-mediated actin folding. *J Mol Biol* 355:124-138.

114. Hynes, G. M., and K. R. Willison. 2000. Individual subunits of the eukaryotic cytosolic chaperonin mediate interactions with binding sites located on subdomains of beta-actin. *J Biol Chem* 275:18985-18994.

CHAPTER 2

EXAMINING THE FOLDING AND STABILITY OF γ-ACTIN VARIANTS *IN VITRO* AND IN CULTURED CELLS

ABSTRACT

Recent work from our laboratory and others identified six different point mutations in the highly conserved amino acids of cytoplasmic γ-actin, which were shown to cause similar nonsyndromic, autosomal dominant, progressive, sensorineural hearing loss in different families. Sensorineural hearing loss (SNHL) is the most common type of hearing loss which is caused by a defect in the inner ear. The finding that mutations in this highly conserved and ubiquitously expressed cytoplasmic actin caused only hearing loss was unexpected. We hypothesize that γ-actin performs specific roles in the ear and the different mutations may cause conformational changes that interfere with a range of actin-related functions. I examined the actin protein folding pathway, molecular interaction of actin, and protein stability using a combination of *in vitro* cell free expression system and cell culture system. All six actin mutants behaved like wild-type actin in most of the assays, in which they folded properly, copolymerized with wild-type actin, bound to selected actin-binding proteins (thymosin β4, profilin I, DNase I and vitamin D-binding protein), and were stable when expressed as N-terminally tagged chimeric proteins in COS-7 cells. Immunostaining and confocal microscopy analyses demonstrated that all tagged actin mutants were incorporated into normal actin structures. However, these mutations did cause different conformational changes of the native structure of actin which resulted in the abnormal CAP (cyclase-associated protein) binding observed for the mutants in the present study. CAP is required for proper

organization and rapid remodeling of cellular actin networks. The altered CAP binding could affect the turnover or remodeling of actin cytoskeleton networks during maintenance of normal structures and/or repairing damaged structures caused by aging and noise. A slightly elevated or reduced regulation of actin assembly or disassembly could be significant enough to cause hair cell dysfunction leading to progressive hearing loss. The presented results are not unexpected as γ-actin is ubiquitous but predominantly expressed in the auditory hair cells.

INTRODUCTION

Hearing loss is the most common sensory disorder in humans. It can be caused by infections, drugs, noise, aging and genetic factors (accounts for at least 60%). The majority (~90%) of hearing impairment is due to a defect in the inner ear where the mechanosensor hair cells are located. Much of the function of the inner ear relies on these cells with a specialized structure: namely a staircase arrangement of hair-like actin bundles called stereocilia project from the apical surface of the cell body. Stereocilia are responsible for transduction of the mechanical stimuli into electrical signals, which is a crucial event in the normal hearing process. Thus, hair cell function is highly dependent on the proper functioning of the actin cytoskeleton, including actin bundles in stereocilia and actin filament networks within the cell body (a dense gel-like network in cuticular plate below apical surface, antiparallel filaments in the adherens junction and actin structure in the basolateral region). To maintain the structural integrity and proper function of these actin structures, many actin-binding proteins interplay with actin monomers and/or filaments (1). Thymosin β4 and profilin bind G-actin to maintain a pool of ATP-G-actin ready for polymerization at the fast-growing end while depolymerization factor cofilin/ADF disassociates ADP-G-actin from the opposite end of filaments (slow-growing end). Recent evidence has shown that CAP works together with cofilin and profilin to regulate turnover and remodeling of actin cytoskeleton networks (2-5). Hence dysfunction of either actin or actin-binding proteins could result in hearing loss. Indeed, several genes

coding for actin-binding proteins have been identified which are responsible for different types of hearing loss, such as whirlin, harmonin, espin, cadherin, myosin VIIa, myosin XV, myosin VI (reviewed in (6)). We and others identified mutations in the cytoplasmic γ-actin gene (*ACTG1*) associated with dominant progressive senserineural hearing loss (DFNA20/26) (7-9).

Cytoplasmic γ-actin is the predominant actin isoform in auditory hair cells. There are six actin isoforms in humans including four muscle actins (skeletal α-actin, vascular α-actin, cardiac α-actin, enteric γ-actin) and two non-muscle actins (cytoplasmic β-actin and γ-actin). They are highly conserved through evolution and share high homology. For instance, cytoplasmic β-actin and γ-actin differ from each other by only four amino acids at the N-terminus. β-actin is predominantly expressed in most cells whereas γ-actin is the predominate isoform only in intestinal epithelial cells and auditory hair cells where it is found in stereocilia, the cuticular plate, and adherens junctions (10).

The maturation of actin protein is a unique and complicated process, in which two chaperon proteins, chaperon prefoldin and chaperonin CCT, are required to assist the folding (11-13). It is thought that the newly synthesized polypeptide is transferred by prefoldin from the ribosome to chaperonin CCT, which directly assists the folding and releases the folded native actin. Correctly folded actin monomers can polymerize into filamentous actin to perform varieties of biological functions. During the actin folding process, at least two actin-containing complexes are formed, prefoldin-actin and CCT-actin. A number of studies have shown that these actin-associated species can be visualized by

autoradiography when actin is synthesized *in vitro* as radioactively labeled protein and analyzed by native gel electrophoresis. This method has been widely used for studying the folding pathway of actin variants. For instance, myopathy mutations in α-skeletal-muscle actin and cardiomyopathy variations in α-cardiac actin have been shown to cause a range of defects in protein folding, copolymerization and molecular interactions (14, 15).

This study investigates the folding pathway and stability of γ-actin variants causing dominant hearing loss. Using an *in vitro* transcription and translation system, I examined the actin variants for the following aspects: the folding pathway, the ability to copolymerize with wild-type actin, and the ability to bind selected actin monomer binding proteins. I also examined the protein and mRNA levels of mutant actins expressed as an N-terminally Myc-tagged version in transiently transfected COS-7 cells. In addition, I attempted to estimate the half-life of variant actin proteins using a cycloheximide (CHX) chase assay. Finally, an immunostaining and confocal microscopy analysis of transfected cells was applied to test if the actin variants could incorporate into normal actin filaments. Overall, only altered CAP binding of actin variants was observed, whereas the rest of results showed no differences between wild-type actin and mutants. Although the molecular basis for this finding is not fully understood, I propose that altered CAP binding ability is directly involved in the development of hearing loss.

MATERIALS AND METHODS

Construction of the γ-actin mutants

C-terminal Flag-tagged actin constructs (pCMV-Tag 4 vector, Stratagene). These constructs were used for the preliminary expression tests and immunofluorescence microscopy in cell culture. The coding sequence of γ-actin (*ACTG1)* was obtained using the IMAGE clone 4855463 (Genbank BC015005) as template in a PCR reaction using Pfu Turbo polymerase from Stratagene. The forward primer contains a *BamHI* site and an optimized Kozak sequence (CCACCATGG), and the reverse primer contains an *XhoI* site substituting the stop codon. The PCR product was purified and ligated into the *BamHI* / *XhoI* site of the pDsRed-Monomer-N1 vector (Clonetech), which was used for other studies and contains the same restriction sites as the pCMV-Tag4 vector. To clone the wild-type actin and six mutants into this vector, I first introduced all six mutations into the plasmid pDsRed-monomer-N1-WT actin using QuickChange Site-Directed Mutagenesis (Stratagene), then sequenced the insert to confirm the mutagenesis and the absence of PCR-introduced errors. Finally, the inserts were moved into the pCMV-Tag4 vector.

Non-tagged actin constructs (pcDNA3.1 vector, Invitrogen). These constructs were made for *in vitro* expression of actin mutants. The pcDNA3.1 vector has been widely used and contains the bacterio phage T7 promoter, which is needed for *in vitro* transcription. This vector also has *BamHI* and *XhoI* sites. Thus, the

same forward primer and a new reverse primer bearing the original 3′ end of actin sequence (with stop codon) plus an *XhoI* site were used for PCR. The purified products of wild-type actin were cloned into the pGEM-T-easy vector (Promega) which is designed especially for cloning PCR products. After confirming the plasmids by sequencing analysis, site-directed mutagenesis was performed to introduce each mutation of γ-actin into pGEM-T-easy constructs. The inserts were verified by sequencing and transferred into the pcDNA3.1 vector. Considering the γ-actin mutations may have very subtle affects on protein folding and binding capacity, I also engineered an *ACTA1* (α-skeletal muscle actin) mutation E259V into γ-actin. This mutation affects protein folding and lacks the ability to bind ABPs (14). The amino acid E259 is conserved between *ACTA1* and γ-actin.

N-terminal Myc-tagged actin constructs (pcDNA3.1vector, Invitrogen). The Myc-tag was introduced into the pcDNA3.1-WT actin construct as a linker (Table 1) at *KpnI* and *BamHI* sites. Briefly, 100 pmol of each primer were mixed in hybridization buffer (10 mM TrisHcl, 2 mM $MgCl_2$, 50 mM Nacl and 1 mM EDTA) and incubated at 90°C for 5 minutes, followed by slow cooling at room temperature. The double-stranded DNA fragment (linker) was then digested with *KpnI* and *BamHI*, and the purified product was ligated into pcDNA3.1-WT construct. Once the pcDNA 3.1-Myc-WT plasmid was verified by sequencing the full insert, mutant actin constructs were made by excision of the wild-type

sequence with *BamHI* and *XhoI* and replacing it with mutant actins from non-tagged constructs.

N-terminal EGFP-tagged actin constructs (pEGFP-Actin vector, Clontech). The pEGFP-Actin vector contains β-actin at clone sites *XhoI* and *BamHI*. The EGFP-tagged γ-actin was made by excision of β-actin and replacing it with γ-actin coding sequence amplified by PCR as described earlier. Mutant actin constructs were made by site-directed mutagenesis PCR. All clones were verified by sequencing the entire open reading frames.

Primers used for cloning, mutagenesis PCR, linker and sequencing analyses in this study are listed in Table 2-1.

Native gels. Two different native gels were used in this study. The native gel according to Safer et al. (16) was used for most of the examinations, including time course experiments, band shift assays, and super-shift experiments. The composition and running buffer of safer gels were summarized in Table 2-2. The other native gel according to Hansen et al. (17) was used only for analyzing prefoldin-actin complex, and the composition and running buffers were listed in Table 2-3. Both Table 2-2 and -3 were adapted and modified from tables created by Rommelaere et al. (18).

TABLE 2-1. Primers used in this study

Purpose	Primers[a,b]	
Plasmid construction		
pCMV-Tag4	For:	CGGGATCCACCATGGAAGAAGAGATCGC
	Rev:	GCCTCGAGATAGAAGCATTTGCGGT
pGEM-T easy &	For:	CGGGATCCACCATGGAAGAAGAGATCGC
pcDNA 3.1	Rev:	GCCTCGAGTTAGAAGCATTTGCGGT
pEGFP	For:	GCCTCGAGCTATGGAAGAAGAGATCGC
	Rev:	CGGGATCCTTAGAAGCATTTGCGGTGG
Myc tag linker to pcDNA3.1	For:	CACCATGGAGCAGAAACTCATCTCTGAA -GAGGATCTGG
	Rev:	GATCCCAGATCCTCTTCAGAGATGAGTTT -CTGCTCCATGGTGGTAC
Mutagenesis PCR		
T89I	For:	ATCTGGCACCACA**T**CTTCTACAACGAGC
	Rev:	GCTCGTTGTAGAAG**A**TGTGGTGCCAGA
K118M	For:	CCAACAGAGAGA**T**GATGACTCAGAT
	Rev:	ATCTGAGTCATC**A**TCTCTCTGTTGG
P264L	For:	CGCTGTTCCAGC**T**TTCCTTCCT
	Rev:	AGGAAGGAA**A**GCTGGAACAGCG
T278I	For:	CACGAGACCA**T**CTTCAACTCCATC
	Rev:	GATGGAGTTGAAG**A**TGGTCTCGTG
P332A	For:	TCAAGATCATCGCA**G**CCCCAGAGC
	Rev:	GCTCTGGGG**C**TGCGATGATCTTGA
V370A	For:	CCTCCATCG**C**CCACCGCAAATGCTT
	Rev:	AAGCATTTGCGGTGG**G**CGATGGAGG
E259V	For:	TTCCGGTGTCCGG**T**GGCGCTGTT
	Rev:	AACAGCGCC**A**CCGGACACCGGAA
Sequencing insert	For:	AGGCTACAGCTTCACCACCA
	Rev:	GTGGCCATCTCCTGCTCGAA
Northern Blotting		
3'UTR probe	For:	TAGTTGCCAGCCATCTGTTG
	Rev:	CAGCATGCCTGCTATTGTCT
GFP probe	For:	AAGTTCAGCGTGTCCGGCGA
	Rev:	CTCCAGCAGGACCATGTGAT

[a] Location of restriction sites are underlined
[b] The mutated bases are highlighted in bold

Table 2-2. Safer gel composition and running conditions

For two mini gels	4.5%	7.5%	10%	13%
10 x tris/glysine (250 mM Tris/1.94 M glycine)	1 ml	1 ml	1 ml	1 ml
30% acrylamide	1.5 ml	2.5 ml	3.3 ml	4.3 ml
2% bis-acrylamide	0.6 ml	1 ml	1.3 ml	1.7 ml
H2O	6.77 ml	5.37 ml	4.27 ml	4.27 ml
100 mM ATP (as needed)	20 µl	20 µl	20 µl	20 µl
10% APS	100 µl	100 µl	100 µl	100 µl
TEMED	10 µl	10 µl	10 µl	10 µl

Running buffer: 25 mM Tris, 194 mM glycine, 200 µM ATP (if required)
The final pH at 4°C will be 8.7 (adjusting the pH is not necessary)

Running conditions:

prerun: 1 hour at 4°C and 175 volts

run: at 4°C and 175 volts till the haemoglobin reaches one third of the gel

Table 2-3. Hansen gel composition and running conditions

For four mini gels	6%	13%
30% acrylamide	4 ml	7.52 ml
2% bis-acrylamide	1.875 ml	3.525 ml
1.5 M 6-aminocaproic acid, 150 mM BisTris, pH 7	7 ml	6 ml
H2O	8.025 ml	0.255 ml
glycerol		3.6 ml
10% APS	90 µl	60 µl
TEMED	9 µl	6 µl

Running buffer:
Anode bufer: 50 mM BisTris, pH 7
Cathode buffer: 50 mM Tricine, 15 mM BisTris, pH 7

2X loading buffer: 100 mM BisTris pH 7, 10% glycerol, 4 mM glutathione, 2 mM methionine, 2 mM cysteine and spatula point Ponceau S

Running conditions: 20 minutes at 50 volts (± 5 mA) at 4°C, remaining time at 150 volts (13 mA) till red front reaches the bottom of the gel

Expression of actin mutants *in vitro*. Wild-type and mutant γ-actins were expressed as ^{35}S-labeled proteins in *in vitro* transcription and translation reactions using reticulocyte lysate (Cat# L-4610, Promega) according to the manufacturer's instructions. Briefly, 0.5 μg of pcDNA3.1-actin plasmid DNAs and 10 μCi of ^{35}S-methionine (Amersham Biosciences) were used in a 25 μl reaction. After incubation at 30°C for 60 minutes, 3 μl of reaction products were analyzed on 10% sodium dodecyl sulfate (SDS)-polyacrylamide gel electrophoresis (PAGE) (19) to determine the total amount of expressed protein, and on non-denaturing (native) gels either with or without 200 μM ATP (16) to determine the amount of ^{35}S-actin in the various complexes. The native gels were pre-run in 25 mM Tris/194 mM glycine for one hour at 175 volts at 4°C in a cold room. After the samples were loaded, the gels were run at the same voltage (175 V) until the haemoglobin reaches one third of the gel (18). The gels were then fixed in fixing solution (50% methanol, 10% glacial acetic acid) for 30 min, followed by soaking in drying solution (7% Methonal, 7% glacial acetic acid and 1% glycerol) for 5 min, and then dried in vacuum dryer at 80°C for 30min. The radio-labeled protein products were analyzed by phosphor imaging (Typhoon 9200 variable mode imager, Amersham Biosciences) and the Image Quant software package.

Band shift assays with actin-binding proteins (ABPs). All ABPs examined in this study were purchased commercially. DNase I was ordered from Worthington, vitamin D-binding protein (VDBP) from Calbiochem. Profilin I was purchased from Cytoskeleton Inc and thymosin β4 from BACHEM. I performed

this assay by following a standard protocol (18). Briefly, I µl of each ABP was added to 3 µl of an *in vitro* transcription and translation reaction. After one minute incubation at room temperature, the mixture was analyzed on 10% non-denaturing gels with 200 µM ATP. Taking the protocol as a reference, I first started by doing a concentration series to determine the minimal amount of each ABP needed to cause a band shift of wild-type γ-actin. The final concentration of the respective actin-binding proteins was 2 µM for DNase I, 1 µM for VDBP, 7.5 µM for profilin I, and 14.5 µM for thymosin β4.

Time course experiments. In this study, two sets of time course experiments were performed. The first set was designed to determine the time needed for maximum production of mature actins. Fifty microliters of an *in vitro* transcription and translation reaction of wild-type actin was performed at 30°C. Three microliters of the reaction were taken at 10 minutes intervals up to 120 minutes and analyzed on a native gel with 200 µM ATP followed by autoradiography. The amount of CCT-bound and released actin for each time point was plotted on a graph. The second set of time course experiments was designed to examine if the mutant has prolonged interaction with CCT. After 6 minutes incubation of an *in vitro* reaction, an excess of cold methionine (1 mM final concentration) was added. Aliquots of 5 µl were taken at 6, 9, 12, 15, 18, 21, 25, 30, 50 and 60 minutes after chasing and put on ice to stop the reaction. 3 µl was analyzed on a native gel (4.5% - 7.5% discontinuous gel) with 200 µM ATP to quantify the amount of CCT-bound and released actin. One microliter was analyzed on a

SDS-PAGE gel (4% stacking and 10% separating) to quantify the total amount of actin produced at each time point. The relative amount of CCT-bound and released actin for each time point was plotted on a graph.

Copolymerization assays. This assay was done by following the protocol of Rommelaere et al. (18). Briefly, *in vitro* transcription and translation reactions of wild-type or mutant γ-actin was performed in a total of 26.5 µl for 60 minutes at 30°C. After the reaction, 1 µl of the sample was removed to analyze the yield of the protein and the remaining 25 µl of the sample was centrifuged at 25 psi (95,000 rpm) for 20 minutes in a Beckman airfuge to remove aggregates (resuspended in 50 µl Laemmli buffer and saved for analysis). To the supernatant, 25 µl of 12 µM non-muscle actin (Cytoskeleton Inc.) in G-buffer (2 mM TrisHcl, pH 8, 0.2 mM $CaCl_2$, 0.5 mM DTT, 0.2 mM ATP) was added. Polymerization was induced for 2 hours at room temperature by adding 1.6 µl of 3 M KCl and 0.5 µl 100 mM $MgCl_2$ (final concentration of 100 mM and 1 mM, respectively, F-buffer conditions) . The actin filaments (F-actin) were pelleted by centrifugation at 25 psi for 20 minutes. The supernatant (Sn1, 50 µl) that contains the unpolymerized actin was removed and saved for analysis. The pellet (P1) was washed gently with G-buffer and resuspended in 80 µl G-buffer for an overnight depolymerization at 4°C. A second round of polymerization was induced for 2 hours. F-actin was again centrifuged at 25 psi for 20 minutes, and supernatant 2 (Sn2, 80 µl) was removed from the final pellet (P2) that contains the F-actin and resuspended in 50 µl Laemmli buffer. Aggregates (2 µl),

supernatant 1 (2 µl) and 2 (10 µl), and the final pellet (10 µl) were analyzed on a 10% sodium dodecyl sulfate (SDS) gel followed by autoradiography and Coomassie brilliant blue (Sigma) staining (for Sn1and 2 and P2). The total amount of ^{35}S-labeled actin in each fraction was analyzed using phosphorimaging and the ImageQuant software. The percentage of actin in each fraction is the amount in each fraction divided by the total amount *in vitro* synthesized actin. All wild-type and mutant actins were analyzed four times.

Cell culture and transfection. COS-7 cells (green monkey kidney cells) were maintained in Dulbecco's modified Eagle's medium (DMEM, cat# 10313-021, Gibco BRL) supplemented with 10% fetal bovine serum (Gibco BRL) and 4 mM L-glutamine (Gibco BRL) at 37°C with constant 5% CO_2 humidified atmosphere. Cells were transiently transfected by the use of FuGene 6 reagent (3 µl per one microgram of plasmid) according to the manufacturer's instruction (Roche) and were harvested 30 hours after transfection. The total amount of plasmid used for a 60 mm diameter dish was 4 µg. The ratio of co-transfected wild-type or mutant actin to control vector (pEGFP-C1) was 9:1.

Northern blotting. Total RNAs were isolated from transfected cells using TRizol reagent (Invitrogen) according to the manufacturer's instruction. Five micrograms of each RNA sample was resolved in a 1% formaldehyde-agarose gel and then transferred to a Hybond-N membrane (Stratagene) by standard techniques. The membranes were hybridized with a ^{32}P-labeled probe in a

formamide-containing solution (6X SSC, 5X Denhardt's solution, 100 µg/ml herring sperm DNA, 25 mM sodium phosphate, pH 6.5, 50% of formamide and 5% Dextran sulfate) at 42°C for overnight, washed to high stringency in 0.5 x SSC / 0.1% SDS at 65°C and then subjected to autoradiography. Hybridization probes were prepared using a Random Primers DNA Labeling System (Invitrogen) with incorporation of α-[^{32}P] dCTP (PerkinElmer) and purified using CHROMA spin columns (Cat# K1302-1) from Clontech. To avoid non-specific probing with actin homologues and other actin isoforms (highly conserved), the probe for Myc-tagged γ-actins was PCR amplified from the DNA sequence (194 bps) of 3′ UTR after the stop codon of the Myc-actin fusion transcript from the pcDNA3.1 vector. The EGFP probe was also a PCR fragment (591 bps) of EGFP coding sequence. The amount of actin and EGFP transcripts were analyzed using ImageJ software (NIH), and the relative number of actin transcripts were normalized to EGFP transcripts.

Western blotting. COS-7 cells cotransfected with Myc-tagged actin (wild-type and mutants) plasmid (3.6 µg) and pEGFP-C1 plasmid (0.4 µg) were harvested using RIPA buffer (Upstate) supplemented with a complete protease inhibitor mixture tablet (Roche). Protein concentrations were determined using a Bio-Rad protein assay kit (Bio-Rad) with bovine serum albumin as the standard. Five micrograms of each protein sample was used for standard10% SDS-PAGE with the buffer described by Laemmli (19). Separated proteins were transferred to PVDF (polyvinylidene difluoride) membrane (Bio-Rad) using standard

transferring systems (Bio-Rad). The membranes were blocked in 5% non-fat milk-0.05% tween 20-1X PBS (Invitrogen) for one hour, then incubated with a polyclonal anti-Myc antibody (Abcam) or anti-EGFP antibody (Clontech) overnight at 4°C, followed by incubation with a HRP-conjugated anti-rabbit antibody for one hour at room temperature. The immunodetection of proteins was performed using the ECL western blotting detection system (Amersham Biosciences/GE). Quantitation analyses were done using ImageJ software (NIH).

Protein stability assay. To measure the rate of degradation of wild-type and mutant actin proteins, a cycloheximide (CHX) chase analysis was performed. COS-7 cells at ~ 50% confluence (3 x10^5 cells were seeded one day before) on a 60 mm diameter dish were transfected with 2 µg of Myc-tagged actin constructs using FuGene 6 reagent (Roche). After 24 hours of incubation, cells were treated with 20 µg of CHX/ml to prevent further protein synthesis. Whole-cell extracts from samples taken at different time points were prepared in 200 µl of RIPA lysis buffer (Upstate) with protease inhibitors (Roche) (one tablet per 7-9 ml lysis buffer) by following the manufacturer's instructions. The amount of wild-type and mutant γ-actin proteins were determined by western blotting with anti-Myc antibody to probe for transfected γ-actin and anti-γ-actin antibody to probe for both the transfected and endogenous γ-actins.

Immunofluorescence and confocal microscopy. COS-7 cells plated on glass coverslips in a 6-well plate were transfected with 1 µg of C-terminal Flag-tagged

actin constructs, N-terminally Myc-tagged, and equal amounts of N-terminally EGFP-tagged wild-type actin (0.5 µg) and N-terminally Myc-tagged mutants (0.5 µg), respectively. After 30 hours of incubation, cells were washed twice in PBS and fixed with 4% paraformaldehyde (PFA, Electron Microscopy Sciences) for 20 minutes at room temperature. Cells were then washed in PBS and permeabilized with 0.1% Triton X-100 (Sigma) in PBS for 5 minutes, and blocked in 1% bovine serum albumin (BSA, Cat# 15260, Gibco BRL) in PBS for 20 minutes. Cells were incubated with anti-Myc antibody (Abcam), or anti-Flag antibody (Sigma) for one hour at room temperature followed by a Cy3 anti-rabbit secondary antibody (Cat# C2306, Sigma) and Alexa Fluor 488 phalloidin (Molecular Probes, Invitrogen) for 30 minutes. There was no phalloidin staining in the case of cotransfection with EGFP-tagged wild-type and Myc-tagged mutants. DAPI (4′, 6′-diamidino-2-phenylindole, Invitrogen) was used as a nuclear counterstain. Finally, coverslips were rinsed, dried completely and mounted onto a slide with anti-fade mounting reagent (Cat# 170-3140, Bio-Rad). Fluorescently labeled cells were examined with an Olympus FluoView 1000 confocal laser scanning microscope using a 60X PlanApo (NA1.42) objective. At least two independent experiments were performed for each transfection design. An average of 50 cells were examined for each slide and 3-5 images were documented per mutant.

RESULTS

Actin variants folded properly but with altered CAP binding ability.

It is known that actin polypeptide must fold into its native structure to perform biological functions both *in vitro* and *in vivo* (13, 20). I studied the folding pathway of wild-type and six mutant γ-actin polypeptides and an engineered control mutant using a cell-free transcription and translation system. The wild-type and variant actins were expressed in the presence of [^{35}S]methionine in reticulocyte lysates, which contain the actin folding machinery: prefoldin and CCT (13, 20, 21) as well as actin-binding protein CAP (22). A non-folding variant E259V identified in the skeletal actin gene (14) was used as a control for this experiment and also for all other *in vitro* and cell culture experiments in this study. This mutant did not have any biological function due to its inability to fold properly.

A time course experiment was performed to determine the optimal reaction time for *in vitro* synthesis of wild-type actin. Fifty microliters of the *in vitro* reaction were incubated at 30°C for up to 2 hours. Aliquots of 3 µl were taken every ten minutes for the first 120 minutes. Samples from each time point were separated on native polyacrylamide gel electrophoresis (PAGE) and visualized by phosphorimaging as shown in Fig. 2-1A. The samples showed a fast-migrating band corresponding to released native actin, a slow-migrating band corresponding to the actin-CCT complex, and an intermediate band corresponding to the actin-PFD complex. I found that the *in vitro* reaction

Figure 2-1: Time course experiment to determine the *in vitro* reaction time. (**A**) Fifty microliters of an *in vitro* transcription and translation reaction for wild-type actin was performed at 30°C. Three microliters of the reaction were taken at 10 minutes intervals up to 120 minutes and analyzed on a native gel with 200 μM ATP followed by autoradiograph. (**B**) The amount of CCT-bound and released actin for each time point was plotted on a graph.

A

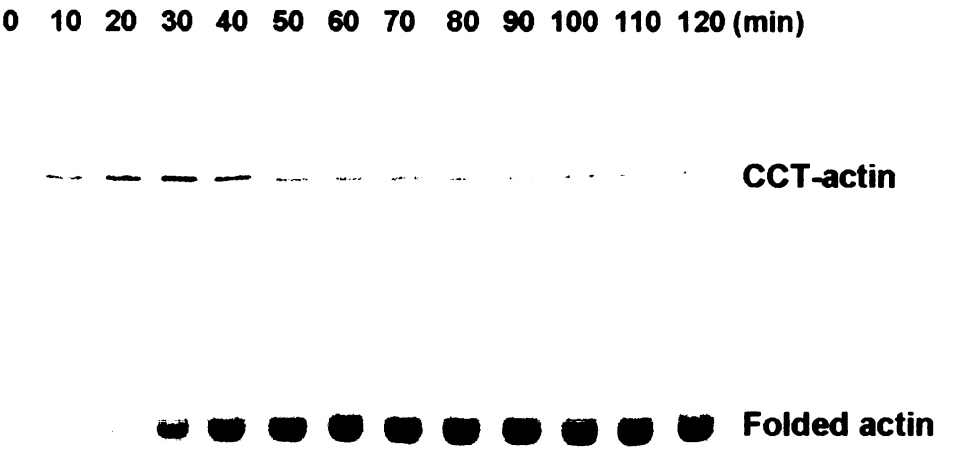
0 10 20 30 40 50 60 70 80 90 100 110 120 (min)
CCT-actin
Folded actin

B

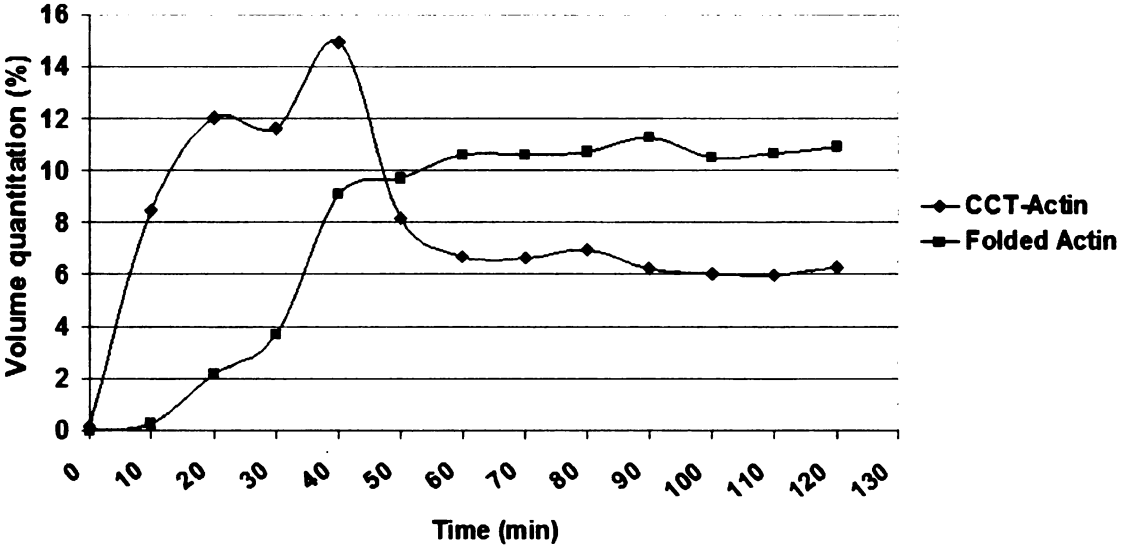
Volume quantitation (%)
16
14
12
10
8
6
4
2
0
0 10 20 30 40 50 60 70 80 90 100 110 120 130
Time (min)
CCT-Actin
Folded Actin

reached a maximum production of folded actin and stable CCT-associated state between 40 and 50 minutes (Fig. 2-1B) and this state was constant up to 2 hours. Thus 60 minutes of incubation was used for all *in vitro* transcription and translation reaction performed in this study.

I then examined if the mutant actin peptides were able to fold properly, be released from CCT and PFD, and associate with CAP. The ^{35}S-labeled wild-type and variants (including control E259V, hereafter the variants include this control) were analyzed by both SDS-PAGE and native PAGE. SDS-PAGE was used to determine the total production of proteins, which showed a single band of 42 kDa with similar intensity for the wild-type and all actin variants (data not shown), indicating homogeneous production of the polypeptides for all constructs. The native PAGE was run in the presence and absence of ATP, and visualized by phosphorimaging. In the presence of ATP (Fig. 2-2A), as described above, of six actin variants, five had similar migrating patterns as wild-type actin while the released variant K118M displayed a sharp and relative fast-migrating band corresponding to the native form. In the absence of ATP, another slow-migrating band corresponding to CAP-actin was observed below the CCT-actin band (Fig. 2-2B), and interestingly the migrating patterns of some variants have changes compared to that exhibited from the native PAGE in the presence of ATP (Fig. 2-2A). For instance, the released variants of P264L and P332A displayed a diffuse, relative slowly migrating band while the migration pattern for the rest of variants remained unchanged, implying that P264L and P332A mutations might cause differential conformational changes when compared to the native proteins. More

Figure 2-2: γ-Actin mutants behaved differently on native gels. Wild-type and mutant actins were produced as ^{35}S-labeled proteins by *in vitro* transcription and translation reaction using reticulocyte lysate. The radioactively labeled products were separated on native polyacrylamide gels with or without ATP and visualized by autoradiography. All mutants folded and were released from CCT. (**A**) On the native gel with ATP, almost all mutant actins behaved like wild-type actin except the folded K118M mutant, which displayed a sharper band indicating a possible uniform and/or compact structure. (**B**) On the native gel without ATP, mutant actins showed different levels of association with CAP. The T89I and V370A mutants showed significant reduction in binding to CAP while the P264L and P332A mutants showed relatively increased binding to CAP compared to wild-type actin. In addition, the released P264L and P332A mutant proteins displayed diffuse migration patterns, which indicate they might have unstable structures. The folded K118M retained the same migration pattern on native gel without ATP as on the native gel with ATP. The E259V mutant was used as a negative control which did not fold and remained bound to CCT and PFD. These two gels represent four independent experiments.

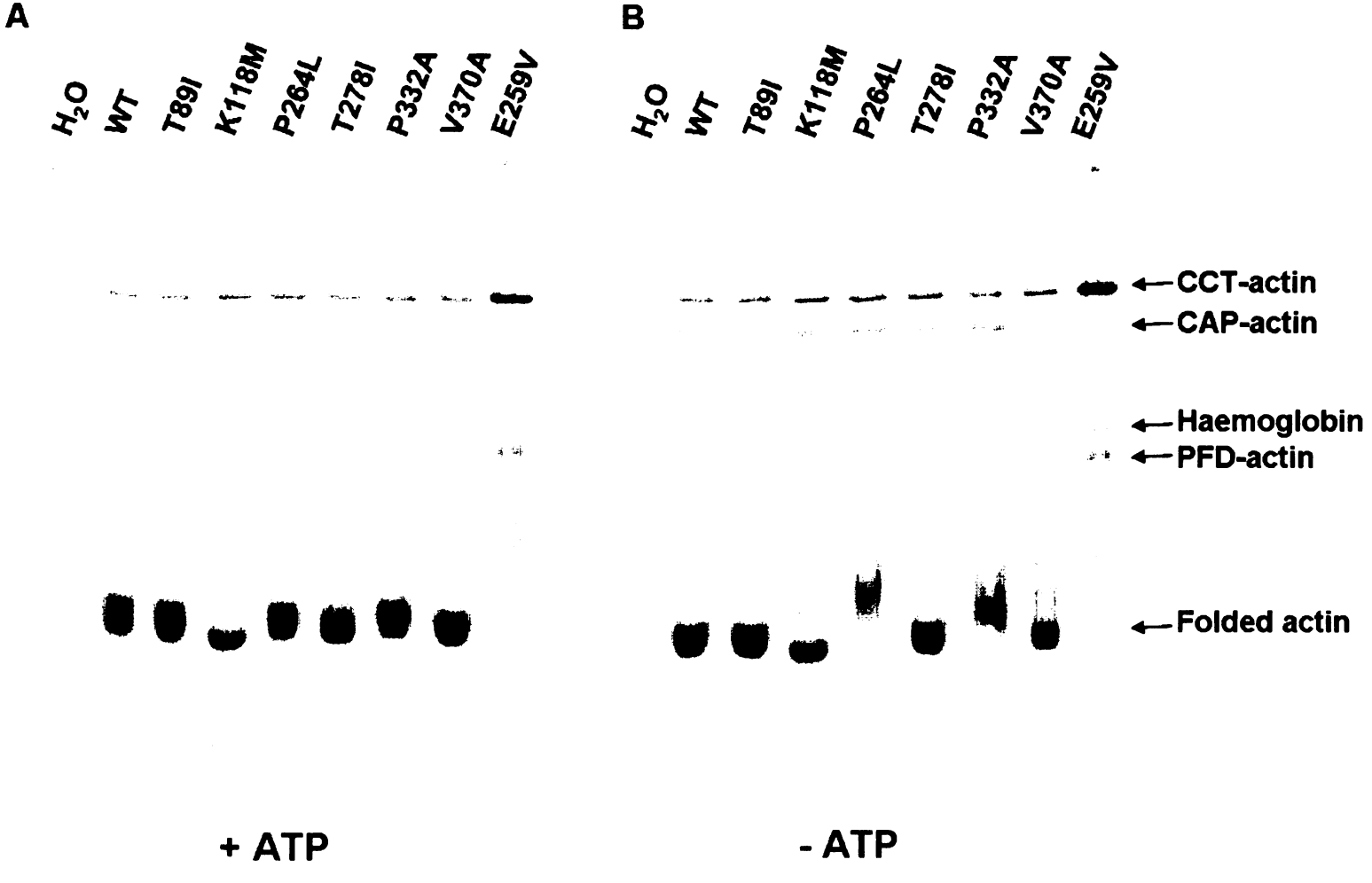
A
B
H2O
WT
T89I
K118M
P264L
T278I
P332A
V370A
E259V
CCT-actin
CAP-actin
Haemoglobin
PFD-actin
Folded actin
+ ATP
- ATP

interestingly, I observed altered CAP binding as shown in Fig. 2-2B. Variants T89I, V370A, T278I and K118M had less association with CAP (4.2%, 5%, 9.2% and 10.2% respectively) while P264L and P332A had more association with CAP (12.8% and 13% respectively) compared to the wild-type actins (11%) (Fig. 2-3). However, a significant change with $p < 0.05$ (student's t-test, n=4) was found only in variants T89I, V370A and T278I.

To assess the chaperone interaction of the actin mutants association with CCT and PFD was examined. All actin variants were properly released from CCT and no abnormal association with CCT compared to wild-type actin from four independent experiments (Fig. 2-4). To analyze and quantitate the PFD-actin complexes, a discontinuous native PAGE (6%-13%) according to Hansen et al. (17) was used to produce a relatively sharper PFD-actin band compared to Safer gels (Fig. 2-2A). Similar to the results seen with CCT-actin variants, all mutants were properly released from PFD and no difference in association with PFD compared to wild-type actin (Fig. 2-5A-B), indicting these mutations did not alter the conformations of the native variants enough to interfere with their interaction with CCT and PFD. Functioning as a negative control, the E259V variant was not released from CCT and PFD, and displayed no CAP binding which is consistent with the findings from previous studies with this skeletal actin mutation (14).

Temperature sensitivity is a phenomenon that is often seen in proteins with altered folding. Thus, I next examined if the variants' folding pathways as described above were affected by different temperatures. I expressed the wild-

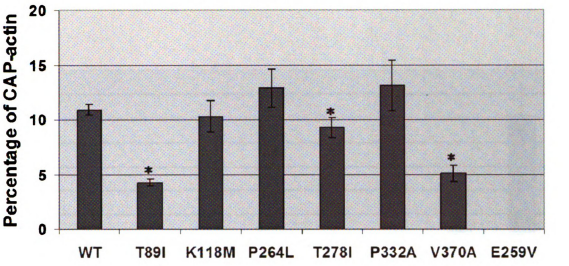

Figure 2-3: γ-Actin mutants showed differences in binding ability to CAP. The ^{35}S-labeled wild-type actin and mutants produced using *in vitro* transcription and translation reaction were run on native PAGE without ATP and standard SDS-PAGE followed by autoradiography and phosphorimaging analysis. The native PAGE was used to determine the amount of CAP-bound actin and the SDS PAGE was to estimate the total yield of proteins produced *in vitro*. The percentage of CAP-bound actin for each mutant was calculated by the amount of CAP-actin compared to the total yield of ^{35}S-labeled actin and plotted on a graph. * indicates statistical significance with $p < 0.05$ from student's t-test, n=4. The mutants T89I and V370A showed over 2 fold reduction in binding with CAP (2.6 and 2.2, respectively) and the T278I also showed significantly decreased CAP binding (1.2 fold with $p = 0.02$). However, the P264L and P332A showed increased CAP binding with p values at 0.06 and 0.09, respectively. As a control, the mutant E259V has no CAP binding.

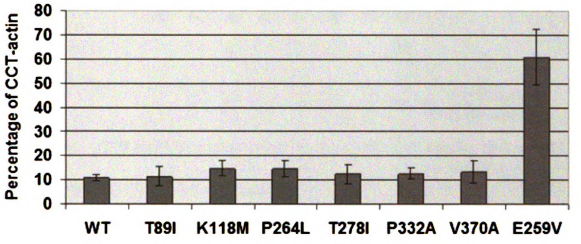

Figure 2-4: γ-Actin mutants were released from CCT upon folding properly. The ^{35}S-labeled wild-type actin and mutants produced *in vitro* were run on native PAGE with ATP and on standard SDS-PAGE followed by autoradiography and phosphorimaging analysis. The native PAGE was used to determine the amount of CCT-bound actin and the SDS PAGE was to estimate the total produced protein. The percentage of CCT-bound actin for each mutant was calculated by the amount of CCT-actin compared to the total yield of ^{35}S-labeled actin and plotted on a graph. The E259V was used as a control, which showed about 6 fold increase in association with CCT. All six γ-actin mutants showed no defect in releasing from CCT. This data was based on four independent experiments.

Figure 2-5: γ-Actin mutants were properly released from PFD. (**A**) ^{35}S-Labeled wild-type γ-actin and mutants were produced by *in vitro* transcription and translation. Three microliters of the reaction were analyzed by SDS-PAGE for quantifying the total produced protein and by native PAGE without ATP for measuring the PFD-bound actin. (**B**) The relative PFD-bound actin was plotted on a graph. The non-folding mutant E259V was produced as a control and showed dramatically increased association with PFD (> 35%). None of the mutants were retained in PFD compared to wild-type actin. Data shown are representative of three experiments.

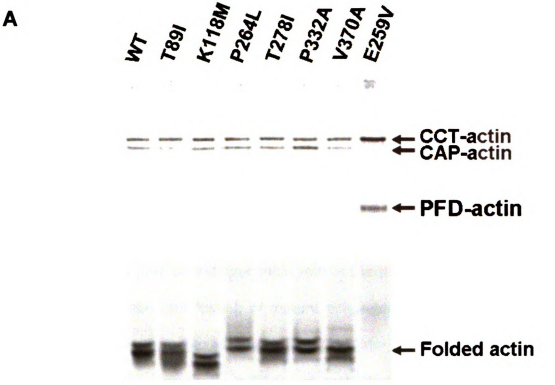
A
WT
T89I
K118M
P264L
T278I
P332A
V370A
E259V
CCT-actin
CAP-actin
PFD-actin
Folded actin

Hansen gel

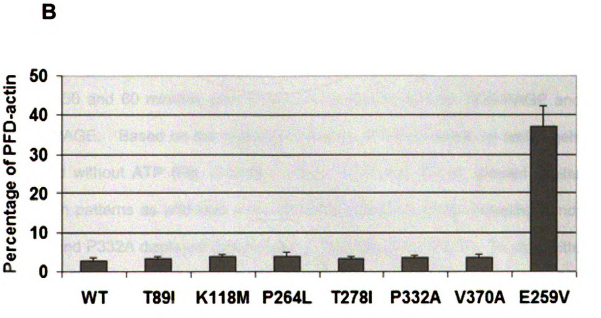
B
Percentage of PFD-actin
50
40
30
20
10
0
WT
T89I
K118M
P264L
T278I
P332A
V370A
E259V

type and mutant actins at either 37°C or 25°C in reticulocyte lysates for one hour and analyzed them on discontinuous native PAGE (4.5%-7.5%) in the presence and absence of ATP (Fig. 2-6). Compared to that performed at 30°C, all variants produced from the three different temperatures have similar migration patterns and binding patterns with CAP. At a lower temperature (25°C), both wild-type actin and variants were shown to have more associate with CCT and PFD compared to wild-type, which is not unexpected. Therefore, no pronounced change was observed from this experiment.

CCT is thought to play an indispensable role in the folding process of actin (13, 21). In addition, aberrant folding of mutant polypeptides usually results in prolonged interaction with molecular chaperons (23). Moreover, I examined the behavior of folded actin variants from 60 minutes of incubation, which is in the plateau phase of an *in vitro* reaction (Fig. 2-1B). To examine if there is any delayed release of native actin from CCT, I performed a pulse chase time course experiment. After 6 minutes of an *in vitro* reaction an excess of cold methionine (1mM final concentration) was added. Aliquots were taken 6, 9, 12, 15, 18, 21, 25, 30, 50 and 60 minutes post chase and analyzed by both SDS-PAGE and native PAGE. Based on the migration patterns of mutant actins on native gels with and without ATP (Fig. 2-2A-B) – T89I, T278I and V370A showed similar migration patterns as wild-type actin; K118M exhibited a sharp migrating band; P264L and P332A displayed diffuse bands in the absence of ATP. To start with, I chose to test variants T89I, K118M and P264L. The relative CCT-actin and released actin (quantified from native PAGE) were compared with total

Figure 2-6: Behavior of γ-actin mutants produced at different temperatures on native PAGE. ^{35}S-Labeled wild-type γ-actin and mutants were produced by *in vitro* translation at three different temperatures (25°C, 30°C, and 37°C) and separated on native gels with or without ATP, followed by autoradiograph. The mutant E259V was produced as a control and showed similar migration patterns on all gels analyzed. Each actin mutant displayed similar migration patterns on native gels examined for proteins produced at different temperatures. No significant behavioral difference between wild-type actin and the six mutants was observed from this test.

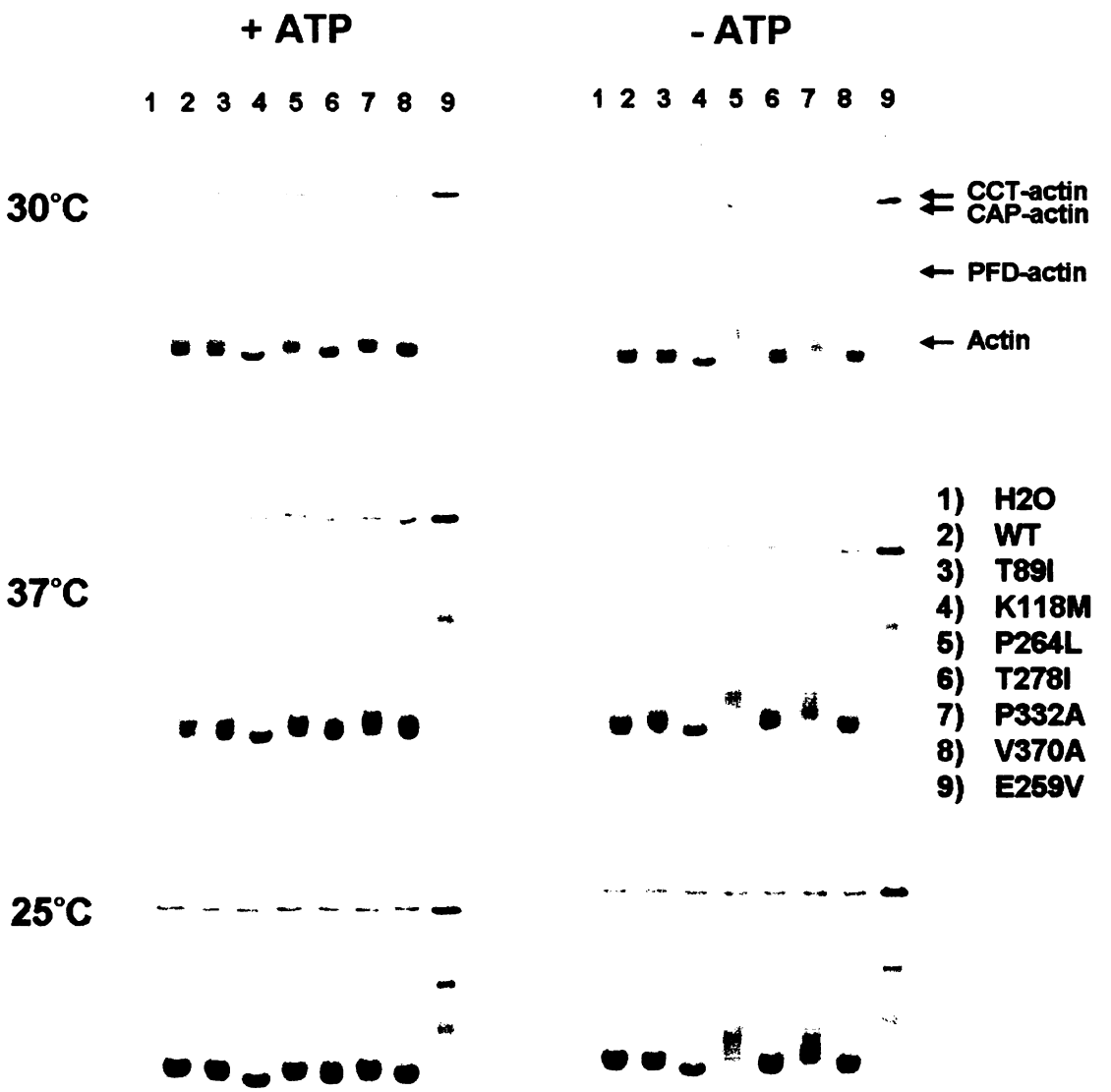
+ ATP
- ATP
1 2 3 4 5 6 7 8 9
1 2 3 4 5 6 7 8 9
30°C
37°C
25°C
CCT-actin
CAP-actin
PFD-actin
Actin
1) H2O
2) WT
3) T89I
4) K118M
5) P264L
6) T278I
7) P332A
8) V370A
9) E259V

production of wild-type and variants (quantified from SDS-PAGE) at each corresponding time point. As shown in Fig. 2-7, all three variants displayed a very similar release rate from CCT compared to that of wild-type actins, indicating these mutants folded properly like wild-type actins. Since no dramatic change was observed from these three mutants, I did not test the rest of mutants, assuming they likely behave the same way.

In summary, none of the six γ-actin mutations affect protein folding or release from CCT and PFD, however, they do cause a range of conformational changes on folded proteins. These were evidenced by the different migration patterns seen on the native PAGE in the presence or absence of ATP. Most significantly, these mutations alter the binding ability of mutant actin proteins to CAP.

Actin variants do not demonstrate altered binding ability with selected ABPs

It is well known that the function of actin is largely dependent on its interaction with many actin-binding proteins (ABPs) and only correctly folded actins with the appropriate binding domain can form a high-affinity complex with them. To test whether these mutant actins can interact with other proteins, I examined their ability to bind selected ABPs using a band shift assay (18), where a relative upward or downward shift of native monomeric actin is observed when it binds to an ABP. Thymosin β4, profilin I, DNase I and vitamin D-binding protein (VDBP) were examined in this study. First, all of them form a very tight complex with folded monomeric actin and interact with different surface areas of

Figure 2-7: Pulse chase time course of CCT and actin interaction. To determine if the actin mutants have prolonged interaction with CCT, I performed a pulse chase time course experiment. Fifty microliters of an *in vitro* transcription and translation reaction for wild-type actin was performed at 30°C. After 6 minutes of incubation, an excess of cold methionine was added. Aliquots of 5 µl were taken 6, 9, 12, 15, 18, 21, 25, 30, 50 and 60 minutes post chase. Three microliters were analyzed by native PAGE with ATP to estimate the amount of CCT-bound actin, and 1 µl was run on SDS-PAGE to determine the total yield of ^{35}S-labeled wild-type γ-actin. The relative amount of CCT-bound actin and released actin for each time point was plotted on a graph. The three mutants (T89I, K118M and P264L) tested exhibited similar rates of release from CCT as the wild-type actin.

Percentage of 35S-labeled actin
5
4.5
4
3.5
3
2.5
2
1.5
1
0.5
0
0
6
12
18
24
30
36
42
48
54
60
Time (min)
CCT-WT
released WT
CCT-K118M
released K118M
CCT-T89I
released T89I
CCT-P264L
released P264L

the monomeric actin. Second, the actin contact sites or regions for these proteins are known from their crystal structures (DNase I, VDBP, profilin I) and cross-linking experiments (thymosin β4). VDBP, profilin I and thymosin β4 interact with subdomains 1 and 3 of actin where most of the deafness-associated mutations in γ-actin are located. Finally, these ABPs have been extensively used for studying the structural stability and folding of variant actins including α-skeletal muscle, α-cardiac muscle and β-actins (14, 15, 18, 24).

First, based on the previous data from others (14, 18), a concentration series was conducted to determine the minimal amount of the actin binding protein needed to cause a complete band shift of wild-type actins. The final concentration of the respective actin-binding proteins was 14.5 μM for thymosin β4, 7.5 μM for profilin I, 2 μM for DNase I and 1 μM for VDBP. The final concentration was defined by the minimal amount of the chosen ABP to cause a complete band shift in a total 4 μl reaction (3 μl of *in vitro* reaction and 1 μl of ABP). The binding of profilin I, DNase I and VDBP to G-actin causes an upward mobility shift while the binding of thymosin β4 causes a downward shift (Fig. 2-8). The N-terminally Myc-tagged wild-type actin was also included in this experiment. This is to verify that Myc-tagged actin behaves like the non-tagged version with respect to the binding ability to ABPs (Fig. 2-8).

Next, I performed the band shift assay by incubating 3 μl of *in vitro* transcription and translation reaction and 1 μl of each ABP for one minute at room temperature, and analyzing the mixture of the reaction on native PAGE with ATP (200 μM) and visualized by phosphorimaging (Fig. 2-9). I found that all actin

Figure 2-8: Determining the final concentration of selected ABPs for band shift assay. ^{35}S-Labeled wild-type γ-actin and mutants were produced by *in vitro* transcription and translation. A concentration series was performed for each ABP where one microliter of an ABP was added to three microliters of the *in vitro* reaction. After one minute incubation, the mixture was analyzed on native gel with 200 μM ATP followed by autoradiography. N-terminally Myc-tagged and non-tagged wild-type actin were examined in this experiment. (**A**) The final concentration of VDBP needed for a complete shift of wild-type actin. Final concentrations of 0.25, 0.5 and 0.75 μM of VDBP were tested to interact with wild-type actin and the final concentration of 0.75 μM completely shifted the complex of actin and VDBP. (**B**) The final concentration needed for DNase I to shift actin is 2 μM. (**C**) The final concentration of thymosin β4 for band shift assay is 14.5 μM. (**D-E**) The final concentration of profilin I was determined twice at lower concentration in the first attempt and it was 7.5 μM from the second test.

A

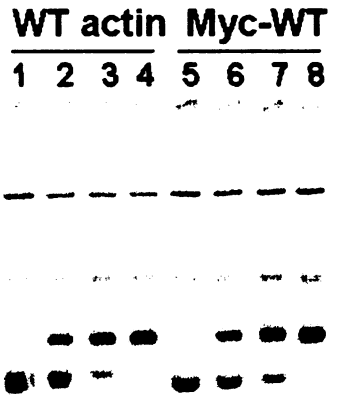

VDBP:actin

Lane 1: WT actin
Lane 2: WT actin + 0.25 μM VDBP
Lane 3: WT actin + 0.5 μM VDBP
Lane 4: WT actin + 0.75 μM VDBP
Lane 5: Myc-WT actin
Lane 6: Myc-WT actin + 0.25 μM VDBP
Lane 7: Myc-WT actin + 0.5 μM VDBP
Lane 8: Myc-WT actin + 0.75 μM VDBP

B

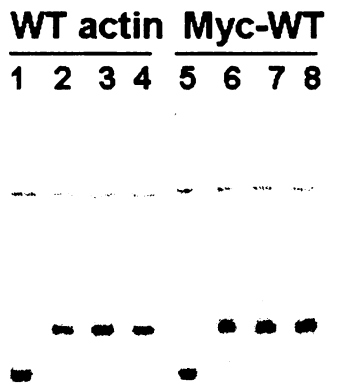

DNase I:actin

Lane 1: WT actin
Lane 2: WT actin + 1 μM DNase I
Lane 3: WT actin + 2 μM DNase I
Lane 4: WT actin + 3 μM DNase I
Lane 5: Myc-WT actin
Lane 6: Myc-WT actin + 1 μM DNase I
Lane 7: Myc-WT actin + 2 μM DNase I
Lane 8: Myc-WT actin + 3 μM DNase I

C

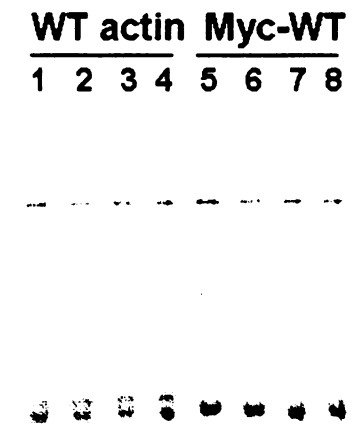

Thymosin β4:actin

Lane 1: WT actin
Lane 2: WT actin + 12.5 μM thymosin β4
Lane 3: WT actin + 14.5 μM thymosin β4
Lane 4: WT actin + 16 μM thymosin β4
Lane 5: Myc-WT actin
Lane 6: Myc-WT + 12.5 μM thymosin β4
Lane 7: Myc-WT + 14.5 μM thymosin β4
Lane 8: Myc-WT + 16 μM thymosin β4

Figure 2-8 continue

D

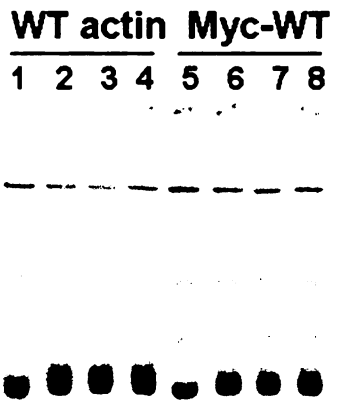

Profilin I:actin

Lane 1: WT actin
Lane 2: WT actin + 3.25 μM profilin I
Lane 3: WT actin + 3.5 μM profilin I
Lane 4: WT actin + 3.75 μM profilin I
Lane 5: Myc-WT actin
Lane 6: Myc-WT + 3.25 μM profilin I
Lane 7: Myc-WT + 3.5 μM profilin I
Lane 8: Myc-WT + 3.75 μM profilin I

E

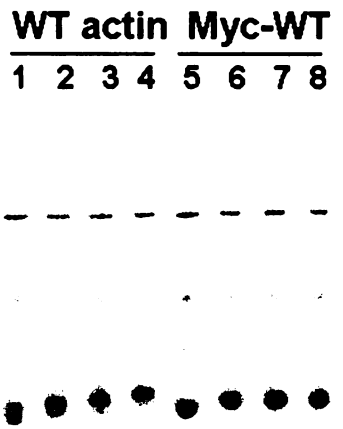

Profilin I:actin

Lane 1: WT actin
Lane 2: WT actin + 5.85 μM profilin I
Lane 3: WT actin + 7.5 μM profilin I
Lane 4: WT actin + 11.75 μM profilin I
Lane 5: Myc-WT actin
Lane 6: Myc-WT + 5.85 μM profilin I
Lane 7: Myc-WT + 7.5 μM profilin I
Lane 8: Myc-WT + 11.75 μM profilin I

Figure 2-9: Band shift assay of wild-type actin and mutants. ^{35}S-Labeled wild-type γ-actin and mutants were produced by *in vitro* transcription and translation. Three microliters of the *in vitro* reaction were incubated with one microliter of thymosin β4, profilin I, DNase I or VDBP for one minute, then the mixtures were subjected to native PAGE analyses followed by autoradiography. Wild-type actin shifted down in complex with thymosin β4 and shifted up in complex with profilin I, DNase I or VDBP compared with wild-type or mutant actin alone. The non-folding mutant E259V was used as a control and showed no interaction with any selected ABPs. All six actin mutants were able to bind and shift the selected ABPs.

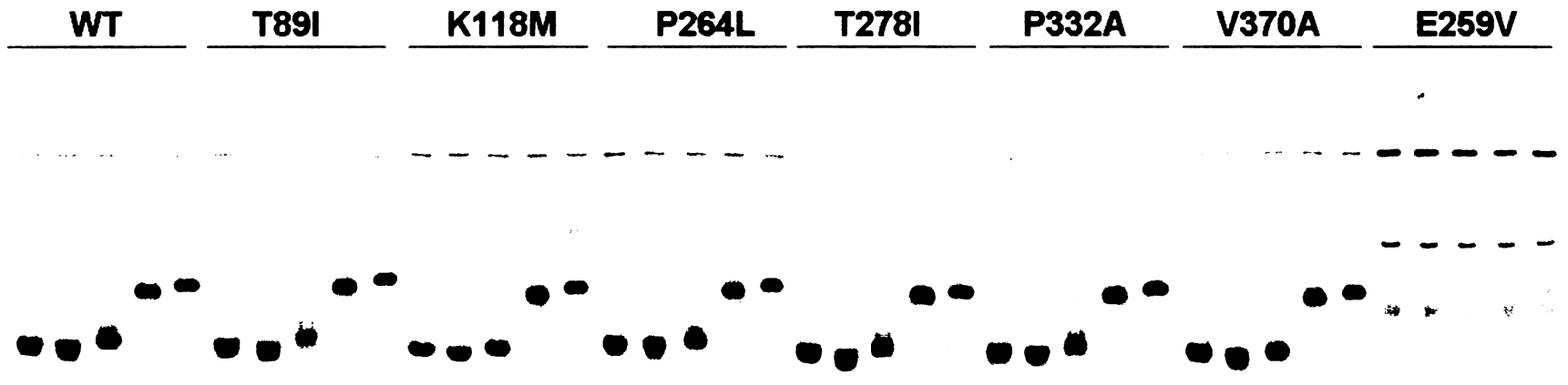

Left to right for each group:

actin (wt/mt), + thymosin β4, + profilin I, + DNase I, + VDBP, respectively

mutants could be shifted by profilin I, thymosin β4, DNase I and VDBP, indicating either the mutant proteins folded properly, or the conformational changes did not affect the interaction of actin with the ABPs tested here.

I would also like to mention here that I have worked on both confirming and improving the band shift pattern of thymosin β4 and actin, which showed a small, marginal downward shift. I attempted this in many ways: first, higher or lower concentration native gels (12-13% and 7.5% respectively) were used. The patterns of band shifting observed from the 7.5% gels were similar to that on 10% native gels (data not shown). The 12% or 13% gels always exhibited double bands for the released actin, even in sample lanes without the addition of thymosin β4, which made it impossible to evaluate the band shift (data not shown). Next, I tried to change the band shift pattern by performing a super-shift experiment using specific antibodies. Briefly, 1 µl of concentrated or serial diluted polyclonal anti-thymosin β4 antibody (whole antiserum for two antibodies were used; derived from either the entire 43 aa molecule, or the C-terminal 10 aa of thymosin β4) (Abcam) was added to either thymosin β4-actin mixture or to thymosin β4 before adding *in vitro* produced actin, and incubated on ice for at least 30 minutes before analyzing on native PAGE. Unfortunately, although the antibodies shifted the thymosin β4-actin complex they also shifted actin alone (data not shown), indicating a non-specific cross reaction of anti-thymosin β4 with actin. Hence I tried to pre-incubate anti-thymosin β4 with purified non-muscle actin (Cytoskeleton Inc.) for 30 minutes on ice before conducting the super-shift experiment. This time, the pre-incubated antibodies did not shift the ^{35}S-labeled

actin and neither shifted the thymosin β4-actin complex (data not shown). Surprisingly, I found that the affinity purified polyclonal anti-γ-actin antibody (developed by our own lab) and anti-profilin antibody (Abcam) were not able to shift γ-actin (with a trace shift) and profilin I-actin complex in my super-shift experiment (data not shown). All antibodies used in the super-shift experiments were tested for their specific function by western blotting (data not shown). In addition, all ABPs tested in this study were examined by SDS-PAGE for their quantity and quality (the integrity and purity), and by native PAGE for their ability to migrate into the native gel. Moreover, I tested and verified using Coomassie brilliant blue stained native gels that thymosin β4 and actin formed a complex which shifted downward compared to non-complexed actin and thymosin β4, however, neither of the two anti-thymosin β4 antibodies was able to shift the complex of actin and thymosin β4. Taken together, the failure of my super-shift experiment may be due to these antibodies not recognizing native proteins or protein complexes, or they may not function well in the reticulocyte lysate. After experiencing many difficulties without a promising result, I finally tested the band shift assay on N-terminally Myc-tagged mutants, which all had been confirmed to behave like non-tagged proteins on native gels with or without ATP (data not shown). I also included profilin I in this experiment. As shown in Fig. 2-10, all Myc-actin mutants except the control Myc-E259V showed a downward shift with thymosin β4 and an upward shift with profilin I.

Actin variants have the ability to copolymerize with wild-type actin *in vitro*

Figure 2-10: Band shift assay of N-terminally Myc-tagged wild-type actin and mutants. Myc-tagged wild-type γ-actin and mutants were produced as ^{35}S-labeled protein *in vitro*. Three microliters of the *in vitro* reaction was incubated with one microliter of thymosin β4 and profilin I. The Myc-tagged wild-type actin was also examined for the binding to VDBP and DNase I. The mixed samples were run on native PAGE in the presence of 200 μM ATP final concentration (both in gel and buffer) followed by autoradiography. The Myc-tagged wild-type actin shifted down in complex with thymosin β4 and shifted up in complex with profilin I, VDBP, and DNase I compared with wild-type or mutant actin alone. The non-folding mutant E259V was used as a control and showed no interaction with any selected ABPs. All six actin mutants with an N-terminal tag showed the ability to bind and shift thymosin β4 and profilin I.

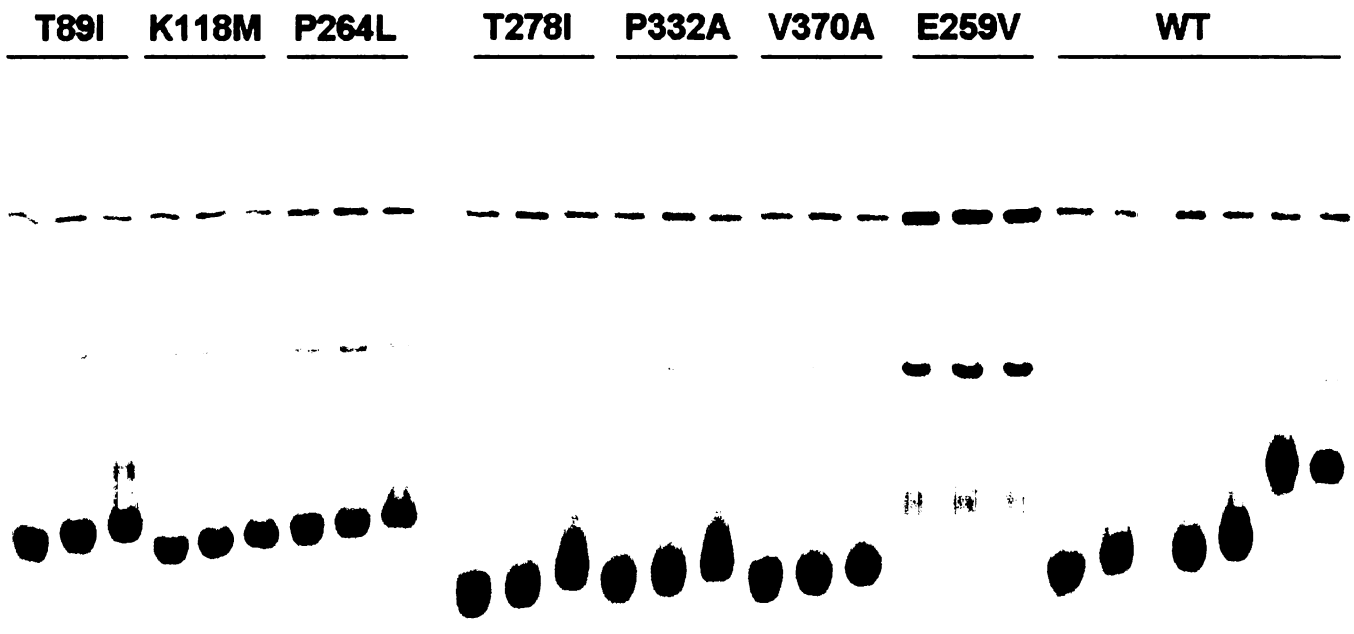

Left to right for each mutant (mt):

Myc-actin mt + thymosin β4, Myc-actin mt, and Myc-actin mt + profilin I, respectively

Left to right for WT:

WT + thymosin 4, WT, WT, WT + profilin I, WT + DNase I, and WT + VDBP, respectively

It is well known that actin has a strong inherent tendency to form filamentous actin, which is the principle functional form in living cells. Hence, it is necessary to test if actin variants are able to polymerize into filaments. Since the *in vitro* transcription and translation reaction only produces a limited protein yield, in order to test the polymerization ability, wild-type carrier actin was added to induce copolymerization of wild-type and variant. Thus, in this experiment, I actually examined the ability of variants to polymerize with wild-type actin. The carrier actin used in this study is a mixture of non-muscle actin (20% γ-actin and 80% β-actin) (Cytoskeleton Inc.), which is well suited for studying γ-actin variants. Studies have shown that different actin isoforms can copolymerize *in vitro* but with different efficiency. For instance, the copolymerization efficiency is higher if the same/similar isoforms (such as all non-muscle actins) were used for the copolymerization assay compared to the assay using different isoforms (such as muscle isoform and non-muscle isoforms). However, most *in vitro* copolymerization studies (14, 18) have been conducted with rabbit skeletal muscle actin, which is easy to purify, even for studying the functionality of non-muscle actin variants, such as β-actin (18). As described in the methods section, the copolymerization assay uses ^{35}S-labeled actins produced *in vitro*. The *in vitro* reaction mixture was subjected to high speed centrifugation to remove aggregates followed by two rounds of polymerization/deploymerization (Fig. 2-11). Mutant actin incorporation into filaments was measured by quantifying ^{35}S levels from each fraction collected in the process of this assay, namely aggregates, supernatant 1 (Sn 1), supernatant 2 (Sn 2) and final pellet (P2), and

Figure 2-11: Copolymerization assays of wild-type γ-actin and mutants. Wild-type γ-actin and mutants were produced as ^{35}S-labeled protein *in vitro*. The reaction mixtures were subjected to high speed centrifugation to remove the aggregates, followed by induction of two rounds of polymerization/depolymerization in the presence of excess cold carrier non-muscle actin. The *in vitro* products, aggregates, two supernatants, and final pellets were analyzed by SDS-PAGE followed by autoradiograph. (**A**) Outline of standard *in vitro* copolymerization assay. The boxed fractions were subjected to western blot analyses. (**B**) Western blot analyses of ^{35}S-labeled actin in different fractions. Yield indicates total yield of wild-type or mutant in an *in vitro* transcription/translation reaction. Agg. represents aggregates from the initial high speed spin. Sn1 is the supernatant collected from the first round of polymerization and contains globular actin. Sn2 is the supernatant collected from the second round of polymerization. P2 is the final pellet of filamentous actin. CBB is the abbreviation of Coomassie brilliant blue and was used for staining the SDS-PAGE gel to visualize the protein. All mutants showed similar signals as the wild-type actin in each fraction analyzed in SDS-PAGE. The non-folding mutant control E259V exhibited no polymerization ability evidenced by comparison of the CBB stained signal (filamentous actin) and the signal from the autoradiograph (^{35}S-labeled E259V).

A

Spin-down copolymerization assay:

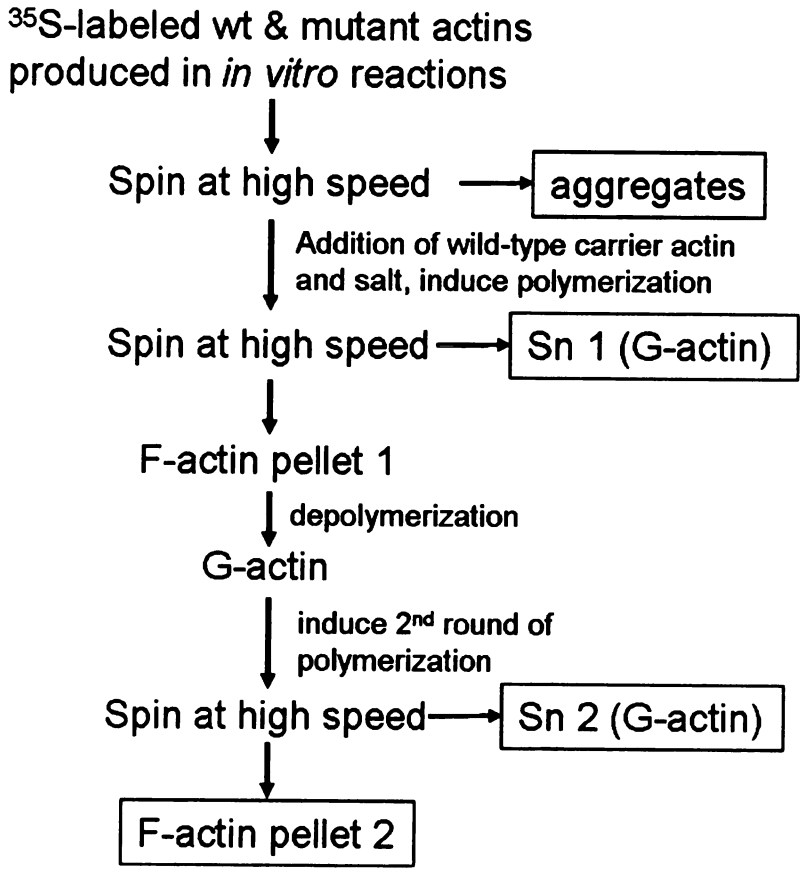

B

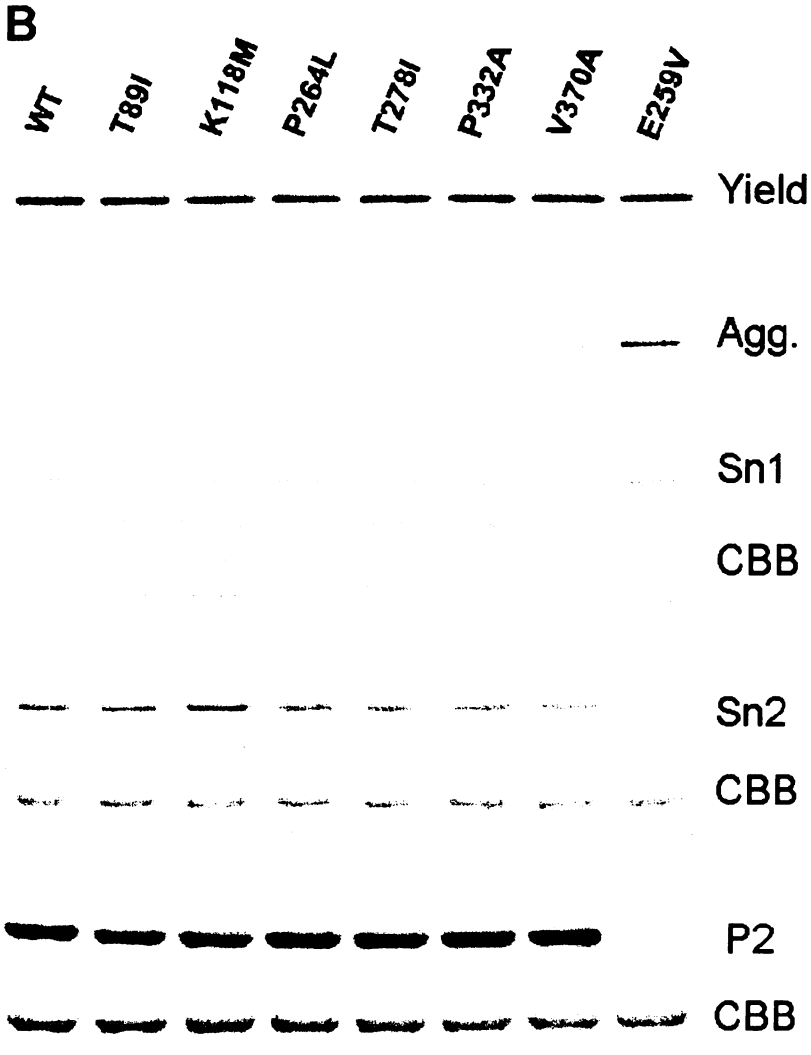

CBB: Coomassie brilliant blue

the percentage of each fraction was plotted on a graph (Fig. 2-12). I found that wild-type actin polymerized to about 60% in this assay, which is similar to that observed from copolymerization of wild-type skeletal muscle actin using the same method (14). The control variant E259V only reached about 4% and the filaments were mainly formed by carrier actin, evidenced by comparing the autoradiograph signal to the Coomassie brilliant blue stained signal (Fig. 2-11B). All six γ-actin variants polymerized to at least 50% which was considered to be similar to wild-type actins (14, 18). In conclusion, the actin hearing loss mutants have the ability to copolymerize with wild-type actin *in vitro*.

Protein and transcript levels of actin variants are relatively stable in transiently transfected cells

To test the hypothesis that γ-actin mutations alter the stability of mRNA and/or protein, leading to a reduced steady-state protein level that triggers the disease, I examined the mRNA and protein levels of wild-type actin and seven variants (including non-folding variant E259V) in transiently transfected cells. My initial test was done by transfection of C-terminally Flag-tagged constructs into 293 T cells. Cells from one of duplicate 60 mm diameter dishes were harvested in RIPA buffer for protein analysis, while cells from the other dish were prepared for total RNA isolation. The protein levels of Flag-tagged variants were examined by standard western blotting and the relative protein levels were normalized by endogenous β-tubulin levels (data not shown). No differences in protein levels were observed between wild-type and variants.

Figure 2-12: γ-Actin mutants demonstrated copolymerization ability to wild-type actin *in vitro*. Wild-type γ-actin and mutants were produced as ^{35}S-labeled protein *in vitro*. The reaction mixtures were subjected to high speed centrifugation to remove the aggregates, followed by induction of two rounds of polymerization/depolymerization in the presence of excess cold carrier non-muscle actin. The *in vitro* products, aggregates, two supernatants, and final pellets were analyzed by SDS-PAGE followed by autoradiograph. The percentage of each fraction to the total yield of *in vitro* reaction was calculated and plotted in a graph. The non-folding mutant E259V was used as a control and showed no polymerization activity. The wild-type actin polymerized to about 60% in this assay. All six γ-actin mutants exhibited over 50% of polymerization of mutant protein, which were considered to be like wild-type in this assay. The data shown are representative of four experiments.

Pellet 2
Sn2
Sn1
Aggregates
Percentage of 35S-labeled actin
110%
100%
90%
80%
70%
60%
50%
40%
30%
20%
10%
0%
WT
T89I
K118M
P264L
T278I
P332A
V370A
E259V

To examine the mRNA levels I first attempted to perform qRT-PCR. However I experienced an unexpected difficulty in cleaning the contaminated plasmid DNA from the total RNA samples. I tried different ways to get rid of the plasmid DNA from the RNA samples. First, I used different methods to isolate total RNAs, including RNeasy® mini and macro kits (QIAGEN) and TRizol reagent (Invitrogen). Second, I treated the RNA samples with RNase free DNase I using one to three rounds of treatment each followed by phenol-chloroform purification. Finally, I even tried to reduce the amount of plasmids for transfection. None of these procedures produced plasmid free RNA preparation so in the end I decided to perform standard northern blotting. Based on the preliminary results from immunostaining and confocal microscopy that the wild-type actin with a C-terminal Flag tag did not behave like the non-tagged version, whereas the version with an N-terminal Myc tag did, I decided to examine the protein and mRNA levels of the actin variants by transfection of N-terminally Myc-tagged constructs in COS-7 cells. A control plasmid, pEGFP-C1, was included in the transfection assay to monitor the transfection efficiency and normalize the protein levels of variants. As described above, N-terminally Myc-tagged wild-type actin or variant and pEGFP-C1 (9:1 ratio) were cotransfected into two 60 mm diameter dishes containing COS-7 cells. Thirty hours after transfection, whole cell extracts were prepared in RIPA buffer and total RNA were isolated using TRizol reagent, followed by standard western blot and northern blot analyses respectively. No significant difference was exhibited between wild-type actin and variants for both levels of protein and mRNA (Fig 13-15), indicating the

Figure 2-13: Examination of protein levels of wild type and mutant actins. Myc-tagged γ-actin constructs were transfected into COS-7 cells and the cells were harvested 30 hours later. Equal amounts of protein were used for western blot analyses of γ-actin and EGFP (cotransfected as loading control) with anti-Myc and anti-EGFP antibodies, respectively. The expression level of endogenous γ-actin was also examined by reprobing the same blot with anti-γ-actin antibody. These results were shown in panel A. All actin mutants showed similar protein levels to that of wild-type actin. The expression level of Myc-tagged wild-type or mutant actin is much lowever than endogenous γ-actin. The relative actin protein level was calculated by comparing the Myc-tagged actin to the EGFP protein level, and plotted in a graph (panel B) which represents two experiments. The mutant E259V was used as a negative control and showed decreased protein level compared to wild-type actin.

A

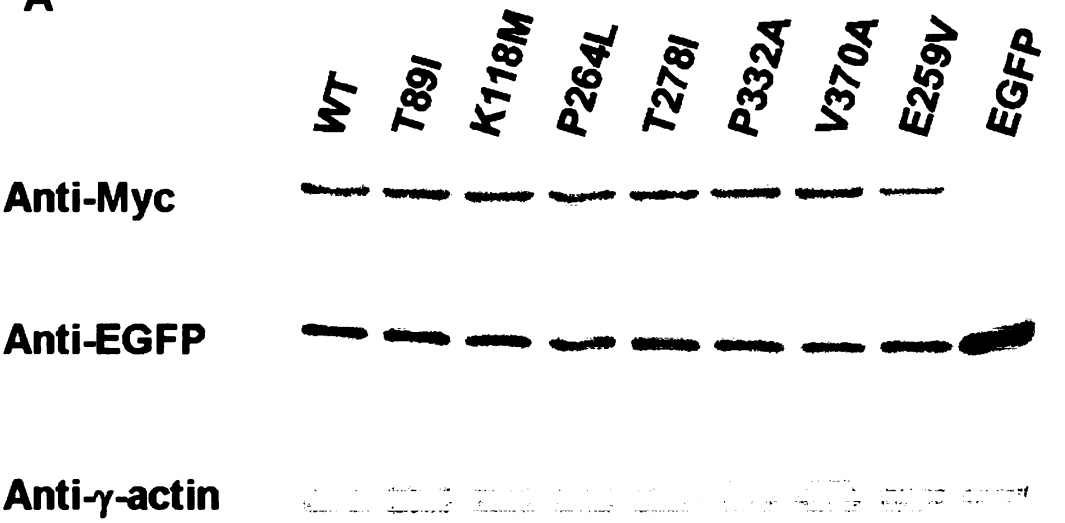
WT
T89I
K118M
P264L
T278I
P332A
V370A
E259V
EGFP
Anti-Myc
Anti-EGFP
Anti-γ-actin

B

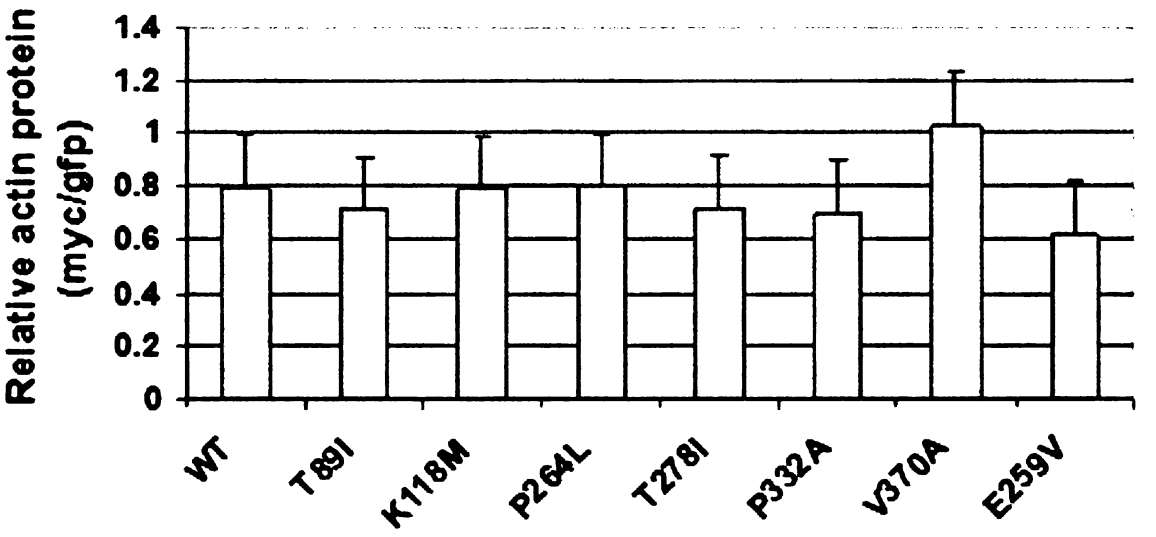
Relative actin protein (myc/gfp)
1.4
1.2
1
0.8
0.6
0.4
0.2
0
WT
T89I
K118M
P264L
T278I
P332A
V370A
E259V

Figure 2-14: Examination of mRNA levels of wild type and mutant actins. COS-7 cells were transfected with Myc-tagged γ-actin constructs and the total RNA were isolated 30 hours later using the TRizol reagent. Five micrograms of total RNAs were subjected to northern blot analyses. A 3′ UTR probe of the pcDNA3.1-actin construct and EGFP probe were used for examining the mRNA levels of Myc-tagged actin variants and cotransfected EGFP, respectively, (panel A). The relative mRNA levels of actin variants were determined by comparing the Myc-tagged actin level to the EGFP mRNA level and plotted in a graph shown in panel B. The γ-actin mutants exhibited similar mRNA levels to the wild-type actin. The mRNA level of mutant E259V is also comparable to the mRNA level of wild-type actin.

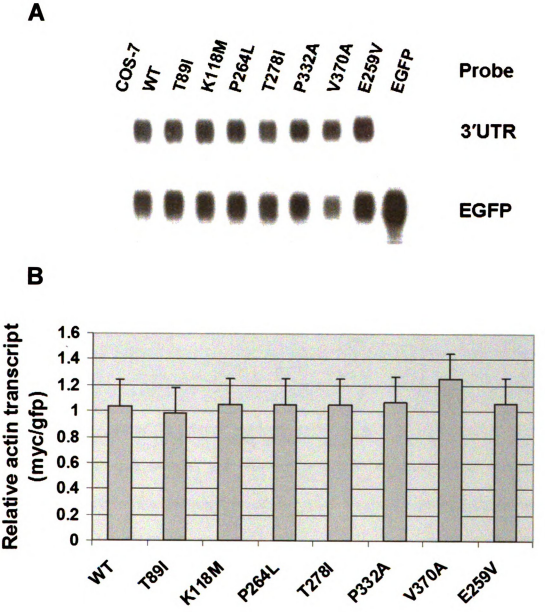
A
COS-7
WT
T89I
K118M
P264L
T278I
P332A
V370A
E259V
EGFP
Probe
3'UTR
EGFP
B
Relative actin transcript (myc/gfp)
1.6
1.4
1.2
1
0.8
0.6
0.4
0.2
0
WT
T89I
K118M
P264L
T278I
P332A
V370A
E259V

Figure 2-15: The relative protein levels of γ-actin mutants in transiently transfected COS-7 cells. Myc-tagged actin constructs and a control plasmid (pEGFP-C1) were transiently co-transfected into two 60 mm diameter dishes of COS-7 cells. The cells from one dish were harvested in RIPA buffer to prepare total protein, and equal amounts of protein were used for western blot analyses of γ-actin and EGFP protein with anti-Myc and anti-EGFP antibodies. The relative protein levels of actin mutants were normalized by the EGFP protein. Cells from the other dish were used for total RNA preparation and equal amounts of total RNA were subjected to northern blot analyses. A 3′ UTR probe of the pcDNA3.1-actin construct and EGFP probe were used for examining the mRNA levels of Myc-tagged actin variants and co-transfected EGFP, respectively. The relative protein levels of actin variants were compared to the relative mRNA levels and the relative expression of actin mutants was plotted on a graph. All γ-actin mutants showed similar expression levels of protein to the wild-type actin. The mutant E259V was used as a control and showed about 30% of reduction of protein level compared to the wild-type actin. The data shown is the mean of two experiments.

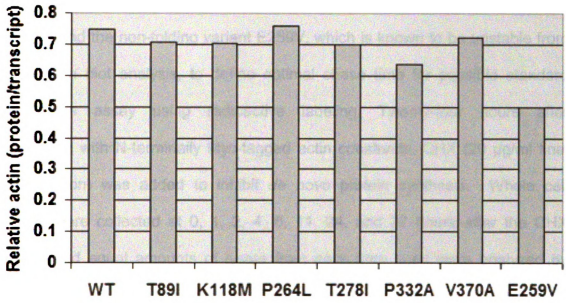
Relative actin (protein/transcript)
0.8
0.7
0.6
0.5
0.4
0.3
0.2
0.1
0
WT
T89I
K118M
P264L
T278I
P332A
V370A
E259V

mutations do not affect the stability of variant protein. The non-folding variant E259V exhibited a reduced relative protein level compared to that of wild-type.

Since the protein levels of variants were examined by transient transfection assays, the relatively stable levels of protein could be due to the overexpression of tagged proteins. Therefore, I felt the stability of the mutant proteins needed to be tested. For an initial attempt to determine the protein turnover rate of actin variants I performed a cycloheximide (CHX) chase analysis. I first tested the wild-type and the non-folding variant E259V, which is known to be unstable from the western blot analysis, to define optimal chase time for possible standard pulse-chase assay using radioactive labeling. Twenty-four hours after transfection with N-terminally Myc-tagged actin constructs, CHX (20 μg/ml final concentration) was added to inhibit *de novo* protein synthesis. Whole cell extracts were collected at 0, 1, 2, 4, 8, 11, 24, and 27 hours after the CHX addition and equal amounts of lysate from each time point were analyzed by western blotting. To my excitement, I observed that the non-folding control variant E259V degraded to about half at a chase time 8 hours; whereas the wild-type actin was relatively stable (Fig. 2-16). Some cell death was observed by 11 hours and more death was seen at 24 hours, therefore a time course of 0, 2, 4, and 8 hours was chosen to test all other actin variants. I did not observe any difference in degradation rate between wild-type and the six γ-actin variants (Fig. 2-17A-B). The levels of endogenous γ-actin at each chase time point were also examined by reprobing the same blot (stripped) with anti- γ-actin antibodies (Fig. 2-16, and data not shown for other variants). The protein levels of both tagged

Figure 2-16: Determining the half-lives of wild-type actin and the non-folding mutant E259V. To determine the half-lives of actin mutants, I first attempted to compare the difference of turnover rate between the wild-type actin and the non-folding mutant. COS-7 cells were transiently transfected with the N-terminally Myc-tagged wild-type actin and the mutant E259V, and treated with 20 μg of cycloheximide (CHX) /ml to stop further protein synthesis. Whole cell lysates were prepared in RIPA buffer at post chase time 1, 2, 4, 8, 11, 24 and 27 hours. Equal amounts of cell lysates were separated on SDS-PAGE followed by western blot analsis (panel A). The endogenous γ-actin was also examined for comparison by reprobing the same blot with anti-γ-actin antibody (panel A) and appeared relatively stable. The relative levels of each mutant were quantitated by ImageJ software (NIH) and the percentage of actin protein at each time point was plotted on a graph (panel B). The non-function mutant E259V showed reduced protein stability with an estimated half-life more than 8 hours. The wild-type actin was relatively stable and its half-life was not able to be estimated using this assay.

A


Time (hr): 0 1 2 4 8 11 24 27
WT
Anti-Myc (1:10,000)
Anti-γ-actin (1:10,000)
E259V
Anti-Myc (1:10,000)
Anti-γ-actin (1:10,000)

B

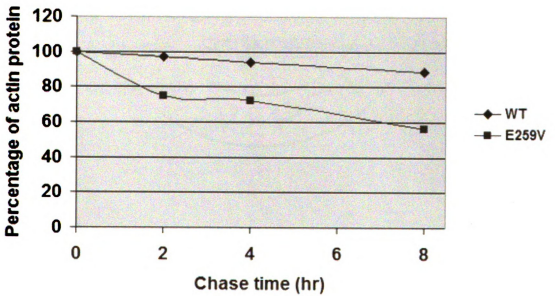
Percentage of actin protein
120
100
80
60
40
20
0
0
2
4
6
8
Chase time (hr)
WT
E259V

Figure 2-17: γ-Actin mutants are stable in transiently transfected COS-7 cells. To determine the relative half-lives of actin mutants, I transfected COS-7 cells with the N-terminally Myc-tagged actin constructs and treated them with 20 µg of cycloheximide (CHX) /ml to stop further protein synthesis. Whole cell lysates were prepared in RIPA buffer at post chase time 2, 4 and 8 hours. Equal amounts of cell lysate were separated on SDS-PAGE followed by western blot analsis (panel A) using anti-Myc antibody. The relative levels of each mutant were quantitated by ImageJ software (NIH) and the percentage of actin protein at each time point was plotted in a graph (panel B). The non-function mutant E259V was used as a control and showed reduced protein stability. All actin mutants showed similar turnover rate as wild-type actin. The data shown here are representative of two experiments.

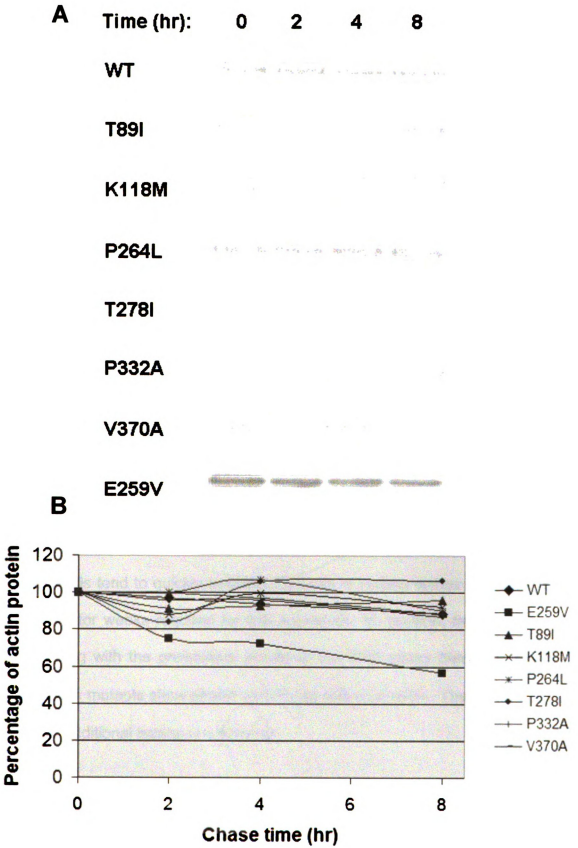
A
Time (hr): 0 2 4 8
WT
T89I
K118M
P264L
T278I
P332A
V370A
E259V
B
Percentage of actin protein
120
100
80
60
40
20
0
0 2 4 6 8
Chase time (hr)
WT
E259V
T89I
K118M
P264L
T278I
P332A
V370A

and endogenous wild-type actin as well as variants (exclude E259V) are relatively stable and are comparable to each other at each chase time point, indicating variant proteins have similar stability as wild-type actin. In addition, the levels of expressed tagged actin are much lower than the levels of endogenous γ-actin (Fig. 2-13 and Fig. 2-16), which implies that there is no overexpression effect on the protein stability of tagged actin. Since I was not able to estimate the relative half-life of wild-type actin from this CHX assay, which is not suitable for long-lived proteins, I may need to perform the standard pulse chase assay that has been widely used. However, several surprising findings from extensive literature searching made me decide not to pursue any further test. Antecol et al. (25) reported that the estimated half-life of actin in normal fibroblast cells is more than 48 hours. In addition, the half-life of rat cardiac actin was estimated about 13 days by *in vivo* L-[^{3}H]leucine labeling (26). Furthermore, the estimated half-life of rabbit skeletal actin is about 67 days (27). The fact that actin has an unusually long half life makes it difficult and unsuitable to be studied for its turnover rate by standard pulse chase assay in cultured mammalian cells. Cultured cells tend to quickly become confluent in culture dishes and cannot be maintained for weeks required for this approach. In addition, the western blot results along with the preliminary results of the CHX assay demonstrated that these γ-actin mutants show similar stability as wild-type actin. Therefore, it is not likely that additional testing is warranted.

Actin variants behave like wild-type actins in cultured cells

Since actin is a cytoskeletal protein and can form stress fibers (filamentous actin) in cultured cells, the effect of actin mutations on subcellular localization and the ability to polymerize can be tested by transfection of tagged actin mutants. Taking into consideration that a tag may interfere with the normal function of G-actin and F-actin formation, I chose to express wild-type and mutant actin using an expression vector containing a small C-terminal Flag tag (8 aa.), pCMV-Tag4 (Stratagene) as an initial study. The expression of these constructs produced an actin-Flag fusion protein. I transfected the C-terminally Flag-tagged actin constructs into COS-7 cells. The non-folding mutant E259V, identified in the *ACTA1* gene, was also included in this experiment. Transfected cells were stained with primary antibodies against Flag prior to labeling with red fluorescent secondary antibodies (Cy3) and costained with Alexa fluor® 488 phalloidin, which is a standard marker for filamentous actin. The immunostained cells were visualized and examined by Olympus confocal laser scanning microscopy. The image results were shown in Fig. 2-18. Surprisingly, the expressed C-terminally Flag-tagged actins including wild-type and all mutants accumulated in abnormal protrusions that stain with phalloidin at the edges of cells and they did not incorporate into actin stress fibers. This finding is in agreement with the report by Rommelaere et al. (18) that a small C-terminal tag on actin affects actin polymerization. In addition, Rommelaere et al. (18) also examined the N-terminally tagged actin *in vitro* and in cultured cells and they found that a small Myc tag fused to N-terminus of actin did not interfere with actin's function. Therefore, I constructed another set of plasmids containing an

Figure 2-18: Expression of C-terminally Flag-tagged wild-type and mutant actins in COS-7 cells. COS-7 cells were transiently transfected with C-terminally Flag-tagged wild-type and mutant actin constructs. The cells were fixed in 4% PFA and subjected to immunostaining with anti-Flag primary antibody and Cy3-conjugated anti-rabbit secondary antibody (red). The nucleus was counterstained with DAPI (blue). The stained cells were examined with an Olympus confocal laser scanning microscope using 60X PlanApo objective. Left panels are anti-Flag-Cy3 staining for the expressed Flag-tagged wild-type and mutant actin (shown in red). Middle panels are phalloidin staining of filamentous actin (Alexa Fluor 488, shown in green). Right panels are the merged images of left and middle panels, which show yellow if the expressed Flag-tagged mutants colocalized with filamentous actin. The non-folding mutant E259V was transfected as a negative control and accumulated in the cytoplasm. The C-terminally Flag-tagged wild-type actin and mutants were not able to incorporate into stress fibers and mainly accumulated at the edge of transfected cells. The scale bar is 10 um. Images in this dissertation are presented in color.

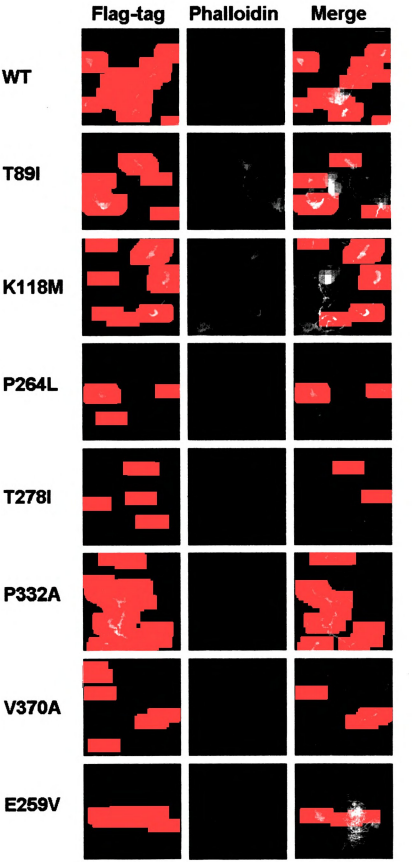
Flag-tag
Phalloidin
Merge
WT
T89I
K118M
P264L
T278I
P332A
V370A
E259V

N-terminal Myc tag using the pcDNA3.1 expression vector as a backbone, producing Myc-actin chimeric protein. The Myc-tagged wild-type actin behaved like the untagged version when tested in the *in vitro* system (Fig. 2-8 and 10). I transfected the Myc-tagged constructs of actin variants into COS-7 cells, which were subsequently stained with anti-Myc primary antibodies and Cy3 red fluorescence labeled secondary antibodies. The filamentous actins, composed of either endogenous actin only or a combination of endogenous and exogenous actin, were stained in green (Alexa Fluor 488 phalloidin). As illustrated in Fig. 2-19, the expressed Myc-actin (red) incorporated nicely into filamentous actin and stress fibers (green), which is indicated by a merged yellow color of red and green signals. No difference was observed in terms of subcellular localization and colocalization with endogenous actin between wild-type and all six γ-actin mutants, indicating correct processing and filament formation of tagged actin variants. The non-folding E259V mutant could not incorporate into any cell structure and mainly accumulated in the cytoplasm. Both these findings are in agreement with the *in vitro* results. However, since phalloidin stains both the endogenous actins and the exogenous actins, the above observation could also possibly be due to colocalization of the tagged filaments and the endogenous filaments instead of copolymerization of the tagged G-actin variants and the endogenous G-actin. This can be verified by cotransfection of wild-type and mutant actin with each having different tags. Thus, a cotransfection of N-terminally Myc-tagged wild-type and N-terminally EGFP-tagged mutant was conducted in COS-7 cells. To avoid the possible effect caused by a relative large

Figure 2-19: N-terminally Myc-tagged actin mutants behaved like wild-type actin in COS-7 cells. COS-7 cells were transiently transfected with N-terminally Flag-tagged wild-type and mutant actin constructs. The cells were fixed in 4% PFA and subjected to immunostaining with anti-Myc primary antibody and Cy3-conjugated anti-rabbit secondary antibody (red). The nucleus was counterstained with DAPI (blue). The stained cells were examined with an Olympus confocal laser scanning microscope using 60X PlanApo objective. Left panels are anti-Myc-Cy3 staining for the expressed Myc-tagged wild-type and mutant actin (shown in red). Middle panels are phalloidin staining of filamentous actin (Alexa Fluor 488, shown in green). Right panels are the merged images of left and middle panels, which show yellow if the expressed Myc-tagged mutants colocalized with filamentous actin. The non-folding mutant E259V was transfected as a negative control and accumulated in the cytoplasm. The N-terminally Myc-tagged actin mutants were able to incorporate into stress fibers, lamellipodia, and generally colocalized with flamentous actin in transfected cells. The scale bar is 20 μm. Images in this dissertation are presented in color.

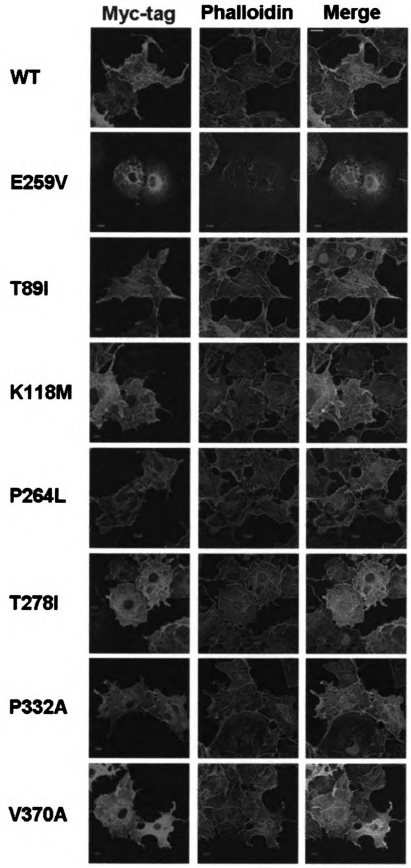
Myc-tag
Phalloidin
Merge
WT
E259V
T89I
K118M
P264L
T278I
P332A
V370A

N-terminal EGFP tag (~27 kDa) on actin, the reciprocal transfection with these two tags reversed was also tested. If cells were transfected with both plasmids and the expressed tagged actins can copolymerize together, a merged yellow image should be observed. Not surprisingly, similar results were obtained from the single plasmid transfection with Myc-tagged construct as were from both cotransfection experiments. No differences were observed between cotransfection of two wild-types and a combination of wild-type and mutant with different tags. Here I show the results from cotransfection of Myc-wt and EGFP-wt/mt. In Fig. 2-20, the red fluorescence image indicates the expressed Myc-tagged wild-type actin (left panels) and the expressed EGFP-tagged wild-type actin and mutants were shown in green (middle panels). All merged images (right panels) of red and green signals from each variant exhibit yellow color, indicating the coexpressed Myc-tagged and EGFP-tagged actins can copolymerize into filamentous actin. Therefore, I conclude that the γ-actin mutations do not affect protein folding process and the ability of copolymerization in COS-7 cells.

DISCUSSION

Actin variants behaved like wild-type actins in most *in vitro* assays but exhibited altered CAP binding ability

To test the hypothesis that the actin folding pathway plays a role in the development of progressive sensorineural hearing loss in DFNA20/26 families,

Figure 2-20: Subcellular localization of coexpressed wild-type and mutant actin each with different N-terminal epitope tags in COS-7 cells. COS-7 cells were transiently transfected with equal amount of N-terminally Myc-tagged wild-type actin plasmid and N-terminally EGFP-tagged wild-type and mutant actin construct, followed by fixation in 4% PFA and immunostaining with anti-Myc primary antibody and Cy3-conjugated anti-rabbit secondary antibody (red). The nucleus was counterstained with DAPI (blue). The stained cells were examined with an Olympus confocal laser scanning microscope using 60X PlanApo objective. Left panels are anti-Myc-Cy3 staining for the expressed Myc-tagged wild-type actin (shown in red). Middle panels are EGFP-fluorescence of the expressed EGFP-tagged wild-type or mutant actin (green). Right panels are the merged images of left and middle panels, which show yellow if the two tagged-actins are colocalized. EGFP-tagged wild-type actin was transfected as a positive control to show normal subcellular localization of expressed actin. The non-folding mutant E259V was transfected as a negative control and accumulated in the cytoplasm. All EGFP-tagged actin mutants were incorporated into stress fibers, ruffles and lamellipodia, and colocalized with Myc-tagged wild-type actin. They all behaved like tagged wild-type actin in cells. The scale bar is 20 μm. Images in this dissertation are presented in color.

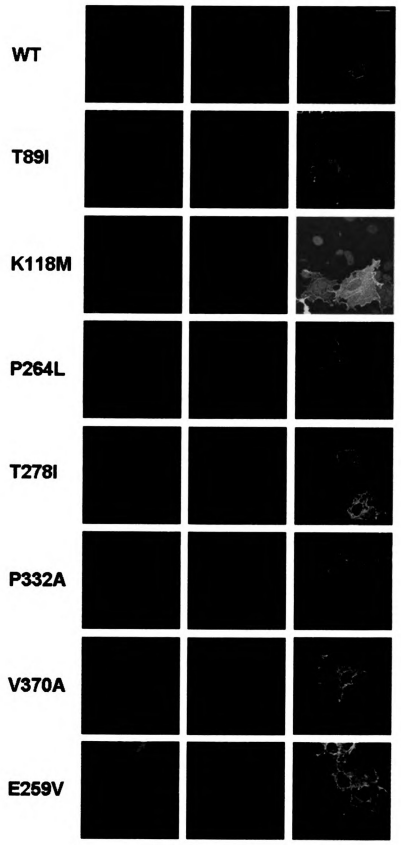
Myc-wt
EGFP-wt/mt
Merge
WT
T89I
K118M
P264L
T278I
P332A
V370A
E259V

six γ-actin variants were examined using an *in vitro* transcription and translation system in rabbit reticulocyte lysates. To my surprise, all six variants could fold properly, were released from chaperones PFD and CCT, bound to the tested actin-binding proteins and copolymerized with wild-type actins. However, these mutants did exhibit a range of conformational changes and some exhibited an altered CAP binding ability. A single amino acid substitution causes significantly different effects on the structure and/or function of the altered polypeptide. For instance, the naturally occurring *ACTA1* mutation E259V (or *ACTG1* E259V engineered in this study) totally abolishes the folding of actin, resulting in a non-functional protein. In contrast, the six γ-actin mutations did not affect the folding of the mutant polypeptides. These mutations, however, did cause a range of conformational changes of the mutant proteins, which can be grouped into three phenotypes based on the migration patterns seen from native gels either with or without ATP (Fig. 2-2A-B). The K118M mutant is of particular significance as it is seen as a sharp migrating band in both ATP and non-ATP native gels, which implies that it formed a uniform and/or more compact structure compared to wild-type actin. In contrast, the mutants P264L and P332A showed similar patterns as the wild-type in the presence of ATP, but displayed diffuse migration patterns in the absence of ATP (Fig. 2-2B). The amino acids P264 and P332 are located near the ATP binding site. Note that an impaired nucleotide binding in actin usually results in an unstable structure (18, 24). Thus the P264L and P332A mutations might impair nucleotide binding. Although this impairment may not be severe enough to cause a phenotype in the native gel with ATP (Fig. 2-2A), in

the absence of ATP, these two mutants become unstable or even denatured, resulting in slowly migrating species (denatured mutant proteins) displayed as smear in the non-ATP native gel (Fig. 2-2B). This is likely due to the fact that actin needs ATP for its stability. The T89I, T278I and V370A mutants exhibit similar migration behavior as the wild-type actin in native gels with or without ATP (Fig. 2-2A-B), indicating they folded into similar overall stable structures as the wild-type actin.

In vitro studies of mutations in other actin isoforms such as skeletal muscle actin (*ACTA1*) and cardiac muscle actin (*ACTC*) have revealed a range of molecular defects involved in the development of muscle diseases (14, 15). Altered CAP binding was also observed in some of the *ACTA1* mutants with either more or less association and even a complete lack of association. *ACTA1* mutants with no CAP binding were mainly found in severe nemaline myopathy (28) patients, while mutants arrested in CAP (even in the presence of ATP) were seen in typical NEM and other forms of myopathy including actin myopathy (AM) and intranuclear-rod myopathy (IRM). However, most of these mutants with altered CAP binding were also associated with other defects such as reduced polymerization ability and inability to bind certain ABPs. Thus, the significance of altered CAP binding in the development of muscle diseases was not well addressed. The lack of other changes besides the altered CAP binding from my *in vitro* assays suggests: some functions of mutant actins have not been determined yet by this approach, or defects caused by mutations are too subtle

to be detected by these assays, or altered CAP binding is a common defect responsible for the hearing loss seen in the six DFNA20/26 families.

CAP has been thought to stabilize nucleotide-free actin and may act as an ATP-loading machine post CCT (24). Increased CAP binding often suggests that the mutant has an unstable structure; in contrast, reduced or diminished CAP binding is usually due to the fact that mutations are close to or in the CAP interface, or mutated polypeptides do not fold (24). Of six actin mutations studied in this project, two mutations (P264L and P332A) reside near the ATP binding site while the remaining four (T89I, K118M, T278I and V370A) reside in subdomains 1 and 3 on the exterior of the protein (Fig. 1-4), where CAP is suggested to interact. As mentioned earlier, the P264L and P332A mutants might have impaired nucleotide binding due to the conformational changes of the mutant molecules. Interestingly, similar results were also observed from the yeast studies of γ-actin mutants (29). The yeast P264L and P332A demonstrated increased nucleotide exchange rates 5 and 3.5 times faster than wild-type actin, respectively. This consistence between yeast actin and human *ACTG1* implies that the P264L and P332A mutations do indeed impair nucleotide binding. Three (T89I, T278I and V370A) of the remaining four mutants (T89I, K118M, T278I and V370A) had reduced CAP binding with statistically significant ($p < 0.05$, n=4, Fig. 2-3). Particularly, the T89I and V370A mutants showed a greater than 2 fold reduction in binding to CAP (2.6 and 2.2, respectively) compared to wild-type actin (Fig. 2-3). The decreased CAP binding observed in these three mutants could be due to the fact that these amino acids are located close to predicted

CAP interface regions in the actin molecule and amino acids substitutions in these positions affect the normal interaction between CAP and actin. Interestingly, the yeast T89I has been shown to retard the rate of nucleotide exchange (29), which may also suggest that this mutation results in a local conformational change in actin that directly interferes with CAP binding. Recently, CAP was found to increase the rate of nucleotide exchange in plants (30). Although the K118M, P264L and P332A mutants did not show significant changes on CAP binding, these three mutants suggested altered association with CAP from the native gels without ATP which needs further quantitation analysis using other methods.

The consequence of increased or decreased CAP binding to monomeric or filamentous actins is still not fully understood. The emerging view of CAP function is that it is required for proper organization and rapid remodeling of cellular actin networks. CAP catalyzes the dissociation of cofilin-bound ADP-actin complexes, recycling cofilin for filament disassembly (2-4). In addition, CAP and profilin promote exchange of nucleotide (ATP for ADP) on G-actin, then CAP releases profilin-bound ATP-actin to replenish the G-actin pool for filament assembly (5, 31). Thus, CAP functions together with cofilin and profilin to accelerate actin turnover, through a series of exchanging the nucleotide (ATP or ADP) on the actin monomer. Based on these observations, γ-actin mutants with altered CAP binding may function abnormally in the process of turnover and/or remodeling of actin networks in living cells. This effect may be particularly significant for auditory hair cells, whose function relies heavily on the specialized

structures made up of actin bundles and networks (mainly γ-actin). After birth, hair cells become exposed to relatively noisy environments, which could damage them (32). In addition, aging and concomitant repeated exposure to reactive oxygen species also could damage the hair cells (33, 34). Hair cells can not be regenerated; hence, proper turnover and remodeling of actin networks are important for maintaining the hair cell structure and function and for repairing hair cell damage caused by noise and aging. Whether altered CAP binding is solely responsible for the progressive hearing loss remains to be further investigated.

No correlation was found between the altered CAP binding and the average age of onset of hearing loss observed among the six DFNA20/26 families. However, this is not unusual. The lack of genotype-phenotype correlation has been a very common theme in genetic diseases. This is largely due to the heterogeneity of genetic background and different environmental factors which could modify the effects of mutant proteins resulting in different outcomes of disease development. For example, an *ACTA1* mutation M132V causing a polymerization defect was found independently in two patients with mild and typical myopathy, respectively (35).

Properly folded proteins do not necessarily function normally. The majority of *ACTA1* mutants folded properly and were released from CCT and PFD, but roughly half of them had impaired polymerization ability and some did not interact with certain ABPs (14). However, all six γ-actin mutants I examined were able to copolymerize to more than 50%, which is considered to be similar to wild-type actin in this *in vitro* polymerization assay (14, 18), and were released from CCT

and PFD. This is consistent with the yeast study using purified yeast actins with γ-actin mutations, in which all mutants displayed virtually the same rate and extent of polymerization, with the exception of the V370A mutant, which had a faster rate and produced shorter filaments when compared to wild-type actin (29). These results imply that γ-actin mutations cause very subtle changes in protein structure and function, which makes them difficult to study. Interestingly, two similar amino acid substitutions, P332S and V370F, found in the *ACTA1* gene caused different types of myopathy namely, fiber-type myopathy (36) and nemaline myopathy (14), respectively. Both mutations were also studied in yeast by Bryan et al. (29); the P332S mutant displayed the same phenotype as our P332A mutant. In contrast, the V370F mutant is lethal in yeast which is consistent with the *in vitro* functional study, showing that this mutant had no CAP binding and severely reduced copolymerization capacity (less than 25%) when compared to wild-type actin (14). These observations indicate that the P332 and V370 amino acids are highly conserved for certain specific functions, particularly, the V370 is involved in filament formation.

Actin variants demonstrated similar stabilities in protein and mRNA with that of wild-type actins in cultured cells

Increased turnover of mutant proteins by amino acid substitution has been implicated in the pathogenesis of many inherited disorders including phenylketonuria, mitochondrial acyl-CoA dehydrogenase deficiency (SCAD) and deficiencies in tumor suppressor genes (37-41). All of these conditions can

result from loss of function due to reduced steady-state level of protein. In these cases, a dosage effect or haploinsufficiency is the cause of disease. However, this turned out not to be the case for actin mutants. In my study, both protein and transcript levels of γ-actin variants were examined in transiently transfected COS-7 cells. Standard western blot and northern blot analyses demonstrated full-length transcripts and proteins from all variants to be relatively stable. The preliminary CHX chase assay reinforced this finding. In addition, the *in vitro* produced ^{35}S-labeled non-tagged mutant γ-actin proteins displayed similar signal intensity in SDS-PAGE and native PAGE. These indicate that hearing loss caused by these variant actin proteins are not likely through loss of function. In contrast, it is more likely to be a dominant-negative cause of disease pathogenesis. There are two lines of evidence for this suggestion. First, my results demonstrated actin variants could fold properly and copolymerize with wild-type actin both *in vitro* and in cultured cells. Second, the fact that mutant actin isoforms produce dominant-negative effects in other organisms, such as yeast (42), drosophila (43, 44) and human muscle myopathies including skeletal muscle myopathies (45-47) and cardiac myopathies (15), suggests that this is also the likely case in hearing loss patients with *ACTG1* mutations. For instance, in skeletal muscle myopathy, adult heterozygote-null patients are normal while the majority of patients with heterozygote-non-null mutations of *ACTA1* showed a wide range of different types of myopathies (46, 47).

To my knowledge, this is the first study conducted to examine the levels of mutant γ-actin proteins and transcripts in cultured mammalian cells. The fact that

actins are the most abundant proteins with an extended long half-life in all eukaryotic cells and the possible dominant-negative mode of pathogenesis might limit the investigation of mutant actin protein levels. So far, there are few studies that have been conducted to examine the mutant actin levels from muscle biopsies of myopathy patients (35, 45). This study showed unaltered protein levels compared to normal control samples, which was suggested to be due to the abundance of muscle actin. My results pertaining to protein stability of mutant actins are very consistent with others and support the notion of a dominant-negative effect in disease development. Whether or not these unaltered protein levels are due to overexpression of mutant actins in cultured cells needs further investigation, and an animal model will be highly preferred.

One interesting result from this study is that the non-folding mutant E259V (control) did retain some amount of mutant protein in cells while the individual with one copy of this mutation in the skeletal muscle actin gene was normal (14). This implies that the protein quality control system of cells has a high capacity to handle the extra mutant proteins. This was confirmed by the *in vitro* results that the majority of mutant E259V was associated with CCT and PFD chaperone proteins, which prevents the aggregation of mutant proteins to cause disease. In contrast, the hearing loss mutant proteins properly folded, were released from CCT and PFD and can likely interfere with wild-type actins and/or ABPs to cause abnormal regulation of filament dynamics leading to the disease.

Actin variants behaved like wild-type actins in transfected COS-7 cells

I investigated the cellular behavior of actin variants by transfection of a single actin mutant and cotransfection of wild-type and mutants with different tags in COS-7 cells. Results from the experiments using an N-terminally tagged construct are identical, which exhibited colocalization or copolymerization of expressed tagged wild-type actins or mutant actins with endogenous actins or contransfected tagged wild-type actins. These indicate that actin mutants undergo normal folding and incorporate into filaments, which is in agreement with my *in vitro* results. Although COS-7 cells express both cytoplasmic actins in a ratio of β:γ about 2:1, with overexpression of wild-type or mutant γ-actins, I did not observe any morphological changes compared to cells with N-terminally Myc-tagged wild-type β-actin (data not shown). It is also noteworthy that different actin isoforms can copolymerize *in vitro* and in cultured cells (10, 14, 18). Therefore, cell types might not be an issue for studying polymerization of actin. In addition, expression of all six γ-actin mutants in explant cochlea culture did not reveal any differences between wild-type and mutants in inner hair cells (Inna Belyantseva at NIDCD, personal communication).

However, in this study, I observed that tagged and non-tagged actins do not necessarily behave similarly. An important feature of G-actin is its ability to form filamentous actin to perform most biological functions. Therefore, a tag sited in either the C-terminus or N-terminus of actin, both located in subdomain 1 with the C-terminus toward the inside and N-terminus sticking outside (Fig. 1-1), could possibly interfere with actin function. There is controversy in the literature regarding the potential effect of the size and position of tags on actin.

Rommelaere et al. (18) reported a detailed examination of the effects of different tags (sizes and locations) and suggested using a small N-terminal tag, whereas Ilkovski and colleagues (45) demonstrated an actin fusion protein with a C-terminal EGFP tag containing a 17 amino acid linker behaved like wild-type actin in cultured cells. In addition, C-terminally tagged Act88F actins caused flightlessness in *Drosophila* (48). From my study, both the C-terminally Flag-tagged wild-type actins and mutant actins were not able to incorporate into stress fibers and mostly accumulated at the edge of transfected cells, whereas the N-terminally Myc-tagged versions behaved like the non-tagged ones. Interestingly, the N-terminally EGFP-tagged actins behaved like the non-tagged version only in cells with relatively lower levels of expression for this tagged actin and accumulated as aggregates in the cytoplasm when they were highly overexpressed (data not shown), indicating the size of a tag is also a concern when large amounts of tagged protein are present. In conclusion, my results suggested that the N terminus of actin is less sensitive to modifications than the C terminus, because it can be tagged and still polymerize into functional filaments.

Overall, all six mutant proteins folded properly, were stable, and copolymerized with wild-type actins both in *in vitro* assays and in cultured cells. Altered CAP binding, caused by the conformational changes due to amino acid substitution, the only significant observation associated with mutations, is likely to be responsible for the development of DFNA20/26 hearing loss. However,

further investigation of the potential molecular mechanisms involved is imperative. The lack of other findings besides abnormal CAP binding is not completely unexpected because γ-actin is a universally expressed structural protein. The γ-actins with the mutations discussed here cause only hearing loss, implying any change of protein structure and/or function caused by these amino acid substitutions will likely be subtle, or else a more severe phenotype would be expected. Most of my results are in agreement with the observations from studies of γ-actin mutations in yeast (29), implying that the *in vitro* assay system is a good alternative method to study the functionality of mutant proteins.

Future plans

My current study has revealed that γ-actin mutants had different binding abilities to CAP, which could be involved in the development of hearing loss. It would be very interesting to test this hypothesis and explore potential molecular mechanisms involved. From my *in vitro* results, only three mutants (T89I, T278I and V370A) demonstrated significant changes of CAP binding, while the other three mutants also displayed visible changes from repeated experiments but lacked statistical power, which could be due to the limitation of the *in vitro* measurements applied. Therefore, I first would like to quantify the effect of mutations on the binding properties (affinity and kinetics) of mutant actins with CAP using surface plasmon resonance (SPR) analysis (Biacore system). This

study will be extended to include cofilin and profilin because these three proteins have been suggested to work together in the processes of actin turnover and remodeling (49). However, in order to perform this experiment, high quantities of purified mutant actin proteins are required. It has been a well known problem that functional studies of actin mutants have been limited due to the lack of a good expression system to produce high quantities and quality of mutant proteins needed for biochemical and biophysical analyses. Actin cannot be expressed in bacteria because bacteria do not have the eukaryotic chaperonin machinery needed for actin folding, resulting in insoluble actin aggregates (50). So far, most of the studies analyzing actin mutants were done using an *in vitro* cell free transcription and translation system (14, 15, 18) as described in this study. However, one limitation of this method is the low yield of produced proteins, which is usually not enough to perform detailed analyses for biochemical and biophysical information. Recently, several studies have demonstrated the successful expression of actin and its mutant in the baculovirus/Sf9 cell system and have also shown that the expressed actin protein behaved like that purified from tissues (51-54). I have previously engineered both γ- and β-actins into the BaculoDirect™ C-Term Linear DNA plasmid (Invitrogen) and successfully expressed γ- and β-wild-type actins with a C-terminal V5-His fusion tag. However, these tagged actins were found to have defects in polymerization by *in vitro* polymerization assay (personal communication with our collaborator James Sellers at NIH). Right now, we are redesigning the constructs to express non-tagged γ- and β-actins. Preliminary experiments indicate that we can produce

mutant γ-actins in this baculovirus expression system and we can use this protein for quantitative biochemical and biophysical analyses.

To my knowledge, the biological profiles of CAP in different tissues are still not fully understood and there is no information about CAP in the inner ear. To investigate whether altered CAP binding is directly involved in disease development, I would like to first answer some questions: first, which CAP isoform (CAP1 or CAP2) is expressed in the inner ear; second, what is the subcellular localization and expression profile of CAP in normal hair cells; finally, how does the expression of CAP respond to the introduction of mutant γ-actins in the hair cells (explant cochlea culture) in the presence and absence of noise exposure. To address these questions, experiments including in situ hybridization, immunohistochemistry and confocal microscopy analyses, and gene-gun transfection of explant cochlea cultures will be tested in mice.

Above all, to investigate and better understand the disease-causing mechanism of human genetic diseases, an *in vivo* animal model is superior. Either transgenic mice or/and knock-in mice will give us more information about how this disease progresses in human cases.

REFERENCES

1. dos Remedios, C. G., D. Chhabra, M. Kekic, I. V. Dedova, M. Tsubakihara, D. A. Berry, and N. J. Nosworthy. 2003. Actin binding proteins: regulation of cytoskeletal microfilaments. *Physiol Rev* 83:433-473.

2. Moriyama, K., and I. Yahara. 2002. Human CAP1 is a key factor in the recycling of cofilin and actin for rapid actin turnover. *J Cell Sci* 115:1591-1601.

3. Balcer, H. I., A. L. Goodman, A. A. Rodal, E. Smith, J. Kugler, J. E. Heuser, and B. L. Goode. 2003. Coordinated regulation of actin filament turnover by a high-molecular-weight Srv2/CAP complex, cofilin, profilin, and Aip1. *Curr Biol* 13:2159-2169.

4. Bertling, E., P. Hotulainen, P. K. Mattila, T. Matilainen, M. Salminen, and P. Lappalainen. 2004. Cyclase-associated protein 1 (CAP1) promotes cofilin-induced actin dynamics in mammalian nonmuscle cells. *Mol Biol Cell* 15:2324-2334.

5. Bertling, E., O. Quintero-Monzon, P. K. Mattila, B. L. Goode, and P. Lappalainen. 2007. Mechanism and biological role of profilin-Srv2/CAP interaction. *J Cell Sci* 120:1225-1234.

6. Petit, C., J. Levilliers, and J. P. Hardelin. 2001. Molecular genetics of hearing loss. *Annu Rev Genet* 35:589-646.

7. Zhu, M., T. Yang, S. Wei, A. T. DeWan, R. J. Morell, J. L. Elfenbein, R. A. Fisher, S. M. Leal, R. J. Smith, and K. H. Friderici. 2003. Mutations in the gamma-actin gene (ACTG1) are associated with dominant progressive deafness (DFNA20/26). *Am J Hum Genet* 73:1082-1091.

8. van Wijk, E., E. Krieger, M. H. Kemperman, E. M. De Leenheer, P. L. Huygen, C. W. Cremers, F. P. Cremers, and H. Kremer. 2003. A mutation in the gamma actin 1 (ACTG1) gene causes autosomal dominant hearing loss (DFNA20/26). *J Med Genet* 40:879-884.

9. Rendtorff, N. D., M. Zhu, T. Fagerheim, T. L. Antal, M. Jones, T. M. Teslovich, E. M. Gillanders, M. Barmada, E. Teig, J. M. Trent, K. H. Friderici, D. A. Stephan, and L. Tranebjaerg. 2006. A novel missense mutation in ACTG1 causes dominant deafness in a Norwegian DFNA20/26 family, but ACTG1 mutations are not frequent among families with hereditary hearing impairment. *Eur J Hum Genet* 14:1097-1105.

10. Khaitlina, S. Y. 2001. Functional specificity of actin isoforms. *Int Rev Cytol* 202:35-98.

11. Geissler, S., K. Siegers, and E. Schiebel. 1998. A novel protein complex promoting formation of functional alpha- and gamma-tubulin. *EMBO J* 17:952-966.

12. Frydman, J., E. Nimmesgern, H. Erdjument-Bromage, J. S. Wall, P. Tempst, and F. U. Hartl. 1992. Function in protein folding of TRiC, a cytosolic ring complex containing TCP-1 and structurally related subunits. *EMBO J* 11:4767-4778.

13. Gao, Y., J. O. Thomas, R. L. Chow, G. H. Lee, and N. J. Cowan. 1992. A cytoplasmic chaperonin that catalyzes beta-actin folding. *Cell* 69:1043-1050.

14. Costa, C. F., H. Rommelaere, D. Waterschoot, K. K. Sethi, K. J. Nowak, N. G. Laing, C. Ampe, and L. M. Machesky. 2004. Myopathy mutations in alpha-skeletal-muscle actin cause a range of molecular defects. *J Cell Sci* 117:3367-3377.

15. Vang, S., T. J. Corydon, A. D. Borglum, M. D. Scott, J. Frydman, J. Mogensen, N. Gregersen, and P. Bross. 2005. Actin mutations in hypertrophic and dilated cardiomyopathy cause inefficient protein folding and perturbed filament formation. *FEBS J* 272:2037-2049.

16. Safer, D. 1989. An electrophoretic procedure for detecting proteins that bind actin monomers. *Anal Biochem* 178:32-37.

17. Hansen, W. J., N. J. Cowan, and W. J. Welch. 1999. Prefoldin-nascent chain complexes in the folding of cytoskeletal proteins. *J Cell Biol* 145:265-277.

18. Rommelaere, H., D. Waterschoot, K. Neirynck, J. Vandekerckhove, and C. Ampe. 2004. A method for rapidly screening functionality of actin mutants and tagged actins. *Biol Proced Online* 6:235-249.

19. Laemmli, U. K. 1970. Cleavage of structural proteins during the assembly of the head of bacteriophage T4. *Nature* 227:680-685.

20. Vainberg, I. E., S. A. Lewis, H. Rommelaere, C. Ampe, J. Vandekerckhove, H. L. Klein, and N. J. Cowan. 1998. Prefoldin, a chaperone that delivers unfolded proteins to cytosolic chaperonin. *Cell* 93:863-873.

21. Rommelaere, H., M. Van Troys, Y. Gao, R. Melki, N. J. Cowan, J. Vandekerckhove, and C. Ampe. 1993. Eukaryotic cytosolic chaperonin contains t-complex polypeptide 1 and seven related subunits. *Proc Natl Acad Sci U S A* 90:11975-11979.

22. McCormack, E. A., M. J. Rohman, and K. R. Willison. 2001. Mutational screen identifies critical amino acid residues of beta-actin mediating interaction between its folding intermediates and eukaryotic cytosolic chaperonin CCT. *J Struct Biol* 135:185-197.

23. Bross, P., T. J. Corydon, B. S. Andresen, M. M. Jorgensen, L. Bolund, and N. Gregersen. 1999. Protein misfolding and degradation in genetic diseases. *Hum Mutat* 14:186-198.

24. Rommelaere, H., D. Waterschoot, K. Neirynck, J. Vandekerckhove, and C. Ampe. 2003. Structural plasticity of functional actin: pictures of actin binding protein and polymer interfaces. *Structure* 11:1279-1289.

25. Antecol, M. H., A. Darveau, N. Sonenberg, and B. B. Mukherjee. 1986. Altered biochemical properties of actin in normal skin fibroblasts from individuals predisposed to dominantly inherited cancers. *Cancer Res* 46:1867-1873.

26. Morrison, P. R., G. W. Muller, and F. W. Booth. 1987. Actin synthesis rate and mRNA level increase during early recovery of atrophied muscle. *Am J Physiol* 253:C205-209.

27. Velick, S. F. 1956. The metabolism of myosin, the meromyosins, actin and tropomyosin in the rabbit. *Biochim Biophys Acta* 20:228-236.

28. Sonnemann, K. J., D. P. Fitzsimons, J. R. Patel, Y. Liu, M. F. Schneider, R. L. Moss, and J. M. Ervasti. 2006. Cytoplasmic gamma-actin is not required for skeletal muscle development but its absence leads to a progressive myopathy. *Dev Cell* 11:387-397.

29. Bryan, K. E., K. K. Wen, M. Zhu, N. D. Rendtorff, M. Feldkamp, L. Tranebjaerg, K. H. Friderici, and P. A. Rubenstein. 2006. Effects of human deafness gamma-actin mutations (DFNA20/26) on actin function. *J Biol Chem* 281:20129-20139.

30. Chaudhry, F., C. Guerin, M. von Witsch, L. Blanchoin, and C. J. Staiger. 2007. Identification of Arabidopsis cyclase-associated protein 1 as the first nucleotide exchange factor for plant actin. *Mol Biol Cell* 18:3002-3014.

31. Drees, B. L., B. Sundin, E. Brazeau, J. P. Caviston, G. C. Chen, W. Guo, K. G. Kozminski, M. W. Lau, J. J. Moskow, A. Tong, L. R. Schenkman, A. McKenzie, 3rd, P. Brennwald, M. Longtine, E. Bi, C. Chan, P. Novick, C. Boone, J. R. Pringle, T. N. Davis, S. Fields, and D. G. Drubin. 2001. A protein interaction map for cell polarity development. *J Cell Biol* 154:549-571.

32. Hu, B. H., D. Henderson, and T. M. Nicotera. 2002. Involvement of apoptosis in progression of cochlear lesion following exposure to intense noise. *Hear Res* 166:62-71.

33. Hultcrantz, M., and H. S. Li. 1995. Degeneration patterns of actin distribution in the organ of corti in two genotypes of mice. *ORL J Otorhinolaryngol Relat Spec* 57:1-4.

34. Li, H. S., and M. Hultcrantz. 1994. Age-related degeneration of the organ of Corti in two genotypes of mice. *ORL J Otorhinolaryngol Relat Spec* 56:61-67.

35. Agrawal, P. B., C. D. Strickland, C. Midgett, A. Morales, D. E. Newburger, M. A. Poulos, K. K. Tomczak, M. M. Ryan, S. T. Iannaccone, T. O. Crawford, N. G. Laing, and A. H. Beggs. 2004. Heterogeneity of nemaline myopathy cases with skeletal muscle alpha-actin gene mutations. *Ann Neurol* 56:86-96.

36. Laing, N. G., N. F. Clarke, D. E. Dye, K. Liyanage, K. R. Walker, Y. Kobayashi, S. Shimakawa, T. Hagiwara, R. Ouvrier, J. C. Sparrow, I. Nishino, K. N. North, and I. Nonaka. 2004. Actin mutations are one cause of congenital fibre type disproportion. *Ann Neurol* 56:689-694.

37. Pedersen, C. B., P. Bross, V. S. Winter, T. J. Corydon, L. Bolund, K. Bartlett, J. Vockley, and N. Gregersen. 2003. Misfolding, degradation, and aggregation of variant proteins. The molecular pathogenesis of short chain acyl-CoA dehydrogenase (SCAD) deficiency. *J Biol Chem* 278:47449-47458.

38. Waters, P. J. 2003. How PAH gene mutations cause hyperphenylalaninemia and why mechanism matters: insights from in vitro expression. *Hum Mutat* 21:357-369.

39. Corydon, T. J., P. Bross, T. G. Jensen, M. J. Corydon, T. B. Lund, U. B. Jensen, J. J. Kim, N. Gregersen, and L. Bolund. 1998. Rapid degradation of short-chain acyl-CoA dehydrogenase variants with temperature-sensitive folding defects occurs after import into mitochondria. *J Biol Chem* 273:13065-13071.

40. Yaguchi, H., N. Ohkura, M. Takahashi, Y. Nagamura, I. Kitabayashi, and T. Tsukada. 2004. Menin missense mutants associated with multiple endocrine neoplasia type 1 are rapidly degraded via the ubiquitin-proteasome pathway. *Mol Cell Biol* 24:6569-6580.

41. Feldman, D. E., C. Spiess, D. E. Howard, and J. Frydman. 2003. Tumorigenic mutations in VHL disrupt folding in vivo by interfering with chaperonin binding. *Mol Cell* 12:1213-1224.

42. Wertman, K. F., D. G. Drubin, and D. Botstein. 1992. Systematic mutational analysis of the yeast ACT1 gene. *Genetics* 132:337-350.

43. Drummond, D. R., E. S. Hennessey, and J. C. Sparrow. 1991. Characterisation of missense mutations in the Act88F gene of Drosophila melanogaster. *Mol Gen Genet* 226:70-80.

44. Sparrow, J. C., D. R. Drummond, E. S. Hennessey, J. D. Clayton, and F. B. Lindegaard. 1992. Drosophila actin mutants and the study of myofibrillar assembly and function. *Symp Soc Exp Biol* 46:111-129.

45. Ilkovski, B., K. J. Nowak, A. Domazetovska, A. L. Maxwell, S. Clement, K. E. Davies, N. G. Laing, K. N. North, and S. T. Cooper. 2004. Evidence for a dominant-negative effect in ACTA1 nemaline myopathy caused by abnormal folding, aggregation and altered polymerization of mutant actin isoforms. *Hum Mol Genet* 13:1727-1743.

46. Sparrow, J. C., K. J. Nowak, H. J. Durling, A. H. Beggs, C. Wallgren-Pettersson, N. Romero, I. Nonaka, and N. G. Laing. 2003. Muscle disease caused by mutations in the skeletal muscle alpha-actin gene (ACTA1). *Neuromuscul Disord* 13:519-531.

47. Nowak, K. J., C. A. Sewry, C. Navarro, W. Squier, C. Reina, J. R. Ricoy, S. S. Jayawant, A. M. Childs, J. A. Dobbie, R. E. Appleton, R. C. Mountford, K. R. Walker, S. Clement, A. Barois, F. Muntoni, N. B. Romero, and N. G. Laing. 2007. Nemaline myopathy caused by absence of alpha-skeletal muscle actin. *Ann Neurol* 61:175-184.

48. Brault, V., U. Sauder, M. C. Reedy, U. Aebi, and C. A. Schoenenberger. 1999. Differential epitope tagging of actin in transformed Drosophila produces distinct effects on myofibril assembly and function of the indirect flight muscle. *Mol Biol Cell* 10:135-149.

49. Goode, B. L. 2006. Srv2/cyclase-associated protein (CAP): a multi-functional recycling center for actin monomers and cofilin. In "*Actin monomer binding proteins*," Editor: P. Lappalainen. *Landes Bioscience*, pp. 45-52.

50. Frankel, S., J. Condeelis, and L. Leinwand. 1990. Expression of actin in Escherichia coli. Aggregation, solubilization, and functional analysis. *J Biol Chem* 265:17980-17987.

51. Anthony Akkari, P., K. J. Nowak, K. Beckman, K. R. Walker, F. Schachat, and N. G. Laing. 2003. Production of human skeletal alpha-actin proteins by the baculovirus expression system. *Biochem Biophys Res Comm* 307:74-79.

52. Joel, P. B., P. M. Fagnant, and K. M. Trybus. 2004. Expression of a nonpolymerizable actin mutant in Sf9 cells. *Biochemistry* 43:11554-11559.

53. Bookwalter, C. S., and K. M. Trybus. 2006. Functional consequences of a mutation in an expressed human alpha-cardiac actin at a site implicated in familial hypertrophic cardiomyopathy. *J Biol Chem* 281:16777-16784.

54. Yates, S. P., M. D. Otley, and J. F. Dawson. 2007. Overexpression of cardiac actin with baculovirus is promoter dependent. *Arch Biochem Biophys* 466:58-65.

CHAPTER 3

Mei Zhu, Kathryn L. Lovell, Jon S. Patterson, Thomas L. Saunders, Elizabeth D. Hughes and Karen H. Friderici. Beta-Mannosidosis mice: a model for the human lysosomal storage disease. *Human Molecular Genetics*, 2006, Vol. 15, No. 3, 493-500.

I was responsible for this study and have been working on and following the mouse colony since I initiated this project. I designed and constructed the targeting vector, screened the ES cells, and carried out the mouse breeding. I conducted the characterization of the β-mannosidase null mice including examination of the general health and growth, behavior test, enzyme activity assays, dissection of tissues for histological examination and oligosaccharide analysis.

ABSTRACT

β-Mannosidase, a lysosomal enzyme which acts exclusively at the last step of oligosaccharide catabolism in glycoprotein degradation, functions to cleave the unique β-linked mannose sugar found in all N-linked oligosaccharides of glycoproteins. Deficiency of this enzyme results in β-mannosidosis, a lysosomal storage disease characterized by the cellular accumulation of small oligosaccharides. In human β-mannosidosis, the clinical presentation is variable and can be mild, even when caused by functionally null mutations. In contrast, two existing ruminant animal models have disease that is consistent and severe. To further explore the molecular pathology of this disease and to investigate potential treatment strategies, we produced a β-mannosidase knockout mouse. Homozygous mutant mice have undetectable β-mannosidase activity. General appearance and growth of the knockout mice are similar to the wild-type littermates. At >1 year of age, these mice exhibit no dysmorphology or overt neurological problems. The mutant animals have consistent cytoplasmic vacuolation in the central nervous system and minimal vacuolation in most visceral organs. Thin-layer chromatography demonstrated an accumulation of disaccharide in epididymis and brain. This mouse model closely resembles human β-mannosidosis and provides a useful tool for studying the phenotypic variation in different species and will facilitate the study of potential therapies for lysosomal storage diseases.

INTRODUCTION

Lysosomal storage diseases constitute a significant portion of genetic disease. Dysfunction of any one of the more than 40 enzymes that reside in the lysosome results in the accumulation of the associated uncatabolized substrate (1, 2). Accumulation of this substrate or toxic intermediates may lead to cellular toxicity. Storage occurs in various cell types, but clinical symptoms characteristic of lysosomal storage disease are often referable to the nervous system and include progressive mental and motor retardation and impaired hearing, as well as dysostosis, and immune defects. Disease presentation can range from severe and consistent to mild and variable depending on the enzyme involved, the severity of the mutation and the species concerned.

β-Mannosidosis (MIM no. 248510 [OMIM]) is a rare lysosomal storage disease that was identified first in Nubian goats (3) and subsequently in humans (4, 5) The Salers breed of cattle also has the disease (6). Affected goats and cattle have very similar clinical features that include inability to stand, facial dysmorphism (dome-shaped skulls, small palpebral fissures, depressed nasal bridge and elongated, narrow muzzle), intention tremors, multiple muscle contractures and digital joint hyperextension (6, 7). Affected animals die in the neonatal period if intensive care is not provided. Gross neuropathological characteristics include ventricular dilation with a marked paucity of myelin in cerebral hemispheres and cerebellum. Microscopic examination reveals

extensive cytoplasmic vacuolation in the nervous system and visceral organs, restricted to specific cell types. Regionally specific myelin deficiency is present in the central nervous system but not in peripheral nerves (7-9). Affected goats and calves are hypothyroid and thyroid follicular epithelium shows severe vacuolation (10, 11). β-Mannosidosis cases in the two ruminant species result from severe mutations that totally inactivate enzymatic activity of the protein (12, 13).

In contrast with ruminant β-mannosidosis, human cases have a milder and heterogeneous clinical expression (14). The most severe cases are associated with mental retardation, developmental delay, dysmorphology, frequent infections and hearing loss (4, 5, 15-18). Siblings with the disease may have differing levels of severity (19). Onset can be in the neonatal period, with hypotonia, swallowing difficulties or seizures as presenting symptoms (20, 21). In contrast to ruminant β-mannosidosis, many of the affected individuals, including those with null mutations, achieve maturity and can have comparatively mild disease (22-24). None of the human cases had clinical signs indicative of central nervous system hypomyelination. No human β-mannosidosis cases have been submitted to autopsy, so little is known about the distribution of storage material or severity of tissue vacuolation.

In the lysosome, N-linked glycoproteins are degraded sequentially from the non-reducing end of the molecule. β-Mannosidase (*MANBA*; 3.2.1.25 [EC]) is required for the final degradative cleavage of the glycan moiety of glycoproteins in humans, rodents and lagomorphs. In these species, the non-sequential

cleavage of the GlcNAc(β1–4) GlcNAc bond can be accomplished by chitobiase, an enzyme that is not present in ruminants and carnivores (25). Therefore, lack of β-mannosidase in humans results in storage of the disaccharide Man(β1–4)GlcNAc (26, 27), whereas in ruminants, storage of the trisaccharide Man(β1–4)GlcNAc(β1–4)GlcNAc predominates (28, 29). The β-mannoside linkage is unique to N-linked glycoproteins; therefore, unlike most other lysosomal enzymes, β-mannosidase has only a single substrate in the cell. In addition, the accumulated substrate that is stored in β-mannosidosis is an unusually small molecule.

Reasons for the phenotypic differences between human and ruminant β-mannosidosis are unknown but speculation has centered on differences in the size and nature of the storage product and in the different developmental programs of the species (14). To address these aspects of the molecular pathology, we developed and characterized a mouse model of β-mannosidosis.

MATERIALS AND METHODS

Construction of the targeting vector. We cloned and sequenced the full-length cDNA of the murine β-mannosidase gene (GenBank accession no. AF306557, and data not shown). Using mouse-specific sequence information and

the genomic structure of the human β-mannosidase gene, a portion of the β-mannosidase gene bearing genomic sequences from intron 3 to intron 7 was cloned from a 129X1/SvJ mouse genomic library (Stratagene) by using a PCR-based screening (30). We chose exon 5 for disruption because it is an out-of-frame exon; the splicing of exon 4 to exon 6 would result in the introduction of a premature translational stop codon. A 1.4 kb PCR fragment containing a part of intron 4 and 20 bp of exon 5 was cloned into *Xho*I sites in front of the neo cassette of the pPNT vector (31) (Fig. 3-1A). The downstream 5.7 kb segment of the homologous region was cloned into the vector in two steps. First, an *Xba*I/*Eco*RI fragment containing 1.6 kb of intron 5 was inserted into the *Xba*I/*Eco*RI digested vector. Then, a *Sal*I/*Eco*RI adaptor was added to the 4.1 kb *Eco*RI/*Sal*I fragment bearing exons 6 and 7 and subsequently was inserted into the *Eco*RI site of the construct. The final construct was sequenced to confirm the boundaries of the homologous region.

Gene targeting in ES cells and generation of null mutant mice. The vector was linearized with *Not*I restriction endonuclease before electroporation into R1 ES cells (32). After positive (G418 for neo gene) and negative (gangciclovir for TK gene) drug selection, we screened five 96-well culture plates by PCR analysis using primers c, b and d (Fig. 3-1A). The primer sequences were: c, 5'-ACAGGAGTGGTTAGGCATCG-3'; b, 5'-AGATTCCCTGAGAGGGGAAG-3' and d, 5'-CTGTCCATCTGCACGAGACT-3'. Five correctly targeted ES clones were expanded and confirmed by PCR and Southern blot analysis using the 5'-probe and were subjected to a chromosome count. Eventually, four ES clones were

injected into C57BL/6J blastocysts. Chimeric males with 90% or more agouti coat color were back-crossed to C57BL/6J females and 129X1/SvJ females (data not shown). The heterozygous F1 mice were intercrossed for experimental use and back-crossed to C57BL/6J mice to generate a congenic background. The F1 and F2 mice were genotyped by PCR analysis (3 min denaturation at 94°C, then 35 cycles of 30 s at 94°C, 30 s at 60°C and 30 s at 72°C) on tail DNA. Primers for genotyping were a, 5'-CTCAGGACCTTCGGAAGAAC-3', b and d (Fig. 3-1A). The genotypes of F2 mice were further confirmed for gene disruption by Southern blot analysis using the 5'-probe (Fig. 3-1A and B). The 5'-probe is a 781 bp PCR product from intron sequence outside of the homologous region. Total RNA was isolated from tissues (kidney and testis) of homozygous mutant, heterozygote and wild-type mice using TRIzol reagent (cat. no. 15 596, Invitrogen). RT–PCR was performed for detection of transcripts. Mice from two independent lines were analyzed, and there was no phenotypic difference between them.

Enzyme assays. Tissue extracts from 6- and 36-week-old mice were prepared as previously described (Lovell *et al.* (33)). Enzyme activity was determined using the fluorogenic substrate, 4-methyl-umbelliferyl-β-D-mannopyranoside (M0905, Sigma). For comparison, α-mannosidase and acid phosphatase were also assayed fluorometrically using substrates 4-methyl-umbelliferyl-α-D-mannopyranoside (M4383, Sigma) and 4-methylumbelliferyl phosphate (M8883, Sigma), respectively. For enzyme assays, 20 µl of substrate was added to 10 µl of the tissue extract and incubated at 37°C for 30 min (β-mannosidase) or 10 min for other enzymes. Each tissue extract was run in duplicate. Reactions were

stopped by adding 170 µl 0.1 M glycine (pH>10.8). Fluorescence of the liberated 4-MU was measured using a luminescence spectrometer (LS50B, Perkin Elmer). Proteins were determined by the BCA method (no. 23225, Pierce). A one-tailed *t*-test for equality of the mean was used to determine the statistical significance of the difference in α-mannosidase activity between mutant and wild-type mice.

Pathological examinations. Tissue samples (including brain, optic nerve, spinal cord, thyroid gland, kidney, heart, spleen, liver, pancreas, adrenal gland, lung, skin, bone, skeletal muscle, epididymis, peripheral nerve, testes, duodenum, uterus) were removed immediately after euthanasia with carbon dioxide and fixed in 10% formalin for paraffin embedding, 4% paraformaldehyde for Immunobed embedding or 4% glutaraldehyde for Epon embedding. Tissues were examined from 11 mutant animals (one at 4 weeks, two at 6 weeks, four at 18 weeks and four at 37 weeks of age) and six control animals (at least one at each age). H&E-stained 6 µm paraffin sections and/or Toluidine blue-stained, 1 µm sections were examined under light microscopy for all tissues. For some animals, 3 µm Immunobed sections showing one coronal hemisphere were stained with H&E or Toluidine blue. Selected tissues that showed pathological changes were examined by electron microscopy.

Oligosaccharide analysis. Tissue from control and homozygous mutant mice was minced on ice and sonicated for 30 s in 5 ml distilled deionized water per gram of tissue. After centrifugation for 10 min at 15 000*g*, the supernatant was transferred to a fresh tube (34). Lipids and proteins were removed by extraction

with 4 vol of $CHCl_3$/methanol (3:1). The aqueous supernatant was evaporated and the residue resuspended in H_20 at 1/10 the original volume. Two microliter samples were applied to silica gel 60 plates (5721-7, EM Science® Merk®) and developed for 1 h in 4:1 acetonitrile/H_2O (35). Oligosaccharides were visualized with 0.2% orcinal in 20% sulfuric acid.

RESULTS

Generation of β-mannosidase-deficient mice

A targeting vector was constructed to disrupt the murine β-mannosidase gene (*Manba*) (Fig. 3-1A). Following drug selection, 480 ES cell clones were screened by PCR and 108 correctly targeted clones (22.5% recombinant efficiency) were identified. Four euploid clones were injected into blastocysts. In total, 31 chimeric mice (24 males and seven females) were identified by coat color. Three chimeric males with germline transmission from two independent ES clones were backcrossed to C57BL/6J females. Thirty-nine F1 heterozygous mice (17 males and 22 females) were generated and 22 of them (four males and 18 females) were intercrossed for experimental use. A total of 199 F2 mice from two independent ES lines were born, and the offspring showed expected Mendelian ratios: 20.1% for wild-types, 29.1% for homozygous mutants and

Figure 3-1. Targeted disruption of the murine β-mannosidase gene. (**A**) The structure of the endogenous β-mannosidase gene, the targeting construct and the disrupted allele. The targeting construct contains 1.4 kb of 5'-homologous sequence and 5.8 kb of 3'-homologous sequence (bold lines). The 5'probe (bar) and PCR primers (arrows) used to screen for recombinant ES clones (c, b, d) and to screen mouse litters (a, b, d) are indicated. Exons are shown as filled boxes. (**B**) Southern blot analysis of tail DNA. The 5'probe was hybridized to *Bci*VI-digested genomic DNA: wild-type allele, 19 kb; mutant allele, 6.4 kb. (**C**) PCR-based screening for the homologous recombinant ES clones. The primer pairs were c+b for wild-type allele (1.5 kb) and c+d for disrupted allele (1.8 kb). Lanes 1 and 2 are wild-type ES lines; lanes 3 and 4 are targeted ES cell lines. (**D**) PCR analysis of tail genomic DNA with primer pairs of a+b for wild-type mouse (210 bp) and a+d for the disrupted allele (470 bp).

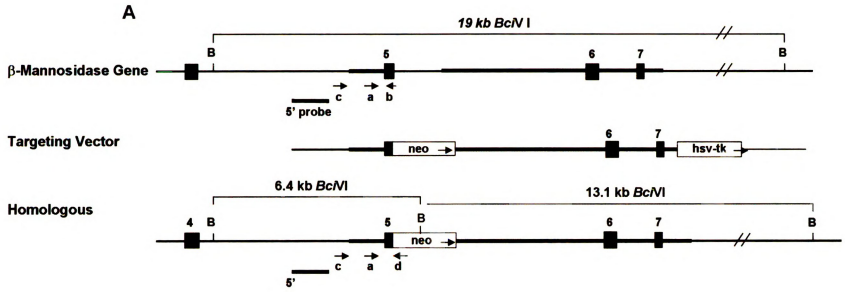
A
19 kb BclV I
B
5
6
7
B
β-Mannosidase Gene
c
a
b
5' probe
Targeting Vector
neo
6
7
hsv-tk
6.4 kb BclVI
13.1 kb BclVI
Homologous
4
B
5
B
neo
6
7
B
c
a
d
5'
B
+/+
+/-
-/-
19.0 kb
6.4 kb
C
1
2
3
4
1.8 kb
1.5 kb
D
+/-
+/+
-/-
+/+
470 bp
210 bp

50.8% for heterozygotes. RT–PCR (data not shown) demonstrated the deletion of exon 5. Homozygous mutant, heterozygous and wild-type mice did not exhibit differences in general appearance, growth or weight. Both males and females were fertile. No obvious mortality and behavior changes were observed to over 12 months of age. There were no phenotypic and biological differences between mutant mice from two independent ES clones.

Biochemical findings

Enzyme activity. β-Mannosidase activity was determined in plasma and tissue homogenates from kidney, liver, spleen, pancreas, brain, testis, epididymis, heart, lung and skeletal muscle. Homozygous mutant mice had no detectable activity in any tissue, confirming the targeted allele was not functional. Heterozygotes had approximately half the enzyme activity of the wild-type (Fig. 3-2A). α-Mannosidase and acid phosphatase were assayed at the ages of 6 and 36 weeks for comparison. The α-mannosidase activity was increased in the mutant when compared with the wild-type, especially at older ages (Fig. 3-2B), whereas the acid phosphatase activity measured at the two ages was not different between mutant and wild-type (Fig. 3-2C).

Pathological characterizations of organs

Tissues from control and mutant mice between the ages of 4 and 37 weeks were analyzed in H&E-stained 6 μm paraffin sections and, for some tissues, in Toluidine blue-stained, 1 μm sections. Histological evidence of storage was

Figure 3-2. β-Mannosidase activity and other lysosomal enzyme activity assay. For each group, four mice were analyzed. Error bars represent one standard deviation. Enzyme activities are expressed as nmol/h/mg protein. **(A)** β-Mannosidase activities were assayed in tissues of homozygous mutant (–/–), heterozygous (+/–) and wild-type mice (+/+). The enzyme activity of the homozygous mutant was non-detectable. **(B)** Activities of α-mannosidase and acid phosphatase were assayed in tissues of homozygous mutant and wild-type mice at two different ages. α-Mannosidase activities increased in the tissues of homozygous mutants when compared with wild-type, and especially at the older age. Significant differences ($P>0.005$) between mutant and wild-type are marked with asterisks (*) **(C)** The enzyme activity of acid phosphatase showed no difference between mutant and wild-type mice.

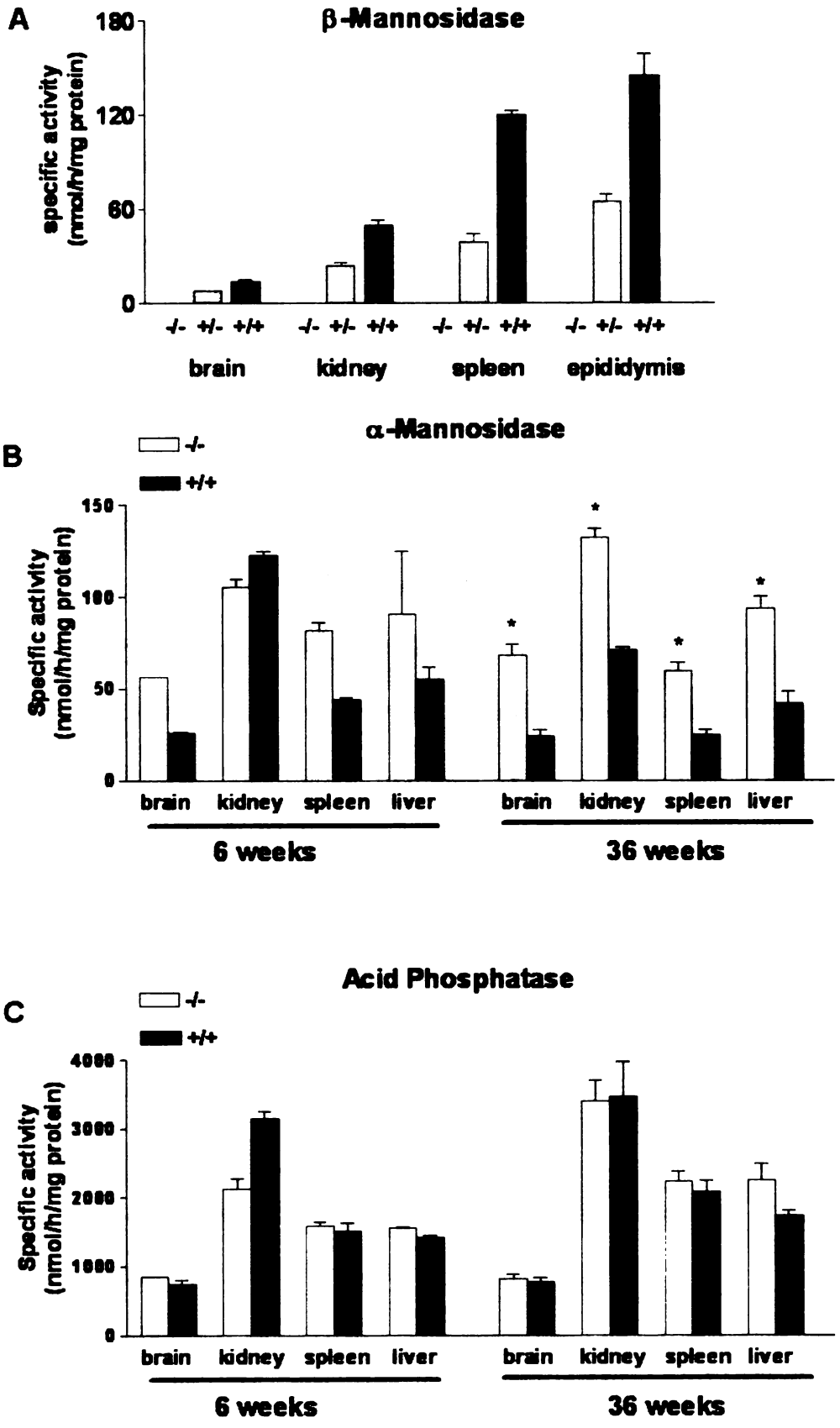
A
β-Mannosidase
specific activity (nmol/h/mg protein)
180
120
60
0
-/- +/- +/+
brain
kidney
spleen
epididymis
B
α-Mannosidase
-/-
+/+
Specific activity (nmol/h/mg protein)
150
100
50
0
brain
kidney
spleen
liver
6 weeks
36 weeks
C
Acid Phosphatase
-/-
+/+
Specific activity (nmol/h/mg protein)
4000
3000
2000
1000
0
brain
kidney
spleen
liver
6 weeks
36 weeks

apparent in selected organs of all mutant mice, although there was variation that did not correlate consistently with age.

Epididymis. Small numbers of epithelial cells lining the ducts in the body of the epididymis contained fine, clear vacuoles in the apical cytoplasm. In a few cells, the cytoplasm was filled diffusely with fine to coarse vacuoles; electron microscopy revealed these vacuoles to be electron-lucent and membrane-bound (Fig. 3-3B+inset). Vacuolation in the epithelium lining the head and tail of the epididymis was not apparent.

Liver. In both control and mutant animals, most hepatocytes showed some degree of indistinctly and finely vacuolated, granular cytoplasm which represented glycogen storage, as confirmed by periodic acid Schiff (PAS) stain. However, in mutant mice only, very small numbers of hepatocytes contained discrete, fine, clear intracytoplasmic vacuoles even in PAS-stained sections. Occasional Kupffer cells and sinusoidal endothelial cells also contained fine intracytoplasmic vacuoles.

Kidney. In the kidney, fine to coarse vacuoles in the apical cytoplasm of both proximal and distal tubular epithelial cells were present in Toluidine blue-stained, 1 μm sections, although the number of affected cells was small (Fig. 3-3D).

Thyroid gland. Fine, intracytoplasmic vacuoles were present in small numbers of follicular epithelial cells from the thyroid gland, and most cells showed no vacuolation (Fig. 3-3F).

Figure 3-3. (A–F) Organ histopathology of β-mannosidase –/– mice compared with wild-type mice. All light microscopic sections were from 18-week-old mice, stained with Toluidine blue. Magnification 50x. (A and B) Body of epididymis of control (A) and mutant (B) mice. Mutant mice have scattered cells with fine, intracytoplasmic vacuoles; the inset shows an electron micrograph of a diffusely vacuolated cell. (C and D) Kidneys of control (C) and mutant (D) mice. Occasional tubular epithelial cells in kidneys from mutant mice contained fine, intracytoplasmic vacuoles. (E and F) Thyroid glands of control (E) and mutant (F) mice. Follicular epithelial cells from mutant mice did not show the level of vacuolation seen in ruminants (**G** and **H**), although they occassionally contained fine, intracytoplasmic vacuoles not evident here. Thyroid glands of control (G) and mutant (H) newborn goats for comparison.

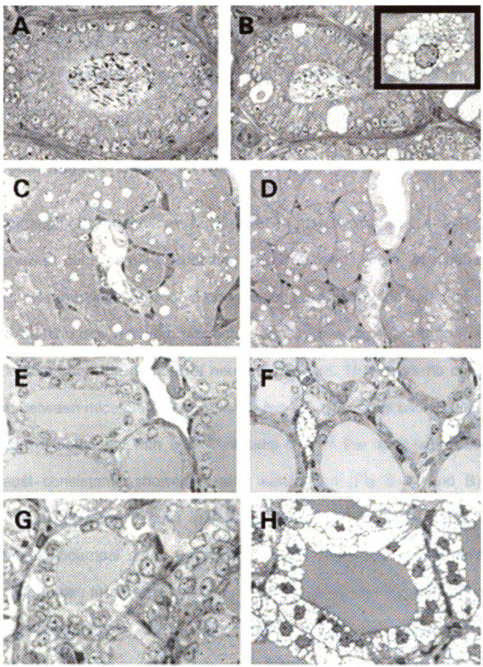
A
B
C
D
E
F
G
H

Other organs. In the duodenum, intracytoplasmic vacuoles were observed in some mutant animals in scattered smooth muscle cells of the outer longitudinal muscular layer and in occasional myenteric plexus neurons. Routine light microscopic examination revealed no significant histological findings in skin, heart, spleen, skeletal muscles (thigh), lung, pancreas, adrenal gland, testis, uterus and bone.

Pathological characterization of central nervous system

Examination of central nervous system of 11 mutant mice from 4 to 37 weeks of age showed cytoplasmic vacuolation in all animals. There was substantial variation in severity of vacuolation among regions examined and variation among animals. Variation occurred with respect to density of vacuoles within a neuron, size of vacuoles and the number of neurons affected. There was no consistent difference between mice generated from the two ES cell clones and no consistent progression of pathology with age. Pyramidal cells in the dorsolateral cerebral cortex most consistently showed severe vacuolation (Fig. 3-4A and B). The choroid plexus also consistently showed conspicuous vacuolation (Fig. 3-4D). Within the hippocampal cornu ammonis, specific segments of Ammon's horn showed differences in severity of vacuolation (Fig. 3-4E and F), with substantial variation among animals. Other regions with neuronal vacuolation to various extents included striatum, amygdala and deep cerebellar nuclei (Fig. 3-4G). Hypomyelination in optic nerve or corpus callosum was not apparent in Toluidine

Figure 3-4. Neuropathology of β-mannosidase –/– mice compared with wild-type mice. (**A**) Dorsal cortex neurons of a 6-week-old mutant show severe vacuolation, 300x. (**B**) Electron micrograph of a cortical neuron from a 19-week-old mutant showing intracytoplasmic vacuolation, 2200x. (**C** and **D**) Choroid plexus from control (C) and mutant (D) mice, showing severe vacuolation in the mutant mouse, 250x. (**E** and **F**) Sections from the hippocampus of a 37-week-old mutant mouse showing absence of vacuolation in CA4 (E) and large vacuoles in pyramidal cells in CA1 (F), 300x. (**G**) Vacuolated neurons in deep cerebellar nucleus of a 37-week-old mutant mouse, 250x. (**H**) Vacuolated spinal cord motor neuron from an 18-week-old mutant mouse, 250x.

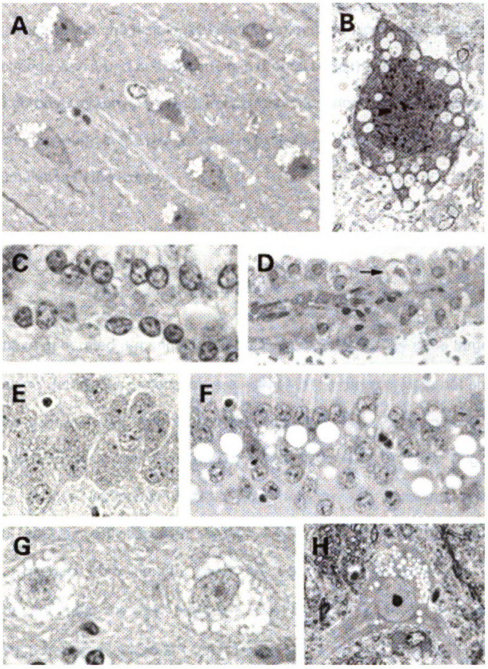
A
B
C
D
E
F
G
H

blue-stained, 1 μm sections. In spinal cord, neuronal cell bodies at all levels (cervical, thoracic, lumbar) contained fine, intracytoplasmic vacuoles (Fig. 3-4H).

Accumulation of oligosaccharides in tissues

In agreement with the histological findings in mutant mice, accumulation of oligosaccharide was found primarily in brain (frontal cortex) and epididymis by thin-layer chromatography (Fig. 3-5). In contrast to the storage seen in goats, the oligosaccharide found in the mutant mice is exclusively disaccharide, and there is little accumulation in the kidney.

DISCUSSION

We have generated β-mannosidase-deficient mouse lines by gene targeting. There was no detectable β-mannosidase activity in the plasma (data not shown) and tissue homogenates from homozygous mutant mice. Heterozygous mice showed approximately half the enzyme activity of wild-type mice (Fig. 3-2). Deficiency of one lysosomal enzyme often causes the elevation of other lysosomal enzyme activities (36), especially those in the same degradation pathway. Tissues from human cases of β-mannosidosis have not been evaluated, but goat tissues have elevated levels of α-mannosidase, α-fucosidase, β-hexosaminidase A and β-glucuronidase in kidney and brain (3, 37). We examined α-mannosidase activity (Fig. 3-2) and found elevation of activity in

Figure 3-5. Thin-layer of oligosaccharides in β-mannosidosis mice. Equal amounts of extract from kidney (kid), frontal cortex (brn) and epididymis (epi) from 9-month-old control (+/+) and homozygous mutant (–/–) mice were applied to silica gel 60 TLC plates. Chromatography controls, not shown here, were 2 µg monosaccharide (glucose), disaccharide (sucrose) and trisaccharide (raffinose). Authentic storage material from affected goat kidney (GK) is shown. Monosaccharide (MS), disaccharide Manβ(1–4)GlcNAc (DS) and trisaccharide Manβ(1–4)GlcNAc(β1–4) GlcNAc (TS) are indicated.

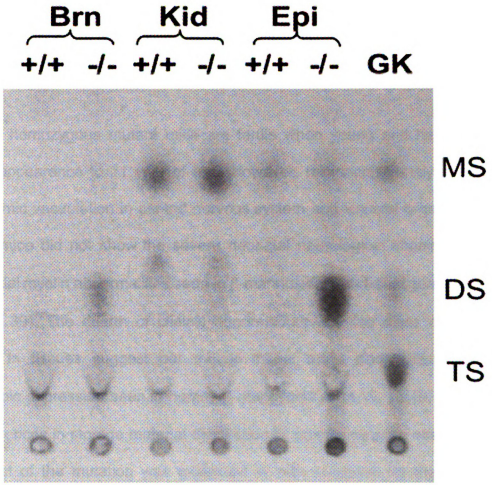
Brn
Kid
Epi
+/+
-/-
+/+
-/-
+/+
-/-
GK
MS
DS
TS

brain, spleen and liver of the mutant mice at young age (6 weeks) and statistically significant increases in all tested tissues at older age (36 weeks). Acid phosphatase, an enzyme not in the N-linked glycoprotein degradation pathway, was assayed for comparison. As expected, acid phosphatase activity (Fig. 3-2) was not different between the mutant and wild-type mice. These enzymatic findings coupled with the genomic findings indicate successful disruption of the β-mannosidase gene.

The homozygous mutant mice are fertile when young and have a normal clinical appearance to >1 year of age. However, microscopic analysis revealed cytoplasmic vacuolation in central nervous system and visceral organs. The null mutant mice did not show the severe neonatal neurological impairment or the substantial myelin abnormalities seen in β-mannosidase-deficient goats and cattle (33, 38, 39). The dearth of clinical abnormalities and the signs of lysosomal storage in tissues suggest our mouse model more closely resembles the phenotypic expression seen in human β-mannosidosis (4, 5, 15-19, 21, 24, 40). No differences in storage material distribution or phenotype were observed when the effect of the mutation was examined in mice congenic for the 129X1/SvJ background (data not shown).

Little is known about the distribution of storage material or severity of cytoplasmic vacuolation in human cases. Only blood and skin biopsy specimens have been examined and these showed cytoplasmic vacuolation of cells in blood and lymph vessels, endothelial cells, fibroblasts, secretary portions of eccrine

sweat glands, neural cells and basal keratinocytes in the epidermis in angiokeratoma lesions (24, 40, 41). Light and electronic microscopic examination of the homozygous mutant mice revealed cytoplasmic vacuolation in the central nervous system and some visceral organs but not in all the organs examined. Many of the affected humans show mental retardation and emotional changes (4, 5, 15-17, 19, 41, 42). We did not see obvious physical or behavioral abnormalities in the β-mannosidase-deficient mice, including preliminary tests such as rotarod, open field and hanging wire (data not shown). Taken together, further behavioral testing in the mice to more specifically analyze learning, working memory, long-term memory and fear conditioning will be necessary to investigate functional effects.

An unusual feature of β-mannosidosis in humans and mice is the nature of the lysosomal storage product. The β-mannoside linkage is found only in the *N*-glycosyl moiety of proteins synthesized in the endoplasmic reticulum. Lack of β-mannosidase activity is expected to result in a trisaccharide, Manβ(1–4)GlcNAcβ(1–4)GlcNAc, produced in the stepwise degradation of glycoprotein glycosyl groups. Humans and mice, but not ruminants, have an additional lysosomal enzyme, chitobiase, that cleaves between the GlcNAc–GlcNAc, which predicts the accumulation of Manβ(1–4)GlcNAc, an unusually small storage product of only 400 molecular weight. We show that the storage product in mice is indeed a disaccharide, similar to that found in humans and different from the ruminant storage products. The smaller sized storage product may contribute to

the phenotypic differences between species. In contrast to our β-mannosidosis mice, α-mannosidosis knockout mice display prominent lysosomal storage in a variety of visceral organs and in both central and peripheral nervous systems (43). This may well be due to the larger and more heterogeneous nature of the stored oligosaccharides found in α-mannosidosis.

Our mouse model will be a valuable tool to better understand the mechanisms of pathogenesis for lysosomal storage disease. The substrates for the enzyme are ubiquitous, the storage product is small and uniform and the storage in the nervous system is consistent. This will be an important model for evaluation of various treatment options, including enzyme-replacement and gene-therapy approaches.

REFERENCES

1. Winchester, B., A. Vellodi, and E. Young. 2000. The molecular basis of lysosomal storage diseases and their treatment. *Biochem Soc Trans* 28:150-154.

2. Neufeld, E. F. 1991. Lysosomal storage diseases. *Annu Rev Biochem* 60:257-280.

3. Jones, M. Z., and G. Dawson. 1981. Caprine beta-mannosidosis. Inherited deficiency of beta-D-mannosidase. *J Biol Chem* 256:5185-5188.

4. Cooper, A., I. B. Sardharwalla, and M. M. Roberts. 1986. Human beta-mannosidase deficiency. *N Engl J Med* 315:1231.

5. Wenger, D. A., E. Sujansky, P. V. Fennessey, and J. N. Thompson. 1986. Human beta-mannosidase deficiency. *N Engl J Med* 315:1201-1205.

6. Abbitt, B., M. Z. Jones, T. R. Kasari, R. W. Storts, J. W. Templeton, P. S. Holland, and P. E. Castenson. 1991. Beta-mannosidosis in twelve Salers calves. *J Am Vet Med Assoc* 198:109-113.

7. Jones, M. Z., J. G. Cunningham, A. W. Dade, D. M. Alessi, U. V. Mostosky, J. R. Vorro, J. T. Benitez, and K. L. Lovell. 1983. Caprine beta-mannosidosis: clinical and pathological features. *J Neuropathol Exp Neurol* 42:268-285.

8. Lovell, K. L., and M. Z. Jones. 1983. Distribution of central nervous system lesions in beta-mannosidosis. *Acta Neuropathol (Berl)* 62:121-126.

9. Patterson, J. S., M. Z. Jones, K. L. Lovell, and B. Abbitt. 1991. Neuropathology of bovine beta-mannosidosis. *J Neuropathol Exp Neurol* 50:538-546.

10. Boyer, P. J., M. Z. Jones, R. F. Nachreiner, K. R. Refsal, R. S. Common, J. Kelley, and K. L. Lovell. 1990. Caprine beta-mannosidosis. Abnormal thyroid structure and function in a lysosomal storage disease. *Lab Invest* 63:100-106.

11. Lovell, K. L., M. Z. Jones, J. Patterson, B. Abbitt, and P. Castenson. 1991. Thyroid structure and function in bovine beta-mannosidosis. *J Inherit Metab Dis* 14:228-230.

12. Leipprandt, J. R., S. A. Kraemer, B. E. Haithcock, H. Chen, J. L. Dyme, K. T. Cavanagh, K. H. Friderici, and M. Z. Jones. 1996. Caprine beta-mannosidase: sequencing and characterization of the cDNA and identification of the molecular defect of caprine beta-mannosidosis. *Genomics* 37:51-56.

13. Chen, H., J. R. Leipprandt, C. E. Traviss, B. L. Sopher, M. Z. Jones, K. T. Cavanagh, and K. H. Friderici. 1995. Molecular cloning and characterization of bovine beta-mannosidase. *J Biol Chem* 270:3841-3848.

14. Cooper, A., C. E. Hatton, M. Thornley, and I. B. Sardharwalla. 1990. Alpha- and beta-mannosidoses. *J Inherit Metab Dis* 13:538-548.

15. Dorland, L., M. Duran, F. E. Hoefnagels, J. N. Breg, H. Fabery de Jonge, K. Cransberg, F. J. van Sprang, and O. P. van Diggelen. 1988. Beta-mannosidosis in two brothers with hearing loss. *J Inherit Metab Dis* 11 Suppl 2:255-258.

16. Wijburg, H., J. de Jong, R. Wevers, J. Bakkeren, F. Trijbels, and R. Sengers. 1992. Beta-mannosidosis and ethanolaminuria in a female patient. *Eur J Pediatr* 151:311.

17. Poenaru, L., S. Akli, F. Rocchiccioli, P. Eydoux, and P. Zamet. 1992. Human beta-mannosidosis: a 3-year-old boy with speech impairment and emotional instability. *Clin Genet* 41:331-334.

18. Levade, T., D. Graber, V. Flurin, M. B. Delisle, M. T. Pieraggi, M. F. Testut, J. P. Carriere, and R. Salvayre. 1994. Human beta-mannosidase deficiency associated with peripheral neuropathy. *Ann Neurol* 35:116-119.

19. Kleijer, W. J., P. Hu, R. Thoomes, M. Boer, J. G. Huijmans, W. Blom, O. P. Van Diggelen, E. Seemanova, and M. Macek. 1990. Beta-mannosidase deficiency: heterogeneous manifestation in the first female patient and her brother. *J Inherit Metab Dis* 13:867-872.

20. Cooper, A., J. E. Wraith, W. J. Savage, M. Thornley, and M. J. Noronha. 1991. beta-mannosidase deficiency in a female infant with epileptic encephalopathy. *J Inherit Metab Dis* 14:18-22.

21. Gourrier, E., M. P. Thomas, A. Munnich, L. Poenaru, D. Asensi, D. Jan, and J. Leraillez. 1997. [Beta mannosidosis: a new case]. *Arch Pediatr* 4:147-151.

22. Alkhayat, A. H., S. A. Kraemer, J. R. Leipprandt, M. Macek, W. J. Kleijer, and K. H. Friderici. 1998. Human beta-mannosidase cDNA characterization and first identification of a mutation associated with human beta-mannosidosis. *Hum Mol Genet* 7:75-83.

23. Bedilu, R., K. A. Nummy, A. Cooper, R. Wevers, J. Smeitink, W. J. Kleijer, and K. H. Friderici. 2002. Variable clinical presentation of lysosomal beta-mannosidosis in patients with null mutations. *Mol Genet Metab* 77:282-290.

24. Uchino, Y., T. Fukushige, S. Yotsumoto, T. Hashiguchi, H. Taguchi, N. Suzuki, I. Konohana, and T. Kanzaki. 2003. Morphological and biochemical studies of human beta-mannosidosis: identification of a novel beta-mannosidase gene mutation. *Br J Dermatol* 149:23-29.

25. Aronson, N. N., Jr., and M. J. Kuranda. 1989. Lysosomal degradation of Asn-linked glycoproteins. *Faseb J* 3:2615-2622.

26. Cooper, A., C. Hatton, M. Thornley, and I. B. Sardharwalla. 1988. Human beta-mannosidase deficiency: biochemical findings in plasma, fibroblasts, white cells and urine. *J Inherit Metab Dis* 11:17-29.

27. van Pelt, J., C. H. Hokke, L. Dorland, M. Duran, J. P. Kamerling, and J. F. Vliegenthart. 1990. Accumulation of mannosyl-beta(1----4)-N-acetylglucosamine in fibroblasts and leukocytes of patients with a deficiency of beta-mannosidase. *Clin Chim Acta* 187:55-60.

28. Jones, M. Z., and R. A. Laine. 1981. Caprine oligosaccharide storage disease. Accumulation of beta-mannosyl (1 goes to 4) beta-N-acetylglucosaminyl (1 goes to 4) beta-N-acetylglucosamine in brain. *J Biol Chem* 256:5181-5184.

29. Jones, M. Z., E. J. Rathke, D. A. Gage, C. E. Costello, K. Murakami, M. Ohta, and F. Matsuura. 1992. Oligosaccharides accumulated in the bovine beta-mannosidosis kidney. *J Inherit Metab Dis* 15:57-67.

30. Israel, D. I. 1993. A PCR-based method for high stringency screening of DNA libraries. *Nucleic Acids Res* 21:2627-2631.

31. Tybulewicz, V. L., C. E. Crawford, P. K. Jackson, R. T. Bronson, and R. C. Mulligan. 1991. Neonatal lethality and lymphopenia in mice with a homozygous disruption of the c-abl proto-oncogene. *Cell* 65:1153-1163.

32. Nagy, A., J. Rossant, R. Nagy, W. Abramow-Newerly, and J. C. Roder. 1993. Derivation of completely cell culture-derived mice from early-passage embryonic stem cells. *Proc Natl Acad Sci U S A* 90:8424-8428.

33. Lovell, K. L., and P. J. Boyer. 1987. Dysmyelinogenesis in caprine beta-mannosidosis: ultrastructural and morphometric studies in fetal optic nerve. *Int J Dev Neurosci* 5:243-253.

34. Jones, M. Z., E. J. Rathke, K. Cavanagh, and L. W. Hancock. 1984. Beta-mannosidosis: prenatal biochemical and morphological characteristics. *J Inherit Metab Dis* 7:80-85.

35. Matsuura, F., and M. Z. Jones. 1985. Structural characterization of novel complex oligosaccharides accumulated in the caprine beta-mannosidosis kidney. Occurrence of tetra- and pentasaccharides containing a beta-linked mannose residue at the nonreducing terminus. *J Biol Chem* 260:15239-15245.

36. Hers, H. G., Van hoof, F. 1973. *Lysosomes and storage Diseases.* Academic Press, New York.

37. Lovell, K. L., R. J. Kranich, and K. T. Cavanagh. 1994. Biochemical and histochemical analysis of lysosomal enzyme activities in caprine beta-mannosidosis. *Mol Chem Neuropathol* 21:61-74.

38. Lovell, K. L., and M. Z. Jones. 1985. Axonal and myelin lesions in beta-mannosidosis: ultrastructural characteristics. *Acta Neuropathol (Berl)* 65:293-299.

39. Bryan, L., S. Schmutz, S. D. Hodges, and F. F. Snyder. 1993. Bovine beta-mannosidosis: pathologic and genetic findings in Salers calves. *Vet Pathol* 30:130-139.

40. Rodriguez-Serna, M., R. Botella-Estrada, A. Chabas, M. J. Coll, V. Oliver, M. I. Febrer, and A. Aliaga. 1996. Angiokeratoma corporis diffusum associated with beta-mannosidase deficiency. *Arch Dermatol* 132:1219-1222.

41. Suzuki, N., I. Konohana, T. Fukushige, and T. Kanzaki. 2004. Beta-mannosidosis with angiokeratoma corporis diffusum. *J Dermatol* 31:931-935.

42. Cherian, M. P. 2004. Beta-mannosidae deficiency in two mentally retarded girls with intractable seizures. *Ann Saudi Med* 24:393-395.

43. Stinchi, S., R. Lullmann-Rauch, D. Hartmann, R. Coenen, T. Beccari, A. Orlacchio, K. von Figura, and P. Saftig. 1999. Targeted disruption of the lysosomal alpha-mannosidase gene results in mice resembling a mild form of human alpha-mannosidosis. *Hum Mol Genet* 8:1365-1372.

CHAPTER 4

SUMMARY AND DISCUSSION

Here I describe in detail using different approaches (*in vitro* and *in vivo* animal model) to explore the molecular mechanisms involved in the development of two different human inherited diseases, progressive sensorineural hearing loss (DFNA20/26) and β-mannosidosis. The causative genes for these diseases were identified as cytoplasmic γ-actin gene (*ACTG1*) and β-mannosidase gene (*MANBA*), respectively. Six missense mutations in the cytoplasmic γ-actin gene were found to associate with the DFNA20/26 hearing loss, while different types of mutations (deletion, insertion, nonsense mutations and missense mutations) in the β-mannosidase gene are responsible for the β-mannosidosis. Interestingly, both γ-actin and β-mannosidase proteins are ubiquitously expressed. So far, the pathological presentations in human tissues for both disease conditions are not known except that a blood and skin biopsy were reported for human β-mannosidosis.

These two diseases are different in many respects. First, these two proteins have different cellular functions: γ-actin is primarily a cytoskeleton protein that plays essential roles in cell activities and viability. In contrast, the β-mannosidase is an exoglycosidase that plays a crucial role in the last step of oligosaccharide catabolism in glycoprotein degradation. It cleaves the single β-linked mannose sugar from the nonreducing end of all N-linked glycoprotein oligosaccharides. Second, the types of mutations identified and disease inheritance are different: only missense mutations were identified to cause dominant DFNA20/26 hearing loss, whereas different types of mutations including deletion, duplication, insertion, missense and nonsense mutations are

responsible for β-mannosidosis which is inherited in an autosomal recessive mode. Third, the two diseases have different clinical presentations: The hearing loss caused by the γ-actin mutations is late onset, bilateral, progressive sensorineural and is the only symptom that is observed among six different families with each carrying a different γ-actin mutation. As discussed in chapter 2, hair cells do not regenerate, and it is likely that these mutations cause very subtle changes on γ-actin function and these effects are only significant in maintaining normal hair cell structures and/or repairing hair cells damaged by noise exposure and/or aging. In contrast, human β-mannosidosis is an inborn error of metabolism and exhibits a wide range of symptoms including mental retardation, hearing loss, angiokeratoma, developmental delay, facial dysmorphism, frequent respiratory infections and skeletal abnormalities. It is worth noting that the hearing loss is one of the common symptoms in β-mannosidosis patients. The hearing loss was usually diagnosed at earlier childhood due to an observation of impaired/delayed speech development, and is likely due to a developmental defect in the inner ear caused by the lack of normal β-mannosidase enzyme activity. Finally, there are two naturally occurring animal models (caprine and bovine) of β-mannosidosis, and the pathogenic mechanism for these ruminant disease models has been extensively studied using biochemical approaches and histologic examinations. In contrast, no animal model is currently available for the newly identified DFNA20/26 deafness gene, γ-actin.

Human β-mannosidosis patients have a milder and very heterogeneous clinical expression compared to the two ruminant animal models of β-

mannosidosis which display very consistent and severe phenotypes usually resulting in neonatal death. Speculation on phenotypic differences has been centered on the size and nature of the storage product and in the different developmental programs of the species. Note that mice and humans have an additional lysosomal enzyme, chitobase, which is lacking in ruminants. This enzyme predicts the accumulation of a smaller storage product (a disaccharide in humans and not a trisaccharide seen in ruminant β-mannosidosis). To address the phenotypic differences between human and ruminant β-mannosidosis, to better understand the disease development in humans, and consider potential therapeutic strategies, we developed and characterized a mouse model of β-mannosidosis. The mouse model resembles human β-mannosidosis in many respects and will be a valuable tool to elucidate the mechanisms of pathogenesis for lysosomal storage disease. Although we did not see obvious physical or behavioral abnormalities in the β-mannosidase-deficient mice, including preliminary tests such as rotarod, open field and hanging wire (data not shown), further behavioral testing in the mice to more specifically analyze learning, working memory, long-term memory and fear conditioning will be necessary. In addition, since the cause of hearing loss observed in human cases of β-mannosidosis is still not understood, complete examination of ear structure and hearing testing on the β-mannosidase null mice are imperative. This study is currently being undertaken. We are breeding the β-mannosidase heterozygous mice and plan to perform auditory brainstem response (ABR) analysis and subsequently examine the ear structures including the three compartments

(outer, middle, and inner ear) and the hair cells in the cochlea of the inner ear. The outcome of this study will provide us important information for understanding the nature and cause of hearing impairment that occurs in human β-mannosidosis patients.

In contrast, I approached differently my studies of the newly identified DFNA20/26 disease gene (γ-actin), as described in chapter 2, using *in vitro* assays to examine the effects of six mutations on γ-actin function. The *in vitro* results revealed an important and novel finding and provide valuable information for further investigation. However, to elucidate the molecular mechanism of disease development with the likely subtle changes on protein function due to mutations, an animal model of *ACTG1* hearing loss will be ideal.

Overall, I present here two examples of inherited disorders with known disease-causing genes and describe two different approaches applied to exploring the molecular mechanisms for the development of these diseases. I show you that both approaches could provide us enough information to upgrade our understanding about the diseases and provide the basis and suggest directions for our further investigation.